Journal Pre-proof

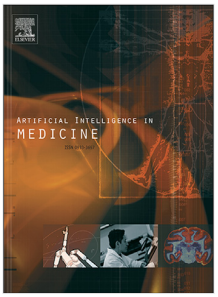

Mapping the brain: AI-driven radiomic approaches to mental disorders

Seraphim S. Moumgiakmas, Eleni Vrochidou, George A. Papakostas

PII: S0933-3657(25)00154-X
DOI: https://doi.org/10.1016/j.artmed.2025.103219
Reference: ARTMED 103219

To appear in: *Artificial Intelligence In Medicine*

Received date : 25 February 2025
Revised date : 4 July 2025
Accepted date : 8 July 2025

Please cite this article as: S.S. Moumgiakmas, E. Vrochidou and G.A. Papakostas, Mapping the brain: AI-driven radiomic approaches to mental disorders. *Artificial Intelligence In Medicine* (2025), doi: https://doi.org/10.1016/j.artmed.2025.103219.

Mapping the Brain: AI-Driven Radiomic Approaches to Mental Disorders

Seraphim S. Moumgiakmas*, Eleni Vrochidou and George A. Papakostas

MLV Research Group, Department of Informatics, Democritus University of Thrace, 65404 Kavala, Greece

ARTICLE INFO

Keywords:
Radiomics
Mental disorders
Artificial intelligence
Neuroimaging
Diagnosis
Treatment response

ABSTRACT

The human brain is the most intricate organ, comprising trillions of synaptic connections and governing every thought, feeling, and action. However, abnormalities in its structure or dysfunction in neural connections can often underpin the development of mental disorders. Mental health conditions affect nearly 1 in 8 people globally, creating a significant challenge for healthcare systems to manage. Advances in neuroimaging and artificial intelligence (AI) hold the potential to transform mental health diagnosis and treatment by enabling the timely detection of these disorders. Radiomics, a technique that extracts quantitative features, has emerged as a promising approach for improving diagnostic accuracy and predicting treatment response. This review explores the current status of radiomics-based applications derived from neuroimaging and AI in addressing various mental disorders categorized under the fifth edition of Diagnostic and Statistical Manual of Mental Disorders (DSM). These include bipolar and anxiety disorders, depressive and neurodevelopmental disorders, schizophrenia spectrum and other psychosis, Post-traumatic stress disorder (PTSD) and Internet Gaming Disorder. The findings highlight the critical role of radiomic features and identify the brain regions associated with each disorder, alongside the tools, algorithms, and methodologies used. While the review also discusses limitations and challenges in radiomics research, it underscores the potential of radiomics and AI to identify significant biomarkers for the precise diagnosis of mental health conditions, as well as to enhance precision in treatment response. The potential of this technology could offer new approaches for the diagnosis and personalized treatment of mental disorders, ultimately improving the well-being of millions people worldwide.

1. Introduction

The human brain is remarkably complex. The average mass varies between genders, ranging from 1.2 kg. to 1.4 kg. (2.65 – 3.09 lbs.). Specifically, the average brain mass for adult women is approximately 1.19 kg. (2.62 lbs.), while for adult males it is about 1.33 kg. (2.93 lbs.) [1]. It comprises approximately 100 billion neurons, each neuron being linked to more than 1000 others, culminating in an estimated total of 60 trillion synaptic connections [2]. The intricate network of neural connections within the brain underpins its role as the central orchestrator of human activities. This encompasses a broad spectrum of functions, including the regulation of the muscular system, the sensory input from the five senses, cognitive computations, the generation of creative thought manifested in art, the processes of learning, the experience of dreams during sleep phases, the control of respiratory functions and emotions. These are merely illustrative of the various physiological and cognitive processes governed by the brain. However, as with any human organ, the brain is also vulnerable to significant health problems.

Health problems caused by the presence of a brain tumor. are dangerous to human life. In addition, neurological disorders resulting from abnormalities in brain functionality or structure are prevalent in the global population. In addition, certain pathologies like mental disorders, are not invariably diagnosed in a timely and accurate manner, leading to serious brain dysfunctions that adversely affect daily functions. The World Health Organization (WHO) reported that mental disorders affected 12.5% of the global population in 2019. Following the COVID-19 pandemic, this percentage enhanced, with the incidence of anxiety disorders and major depressive disorders increasing by 26% and 28%, respectively, over two years. Although there has been a global population growth of 5.19% from 7.7 billion in 2019 to 8.1 billion in 2024, the rise in the rate of mental disorders due to COVID-19 has resulted in a higher number of individuals affected by these conditions. In the recent years, an increase in the prevalence of mental disorders has

*Corresponding author
smoumgia@cs.duth.gr (S.S. Moumgiakmas); evrochid@cs.duth.gr (E. Vrochidou); gpapak@cs.duth.gr (G.A. Papakostas)
ORCID(s): 0000-0002-4890-1022 (S.S. Moumgiakmas); 0000-0002-0148-8592 (E. Vrochidou); 0000-0001-5545-1499 (G.A. Papakostas)

been noticed, according to the Global Burden of Disease (GBD) visualization of the Institute for Health Metrics and Evaluation (IHME) [3]. It is apparent that in the last three decades (1990-2021), the global prevalence has been risen by approximately 64.2%. More specifically, it is estimated that 670 million people were affected by some mental disorder in 1990, a number that increased to approximately 1.1 billion by 2021. This shows a mean annual increase equal to 1.6%, representing approximately 13.87 million people globally. Furthermore, research has shown that the likelihood that an individual develops a mental disorder by age 75 is approximately evenly distributed between genders, with a rate close to 50%. Specifically, for men, the probability was 46.4% and for women, 53.1% [4]. Considering the lifestyle of modern society and the lasting impacts of the COVID-19 pandemic, this upward trend not only persists but appears to be accelerating. These data underscore a significant and growing public health concern that requires urgent attention and intervention.

Based on the above, it is highlighted the increasing prevalence of mental disorders, underscoring the complexity of the brain. This situation emphasizes the critical importance of early diagnosis, or ideally the prediction of mental disorders. Traditionally, diagnosis relies on the identification of a baseline set of symptoms. However, the ability to detect a disorder before such symptoms manifest could significantly enhance treatment prospects by allowing early intervention in the initial stages of the disorder. In many cases, the early symptoms of a mental disorder are similar to those of other conditions, leading to a commonality of symptoms across different disorders [5, 6]. The impact of this overlap is that disorders are not accurately diagnosed in the early stages of their development, and consequently, treatment may not be appropriate. In addition, diagnosis can often be limited to simply describing the patient's thoughts or feelings, and it is incumbent on each psychologist or psychiatrist to determine if the patient has a disorder and, if so, which one. Therefore, it is understandable that diagnoses are not always correct. A further challenge is that even after identifying a mental disorder, the specific subtype must also be determined, as disorders can encompass various categories with different symptoms, some of which may overlap or be entirely distinct. This complexity makes the accurate diagnosis of both the disorder and its subtype even more crucial [7]. As highlighted, the timely and accurate identification of mental disorders is a complex and intricate process, often involving the risk of misdiagnosis. For this reason, the development and application of neuroimaging approaches to study specific brain regions is essential, allowing diagnosis to be based not only on patient-reported descriptions but also on solid evidence derived from the physiology of the organ most directly affected by psychiatric disorders, the brain. Mental disorders can alter both brain function and structure and may even arise as a result of such abnormalities. Consequently, these changes affect the daily functioning of the individual in multiple cases, including cognition, concentration, and even sensory processes such as vision and hearing. In certain disorders, patients may experience hallucinations or sounds that do not exist in reality. Thus, the identification of robust brain biomarkers through neuroimaging techniques is essential for the timely and precise detection of mental disorders.

Radiomics is an evolving field that enhances neuroimaging by extracting quantitative brain features from medical images. These measurable features provide a more comprehensive and data-driven insight into the human body. Radiomics enhances the interpretability of neuroimaging data, enabling more accurate early detection of mental disorders. By analyzing detailed brain information, it improves the precision of diagnosis and allows for a better understanding of treatment responses.

This study seeks to link radiomic technology with the identification and therapeutic outcomes of mental disorders. The scope is to identify and analyze research that applies radiomic approaches integrated with AI techniques to neuroimaging data for the detection and classification of mental disorders. The main objects are:

1. Exploration of the current status of radiomics technology in mental health.
2. Identification of radiomic features associated with various mental disorders.
3. Detection of the most important brain regions highly correlated with each mental disorder.
4. Exploration of software and tools for neuroimaging preprocessing and radiomic feature extraction.
5. Detection of accurate feature selection techniques for identifying the most significant features.
6. Selection of robust and effective AI models for radiomics classification in mental disorders.

Building on the above objectives, the main contribution of this review is to systematically synthesize a research that integrates radiomics, neuroimaging, and AI, offering a detailed overview of the progress and challenges in the diagnosis and treatment of mental disorders. Although there have been previous reviews, they typically focus on a single mental disorder, covering only a limited number of studies based on radiomics, or explore neuroimaging approaches that are not focused on radiomics [8, 9, 10, 11, 12, 13, 14, 15, 16]. Notably, Alizadeh et al. [7] provided a

valuable review of 13 studies applying radiomics to several major mental disorder, including neurodevelopmental disoders and Parkinson's disease. However, the present study offers a more comprehensive and methodologically rigorous exploration of AI-driven radiomics in mental health, expanding the scope to include trauma and stressor-related and neurodevelopmental disorders. Using a clearly defined methodology based on PRISMA 2020 guidelines, we systematically review 28 empirical studies, categorize findings according to DSM-5 mental disorder groups, and compare neuroimaging modalities, radiomic features, AI models, and reported performance metrics. Additionally, we emphasize the role of explainable AI techniques and detail the software tools used across studies. While Alizadeh et al. [7] contribute a strong conceptual foundation, our study advances the field through a deeper, more structured, and practically actionable synthesis of the literature.

The manuscript is structured as follows: The first section introduces the topic, providing an overview of the study's scope and objectives. The second section outlines key concepts and relevant background information concerning mental disorders, neuroimaging, and radiomics. The third section details the research approach and criteria employed in the study. The fourth section presents a comprehensive analysis of the brain regions implicated in mental disorders, the radiomic features detected and selected, and the tools and AI models utilized in each study. The fifth section offers an in-depth exploration of the findings, focusing on the most commonly used tools, algorithms, methods, and the importance of explainable AI (XAI), as well as the results regarding the brain regions associated with each disorder and their implications for future research. Finally, the manuscript concludes with a summary of key insights.

2. Fundamentals

This section analyzes the increasing prevalence of mental disorders, providing a summary of key concepts within the field. It also presents mental disorders as those classified by the DSM. Additionally, a brief introduction to radiomics and neuroimaging is given, explaining the workflow for the identification of radiomic features acquired from neuroimaging data.

2.1. Navigating the Challenges of Mental Health

Before delving into the analysis of risks associated with mental disorders, it is essential to describe the fundamental metrics used in public health, as shown in Table 1. Various health measurements are delineated to assess and quantify the impact of diseases and health conditions on populations. Disability-Adjusted Life Years (DALYs) integrate Years Lived with Disability (YLD) and Years of Life Lost (YLL), offering a comprehensive measure of the overall burden of the disease. This metric reflects the dual aspects of quality and quantity of life impacted by diseases. The incidence rate denotes the frequency of newly occurring instances within a defined group over a particular timeframe and is integral for monitoring the spread and emergence of diseases. In addition, the maternal mortality ratio gauges the rate of maternal deaths in relation to 100,000 live births within a specific timeframe and underscores the risks inherent in childbirth and pregnancy. The prevalence rates provide an understanding of the overall count of present disease cases within a specific group at a given moment, thereby reflecting the community's overall disease burden. YLD focuses specifically on the burden of disability attributable to various health conditions, considering the non-fatal impact on individuals' daily lives. Lastly, YLL determines premature mortality by calculating the potential years of life lost when individuals do not achieve their expected lifespan, a measure often used to guide healthcare priorities and interventions.

Table 1: Key measures

Measures	Definition	Description
DALY	Disease burden measurement	A single DALY signifies the loss of one year of optimal health. DALYs summarize the YLL due to premature mortality and YLD.
Deaths	Total deaths measurement	This measurement accounts for the overall count of deaths within a specific time period caused by a particular disorder.

Continued on next page

Measures	Definition	Description
Incidence	The count of newly diagnosed instances of a disease.	Refers to the emergence of newly identified cases over a specified time period.
Maternal mortality ratio	Maternal deaths	This metric represents the rate of maternal mortality per 100,000 live births within a given time period.
Prevalence	Total instance of disease occurrences	Prevalence shows the detected disease cases in the population within a specified timeframe.
YLD	Health conditions impact	YLD are a calculation of the burden of living with a health condition or its consequences and are measured in terms of non-fatal health outcomes.
YLL	Premature deaths measurement	YLL are determined from the subtraction of age at death from the projected life expectancy, representing the years lost due to not reaching a typical life expectancy [17].

Concerning mental disorders, it is crucial to differentiate between direct and indirect mortality risks. Not all psychiatric conditions pose an immediate threat to life by directly affecting an individual's physiological functions. However, mortality risk can increase through indirect pathways, most notably suicide. This distinction is particularly relevant when examining eating disorders (e.g., anorexia), which are directly life-threatening due to their severe impact on nutritional status and metabolic functioning. In contrast, conditions such as depression pose a significant mortality risk through indirect mechanisms. Although these disorders primarily contribute to mortality by increasing the likelihood of suicide, the connection between the disorder and death is mediated by psychological distress rather than direct physical health consequences. This distinction underscores the importance of recognizing the various ways mental health disorders can lead to mortality, whether through direct physiological decline, as seen in anorexia, or the complex indirect effects observed in depression.

Drawing from data provided by the WHO, over 700,000 individuals lose their lives to suicide annually. This statistic is linked with mental illness, including depression and alcohol addiction disorders [18]. In addition, this figure encompasses cases in which individuals face significant challenges, such as financial distress, dissolution of personal relationships, or the enduring presence of chronic pain and illness. In addition, the incidence of suicide attempts significantly exceeds the number of fatalities resulting from such acts. For example, data from the American Foundation for Suicide Prevention [19] indicate that in 2021, there were 48,183 recorded suicides, compared to approximately 1.7 million attempted suicides. As already mentioned, suicide causes include financial problems, relationship problems, and causes which are not directly related to mental disorders. However, research has proved that people suffering from mental health illnesses have a higher likelihood of suicide [20].

A comprehensive analysis conducted in 2015 [21], which synthesized the results of 148 studies, has underscored the significant impact of mental disorders on global mortality rates. This meta-analysis revealed that the combined comparative risk of all-cause mortality for people diagnosed with mental disorders is 2.22, indicating a significantly greater likelihood of death than in the mentally healthy population. Almost 67% of the deaths in individuals suffering from mental disorders were due to chronic illnesses, while 17.5% were attributed to unnatural causes such as suicide or unintentional injury. This distinction highlights the varied ways in which mental health conditions can affect longevity. Furthermore, has been indicated a median loss of 14.66 years of potential lifespan for those suffering from mental disorders [22]. Interestingly, mental disorders are estimated to account for 14.3% of global deaths annually, translating to approximately 8 million deaths. These findings, based on the above analysis, highlight the urgent need for global health initiatives to address mental disorders more effectively, aiming to reduce their substantial contribution to worldwide mortality. Mental health is crucial not only for individuals' functionality but also for their lives.

2.2. Diagnosing Mental Disorders: The DSM Framework

The Diagnostic and Statistical Manual of Mental Disorders (DSM) [23, 24, 25, 26], although originally developed for healthcare practitioners in the United States, has gained importance as a critical resource worldwide, offering a detailed framework for diagnosing mental health conditions. Its significance is magnified by the manual's periodic updates, which mirror the dynamic nature of mental health understanding within the global scientific community. These revisions ensure that the DSM remains an indispensable evolving tool that incorporates the latest research and clinical practices. Globally acknowledged by mental health experts, DSM guidelines facilitate a consistent process for the diagnosis and treatment of mental disorders. This global adoption highlights its importance not only as a national manual for the US but also as a key document for the international healthcare community. The DSM-5 describes a mental disorder as a condition marked by considerable disruptions in a person's cognition,

emotional regulation, or behavior, which point to an underlying malfunction in the psychological, biological, or developmental processes involved in mental functioning, emphasizing its commitment to a holistic perspective on mental health. Table 2 provides the classification of mental disorders, as listed in the DSM-5. This table shows 23 broad groups of mental conditions in the first column, together with several examples of disorders for each category in the second column. It should be noted that the second column lists only a few examples and does not encompass all mental disorders identified in DSM-5 for each category. This approach was taken because unspecified disorders were recorded for nearly every category, along with subcategories, which would have resulted in a more complex table. The purpose of the table is to highlight the recognized categories of mental disorders and to illustrate the complexity of the human brain from a general psychiatric perspective.

Table 2: Mental Disorder Categories and Examples

Mental Disorder Category	**Examples of Disorders**
Anxiety Disorders	Agoraphobia, Generalized Anxiety Disorder, Social Anxiety Disorder, Panic Disorder
Bipolar and Related Disorders	Cyclothymic Disorder, Bipolar I, Bipolar II Disorders
Depressive Disorders	Persistent Depressive Disorder, Disruptive Mood Dysregulation Disorder, Major Depressive Disorder (MDD), Persistent Depressive Disorder
Disruptive, Impulse-Control, and Conduct Disorders	Kleptomania, Conduct Disorder, Pyromania
Dissociative Disorders	Dissociative Identity Disorder, Depersonalization Disorder, Dissociative Amnesia
Elimination Disorders	Enuresis, Encopresis
Feeding and Eating Disorders	Bulimia Nervosa, Anorexia Nervosa, Avoidant/ Restrictive Food Intake Disorder, Pica
Gender Dysphoria	Gender Dysphoria
Medication-Induced Movement Disorders and Other Adverse Effects of Medication	Tardive Dyskinesia, Tardive Akathisia, Tardive Dystonia
Neurocognitive Disorders	Major or Mild Frontotemporal Neurocognitive Disorder, Delirium
Neurodevelopmental Disorders	Autism spectrum disorder, Tic disorder, Attention-Deficit/Hyperactivity Disorder (ADHD)
Obsessive-Compulsive and Related Disorders	Hoarding Disorder, Body Dysmorphic Disorder, Obsessive-Compulsive Disorder (OCD)
Paraphilic Disorders	Pedophilic Disorder, Sexual Masochism Disorder, Sexual Sadism Disorder, Fetishistic Disorder
Personality Disorders	Paranoid Personality Disorder, Schizoid Personality Disorder, General Personality Disorder
Schizophrenia Spectrum & Other Psychotic Disorders	Schizoaffective Disorder, Catatonia, Schizophrenia
Sexual Dysfunctions	Female Orgasmic Disorder, Female Sexual Interest/Arousal Disorder, Delayed Ejaculation, Male Hypoactive Sexual Desire Disorder, Erectile Disorder
Sleep-Wake Disorders	Narcolepsy, Breathing-Related Sleep Disorders, Parasomnias, Nightmare Disorder, Insomnia Disorder
Somatic Symptom and Related Disorders	Functional Neurological Symptom Disorder, Somatic Symptom Disorder
Substance-Related and Addictive Disorders	Cannabis-Related Disorder, Alcohol-Related Disorders, Hallucinogen-Related Disorders

Continued on next page

Mental Disorder Category	Examples of Disorders
Trauma- and Stressor-Related Disorders	Posttraumatic Stress Disorder (PTSD), Disinhibited Social Engagement Disorder, Adjustment Disorders
Other Conditions That May Be a Focus of Clinical Attention	Suicidal Behavior and Non-suicidal Self-Injury, Abuse and Neglect, Relational problems, Adult Maltreatment and Neglect Problems
Conditions for Further Study	Internet Gaming Disorder, Caffeine Use Disorder, Persistent Complex Bereavement Disorder
Other Mental Disorders	Unspecified Mental Disorder Due to Another Medical Condition, Unspecified Mental Disorder

According to the WHO, Figure 1 illustrates the widespread occurrence of the most prevalent mental health disorders globally. These include anxiety disorders, which affect approximately 301 million people [27], depressive disorders, which affect more than 264 million people [28, 29], and bipolar disorders and related conditions, which affect 40 million people [30]. Additionally, 24 million people are affected by the schizophrenia spectrum [31]. Regarding Post-Traumatic Stress Disorder (PTSD), around 3.9% of the global population (approximately 316 million people) experienced PTSD sometime during their lifetime, although the exact number of those currently suffering remains unclear. As for neurodevelopmental disorders, clear statistics are unavailable due to the complexity and varying severity of these conditions [32]. However, WHO shows that shows that approximately 1 in 100 children is affected by autism spectrum disorder [33], while other sources show one in 44, or one in 300 [34, 35]. It is evident that anxiety and depressive disorders collectively represent over 50% of the worldwide impact of mental disorders, with approximately 565 million people affected out of an estimated 970 million to 1.1 billion people [36, 3].

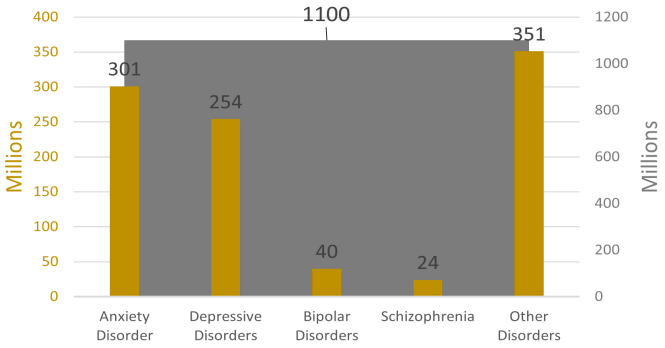

Figure 1: Distribution of mental disorders (millions)

2.3. Neuroimaging Techniques

Human physiology can offer valuable insights into a person's dysfunction or pathology even before obvious symptoms emerge. Advanced biochemical and medical examinations provide health professionals with critical insights into an individual's health [37]. Neuroimaging can be used as a cutting-edge diagnostic technique, offering a window into the intricate workings of the brain. Some well-known neuroimaging techniques include the following:

X-ray Imaging (Röntgen rays)

X-ray imaging, a foundational pillar of diagnostic medicine for more than a century, utilizes high-energy electromagnetic radiation to penetrate the body. The varying absorption rates of X-ray radiation by different tissues allow for the creation of a detailed visual representation. Dense materials, such as bone, absorb more X-rays and appear lighter in the resulting image, whereas softer tissues show in shades of gray. This differential absorption generates a detailed "shadow" image of the internal anatomy, allowing medical professionals to diagnose and monitor various conditions [38, 39, 40, 41, 42]

Computed Tomography (CT)

CT imaging, leveraging the same principles of X-ray radiation, provides cross-sectional views of the body through the acquisition of

images from multiple angles. These images are then computationally reconstructed into two-dimensional slices or three-dimensional models of the internal structures. By analyzing the reduction in X-ray photon intensity as they pass through various tissues, CT scans produce detailed images that are crucial in diagnosing and tracking anatomical and pathological changes within the body [43].

Magnetic Resonance Imaging (MRI)

Magnetic resonance imaging (MRI) differentiates from CT by using magnetic fields and radio waves to generate visualizations based on the hydrogen atom distribution within the body. This technique provides a contrast based on the variations in the proton density and relaxation durations across various tissues, thereby offering a versatile imaging solution. Through selective imaging sequences, magnetic resonance imaging can emphasize particular tissue characteristics, enhancing its diagnostic utility for a variety of clinical conditions. Moreover, MRI's ability to visualize both anatomical structures and functional processes without ionizing radiation makes it indispensable in medical diagnostics [44, 45, 46, 47, 48, 49, 50, 51].

Positron Emission Tomography (PET)

PET imaging introduces a dynamic component to medical diagnostics by tracking metabolic processes through the administration of radioactive tracers. This technique captures the annihilation events resulting from the interaction of emitted positrons with electrons, allowing visualization of physiological activity within the body. The capability of PET to monitor metabolic alterations in real-time offers invaluable insights, particularly in oncology, neurology, and cardiology [52, 53, 54, 55].

Single Photon Emission Computed Tomography (SPECT)

In this case, radiological markers are used to generate comprehensive three-dimensional images of physiological, metabolic, or pathological activities. This method surpasses conventional imaging by providing a more detailed view of the tracer distribution within the body, thus improving the understanding of various diseases and conditions. The introduction of multiheaded camera systems has significantly accelerated the image acquisition process, further solidifying SPECT's role in modern diagnostics [56, 57, 58, 59, 60, 61]

Additional Methodologies

Beyond the above neuroimaging techniques, methods such as electroencephalography (EEG) and magnetoencephalography (MEG) offer alternative approaches to understanding brain function. Although not depicted in structural images, these techniques produce graphical representations of brain activity, providing unique insights into neurological functions and disorders.

Through the neuroimaging methods analyzed, it is possible to identify characteristics present at the sites where the neuroimaging was performed. The choice of the neuroimaging technique depends on the criticality and nature of the disease or disorder. The points of interest in neuroimaging may be related to a tumor or an abnormality and they are not visible to the naked eye and can only be detected using specialized imaging technologies. Additionally, integrating imaging data with omics approaches, such as radiomics, provides deeper insights into the biological underpinnings of these abnormalities. These methods are presented in Table 3, along with some basic techniques associated with each.

Table 3: Neuroimaging Methods and their Techniques

Neuroimaging methods	Techniques of neuroimaging method
X-Ray	• Angiography • Dental X-rays
Computed Tomography (CT)	• Refraction Enhanced CT • Four-Dimensional (4D) CT • Fluorescence Molecular CT

Continued on next page

Neuroimaging methods	Techniques of neuroimaging method
Magnetic Resonance Imaging (MRI)	• Structural MRI (sMRI) -T1-weighted -3D T1-weighted -T2-weighted • Functional MRI (fMRI) -Resting State- Functional MRI (rs- fMRI) • Diffusion MRI (dMRI) -Diffusion Tensor Imaging (DTI) -Diffusion-Weighted Imaging (DWI)
Positron Emission Tomography (PET)	• Amyloid PET Imaging • Tau PET Imaging
Single Photon Emission Computed Tomography (SPECT)	• Brain SPECT (Neurological) • Cardiac SPECT (Cardiovascular) • Tumor Imaging SPECT (Oncological)

2.4. Radiomics: Extracting Quantitative Imaging Data

Radiomics is a rapidly advancing technological field, based on the fundamental principle that neuroimaging is not just an image, but rather imaging data [61, 62]. Radiomic features pertain to the quantitative information that is "hidden" within the human body and everything within it. By "quantitative," we refer to information that is physically measurable and relates to the volume, texture, size, or shape of a specific part of the body, such as a tumor or a segment of an organ [63]. These features are of high quality, precision, and large volume. However, to extract these features, in addition to neuroimaging, a very specific area is required for the extraction algorithms to focus on. These areas are referred to as Region of Interest (ROI) or Volume of Interest (VOI), depending on whether it is a 2D neuroimaging or its 3D model. This process is necessary to avoid extracting a large volume of radiomic features that may pertain to general and potentially vague information not related to the specific target. However, there are cases that as ROI has been selected the whole brain relating a huge number of radiomics which are not always so significant. In summary, radiomic features refer to measurable characteristics extracted with high fidelity from a segment of the human body or organ through neuroimaging and algorithms, imperceptible to the human eye. The identification of these features enables early detection and precise diagnosis of a disease using parameters and criteria established in the fields of radiology and medicine. Figure 2 illustrates the convergence of artificial intelligence, psychiatry, and radiology in advancing radiomics, thereby shaping the concept of psychoradiology [63]. The most common radiomics categories can be identified as follows:

First-Order Features: These features show how voxel intensity values are spread across a ROI without considering the spatial relationships between voxels [64].

Second-Order Features: Unlike first-order, this type of feature focuses on the spatial relationships between voxels [65].

Morphological Features: These features are related to the volume or the shape, describing the geometric characteristics of a specific region [66].

Higher-Order Features: Higher-order features describe the directional movement of water molecules within tissues, providing insights into tissue microstructure and fiber integrity. These features are particularly useful in diffusion imaging [67].

Transform-Based Features: In contrast to second- and higher-order texture features, this type of features are derived after applying a mathematical transformation to the ROI. These features enable analysis in both the spatial and frequency domains [66].

Functional Connectivity Features: These features assess the temporal correlations between different brain regions, typically using resting-state fMRI. They help identify synchronized brain activity patterns, providing insights into brain network dynamics and cognitive functions [68].

To identify and convert radiomic features into useful information for detection, classification, or analysis, a precise and well-defined process must be followed. This procedure is illustrated in Figure 3 [66, 7, 69, 70, 71]. In this subsection, the process will be described at a high level, as it can vary depending on the type of neuroimage used, its quality, or the specific objective. The first

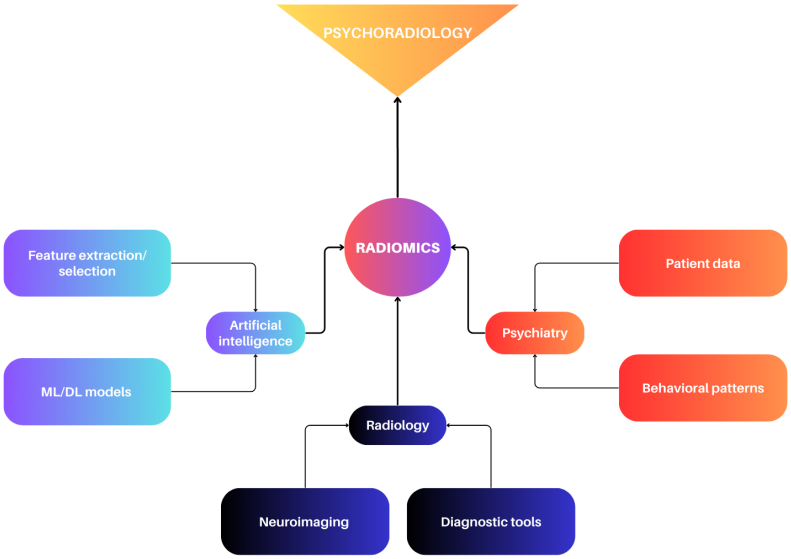

Figure 2: Connecting artificial intelligence, radiology, and psychiatry through radiomics

two steps in this process involve neuroimaging from the patient. Imaging acquisition techniques vary according to the objective of the analysis or the desired outcome. Each of these techniques can be utilized to provide different types of information, such as structural or functional data, varying in quality and depth of detail. The next step is the preprocessing of the acquired images. This stage includes methods such as normalization, segmentation, and identification of the ROIs to remove unnecessary parts of the image and irrelevant information, focusing only on the valuable brain areas. The preprocessing technique would isolate this region as ROI and improve its quality to allow more accurate and precise detection of radiomic features. The following step involves extracting radiomic features. These features are typically obtained as either tabular data or feature maps, which are visualized within the ROI of the neuroimage. Of course, not all extracted features are equally useful and not all provide significant information related to the scope of the analysis. For this reason, the next stage of the process is critical. During the feature selection stage, the most informative and predictive radiomic features must be chosen to enhance the precision and overall performance of the final model. Several algorithms are available for feature selection, which will be described in a subsequent chapter. The final stage of the flowchart involves the implementation of Machine Learning (ML) or Deep Learning (DL), including the training, validation, and testing of selected features, followed by their application for classification, detection, or prediction.

3. Methodology

This section describes the methodology followed for the detection of studies and the criteria applied for their inclusion or exclusion in the present review. A literature search was conducted in the Scopus database on October 23rd 2024, resulting in 702 papers. The query used was as follows:

ALL ((radiomic OR radiomics) AND ("psychiatric disease" OR "psychiatric disorders" OR "psychopathology" OR "mental disorders" OR "mental illness"))

However, not all the papers aligned with the focus of the present review. More specifically, the acceptance criteria were:

- Focus on mental disorders
- Utilize neuroimaging data
- Implementation/description of a radiomic approach using ML/DL/AI

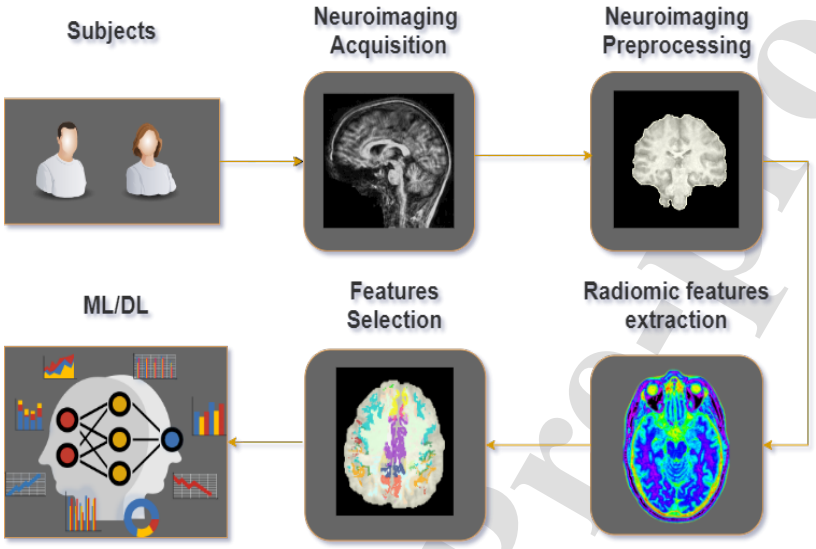

Figure 3: Radiomics application flowchart

The papers that complied with the above criteria are included in the following section which aims to identify significant radiomic features and brain regions for several mental disorders, as well as tools, techniques, and related algorithms. Based on the above, the exclusion criteria were the following:

- Radiomics and neuroimaging data for non- mental disorders (stroke, epilepsy etc.)
- AI approaches without using radiomic features
- Statistical radiomic analyses

In Figure 4, it is shown the process which followed to identify the 28 papers included in the analysis, based on the PRISMA 2020 flow diagram [72]. It is important to note that 36 papers met the acceptance criteria. However, eight of these were review articles. Although the reviews were studied and cited as references, they were not included in the final analysis, since the eligible studies they described had already been considered individually during the screening process. After selecting the eligible studies, data extraction was performed manually. A structured file was developed to systematically record key variables from each study. Extracted data included the mental disorder category, neuroimaging modality, radiomic features analyzed, machine learning or deep learning algorithms applied, main brain regions identified, sample sizes, and reported performance metrics. Based on these data, 28 papers were included in the analysis, focusing on seven categories of mental disorders, as classified in the DSM-5:

1. Anxiety Disorders
2. Bipolar and Related Disorders
3. Depressive Disorders
4. Neurodevelopmental Disorders
5. Schizophrenia Spectrum and Other Psychotic Disorders
6. Trauma- and Stressor-Related Disorders
7. Conditions for Further Study

At this stage, it is essential to emphasize that the category of "Conditions for Further Study", the Internet Gaming Disorder (IGD) is included. The case of this disorder is controversial. In DSM-5, IGD is not classified as a standalone mental disorder but is included in the section "Conditions for Further Study" indicating the need for more research. In contrast, the International

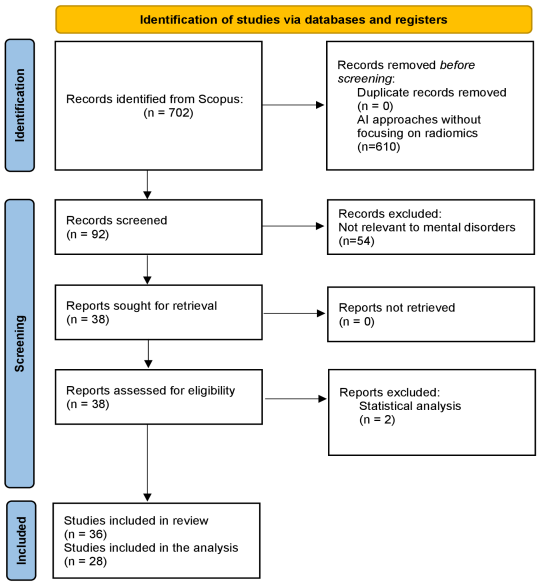

Figure 4: PRISMA 2020 flow diagram

Classification of Diseases (ICD-11) formally classifies IGD as a mental disorder. However, since papers that focus on the IGD were found and the present review is based on the DSM structure, the IGD is included in the "Conditions for Further Study".

Although the total number of results was 702, only 28 papers met the criteria and were selected for inclusion in the final analysis. The selected papers revealed a linear increasing trend in publications from 2017 to 2022, which recorded the highest number of studies. More specifically, the number of studies rose from one to eight, reflecting an increase of 700%. However, this trend did not continue in the following years (up to October 2024). A decline followed, dropping to five and two papers in 2023 and 2024, respectively. Furthermore, 89.29% of the papers included for analysis in the next section were published from 2020 onward, while only 10.71% were published before 2020. This indicates that the combination of radiomics, neuroimaging, and AI for the diagnosis of mental disorders is a relatively recent area, although this combination has already been implemented more widely in healthcare fields focusing on neurodegenerative diseases and tumors. Preliminary findings show that research on radiomic approaches using neuroimaging data and AI for diagnosing mental disorders is very limited. This is evident from the small number of papers that meet the above criteria. Although a large number of studies targeted at detecting various mental disorders through neuroimaging and AI, radiomics remains a technological field that has not yet been thoroughly explored in conjunction with mental disorders and AI. Furthermore, the shortage of publicly datasets could explain the limited number of studies and the decline in publications observed after 2022. Nevertheless, a gradually increasing focus on radiomics and mental health combined with AI has been observed, which is crucial since mental disorders affect millions of people worldwide, and current diagnostic methods are not always accurate. This shift highlights the potential of radiomic technology to improve both the diagnosis of disorders and the prediction of treatment responses.

4. Radiomics in Mental Disorders

The following subsections will examine various radiomics-based approaches, combined with AI, to diagnose and predict treatment responses for several mental disorders. The disorders included in the review have been classified into seven categories based on the DSM. A brief description of each disorder is provided, highlighting which brain regions are affected, and discussing the neuroimaging techniques used in each study. In addition, the radiomic features selected as the significant ones from different

brain areas for each disorder, the types of classifiers used, and the performance of each method are also explored. Additionally, at the end of each subsection, two supplementary tables are provided to summarize the findings for each category. The first table reports the number of features selected, identifies the specific radiomic features and important brain regions associated with the disorder, and summarizes the key findings. The second table presents the performance metrics reported in each study, specifies whether the dataset was public or private, details the number of participants, and indicates the type of cross-validation (CV) employed, if applicable.

4.1. Anxiety Disorders

Anxiety disorders (AD) are among the most prevalent mental health issues that impact adolescents and adults. This disorder manifests fear, worry, emotional distress, behavioral and social problems, and even physical illness [73, 74]. The biological cause of AD is present in the limbic system [75]. More specifically, in the development of AD, the amygdala plays a crucial role [76, 77, 74, 78, 79]. The amygdala is responsible for the creation of anxiety emotions and fear reactions. In addition, among the hippocampus that communicates closely, they are responsible for emotional responses to fear that can be based on memories or stimuli [80]. This type of disorder has various subtypes. Some of these subtypes will be presented in the following paragraphs.

4.1.1. Panic Disorder (PD) with Agoraphobia (PDA)

The basic characteristics of PD are panic attacks, which are unexpected and recurrent, combined with an intense sense of anxiety [81]. One of the main problems of the disorder is that the diagnosis is determined by evaluating clinical symptoms and it is a very complex and difficult process, as they overlap with symptoms of psychical illnesses or were completely missed [82]. Three primary brain regions linked to the pathogenesis of panic disorders are the insula, amygdala, and the Anterior Cingulate Cortex (ACC). All of these structures are also related to the emotions of anxiety and fear [83, 84, 85, 86, 87, 88]. More specifically, the decrease in volume and the hyperactive amygdala are key factors in the development of panic attacks [84, 86]. Furthermore, gray matter irregularities have been observed in the insula and ACC has been observed in patients with panic disorder and agoraphobia [89, 90, 91, 92, 93]. Those three structures show that they could be important brain regions that differentiate healthy patients from patients with panic disorders, and those are the structures on which Bang et al. in [81] focused. T1-weighted MRI data were preprocessed in order for their quality to be increased and also to keep only the important information. More specifically, FreeSurfer is used for automated segmentation of the regions related to the disorder (amygdala, insula and ACC), and N4 bias correction was applied for the correction of the non-uniformity in low frequency intensity. In addition, the images were resampled at a voxel size of $1 \times 1 \times 1$ mm^3 and masks were generated for each ROI. After this procedure, they extracted 1498 radiomics. The extracted radiomics were first and second-order, as well as shape features. With these features, the intensity distribution, spatial heterogeneity, and morphological alterations would be reflected in the ROIs. The feature extraction process was performed with Pyradiomics [94], while for the selection of those features the LASSO method was used. In addition, the best classification performance was achieved with Extreme Gradient Boosting (XGBoost), with an accuracy score of 81.3%, 75% and 86.1% for sensitivity and specificity, respectively, while the AUC was 0.84. In this paper, the authors also used the SHapley Additive exPlantations (SHAP) model towards enhancing the interpretability [95]. Based on that, they concluded that 29 radiomics are the most significant to differentiate patients with panic disorder and healthy patients. More specifically, 18 features were obtained from insular subregions, the amygdala provided six features, while five of them were acquired from the ACC. Of these features, 10 were in the first-order category and 19 in the second-order category. It should be noted that the percentage of reduction in the total number of radiomic features was 98.06%, from 1498 (107 features $\times$ 14 ROI) to 29. The outcome of the SHAP model is the suggestion that the first-order energy of the central sulcus of the insula, the right ACC and the bilateral long insula gyrus show a strong correlation with panic disorder accompanied by agoraphobia.

4.1.2. Social Anxiety Disorder (SAD) & Generalized Anxiety Disorder (GAD)

In this section, the Social Anxiety Disorder (SAD) [79] and the Generalized Anxiety Disorder (GAD) [74] are described. SAD is the type of AD in which the subject feels fear and/or anxiety about social situations. Those emotions lead to having problems with interactions, such as communication issues or the absence of events, which generally avoid any situation related to other people or crowded places [96]. In this type of disorder, with the exception of the amygdala and hippocampus, the crucial role also has the orbitofrontal cortex (OFC). OFC is the region related to decision making, evaluation of reward value, and emotion processing during social situations [97, 98]. Evaluation of the reward value of the social interaction can create negative emotions in the subject caused by fear of the negative outcome of the interaction [99].

In the paper of Kim et al. [79], the authors sought to predict social anxiety levels using resting-state functional magnetic resonance imaging (rs-fMRI) data. For this reason, the preprocessing of the images is performed using the fMRIPrep pipeline, which is based on the Nipype framework [100, 101]. The pipeline comprises a series of preprocessing stages like surface reconstruction, skull stripping, resampling, motion correction, normalization, and segmentation. The research used vectors with 56 elements (7 brain regions $\times$ 4 radiomic features $\times$ 2 hemisphere sides). The radiomic features were fractional amplitude of low-frequency fluctuation (fALFF), regional homogeneity (ReHo), fractional resting-state physiological fluctuation amplitude (fRSFA), and degree centrality (DC) and extracted using the AFNI [102] software. Furthermore, the brain regions were the OFC, posterior cingulate cortex, precuneus, anterior cingulate cortex, parahippocampal gyrus, hippocampus, and the amygdala. XGBoost was the most efficient model, achieving an accuracy of 77.7% and an F1 score of 0.815. An interesting part of this work was the study of

the importance of radiomic features using SHAP [95]. Using this Explainable Artificial Intelligence (XAI) technique, a SHAP metric value is calculated for each radiomic feature to measure their importance and their contribution value to the method. With this method, the results are more transparent, and it becomes more clear why the model extracts those results, leading to human interpretability, which is very important for medical applications. In general, it is crucial for both engineers and doctors to explain why each model extracted a decision and which parameters led to this result. The results showed that the most significant radiomics were the DC of the OFC and more specifically in the left hemisphere.

With regard to GAD, it is characterized by chronic anxiety, restlessness, muscle tension, and sleep disturbance. As in SAD, amygdala also has a crucial role in GAD, as generally in AD. Research has indicated that amygdala volume undergoes changes in patients with anxiety disorders. Based on this, Li et al. [74] selected to use T1-weighted MR data for two classifications: AD patients vs. healthy controls (HC), and GAD patients vs. HC. The radiomic features provided by the bilateral amygdala in both tasks highlighted its role as a key region forming the basis for the clinical diagnosis of AD. However, in order for the feature extraction process to proceed effectively, the authors used preprocessing techniques for the data. The Computational Anatomy Toolbox 12 (CAT12) [103] was used for the quality control of the images. Images that had scores equal to or lower than C+ were excluded. The scoring criteria were the noise, bias field, image resolution, and overall weighted image quality. For images that were high quality and remained in the data set, the FreeSurfer pipeline was used [104]. FreeSurfer is an open-source software for analyzing MRI data and provides tools for brain segmentation, surface reconstruction, and anatomical parcellation. Has the ability for detailed measurements of the brain, and also 3D models can be constructed. In addition, for segmentation of the bilateral amygdala, a probabilistic subcortical structural atlas (Aseg atlas) was used [105]. Using the Pyradiomics [94] toolkit, 107 features extracted from the T1-weighted MRI images. More specifically, those features were 14 shape-based, 14 Gray-Level Dependence Matrix (GLDM) features, five Neighborhood Gray Tone Difference Matrix (NGTDM), 16 Gray-Level Run Length Matrix (GLRLM), 16 Gray-Level Size Zone Matrix (GLSZM), 24 Gray-Level Co-occurrence Matrix (GLCM), and 18 first-order statistics features. The ones with the greatest significance were selected using a 10-fold LASSO regressor. For the AD vs. HC task, two features were chosen from the left amygdala (small dependence emphasis and high gray level emphasis) and four features from the right amygdala (interquartile range, small dependence emphasis, maximum 2D diameter column, and gray level non-uniformity normalized). For the GAD vs. HC task, seven features were chosen from the left amygdala (cluster prominence, cluster tendency, mean absolute deviation, small dependence high gray level emphasis, short-run high gray level emphasis, maximum 2D diameter column, and small area high gray level emphasis) and three features from the right amygdala (interquartile range, maximum 2D diameter column, and cluster tendency). Classification was performed using a linear kernel Support Vector Machine (SVM). For the AD vs. HC classification task, the receiver-operating characteristic Area Under Curve (AUC) was 0.67 and 0.64 for the features of the left and right amygdala respectively. For the GAD vs. HC task, the AUCs were 0.67 for left amygdala features and 0.69 for right amygdala features. For both tasks, radiomic features importance was higher than the importance of the amygdala's volume. The dataset used in this research is available at: Child Mind Institute Healthy Brain Network (HBN) dataset: CMI Healthy Brain Network.

Details on key findings and evaluation performance metrics for Anxiety disorders are included in Tables 4 and 5, respectively.

Table 4: Analysis on Anxiety Disorders

Work	Disorder	Selected features	Radiomics	Important Regions	Key Findings
[81]	PD & PDA	29	First-order, second-order	Amygdala, insula, ACC	The features of energy detected in the central sulcus, bilateral long insula gyrus, right ACC and the insula had increased significance
[79]	SAD	56	ReHo, fALFF, fRSFA, DC	OFC, ACC, posterior cingulate cortex, precuneus, hippocampus, parahippocampal gyrus, amygdala	DC features of OFC of the left hemisphere were crucial features

Continued on next page

Work	Disorder	Selected features	Radiomics	Important Regions	Key Findings
[74]	GAD	(2,4) (7,3) [left and right amygdala for both tasks]	Small dependence emphasis, maximum 2D diameter column, cluster tendency	Left and right amygdala	Amygdala radiomics features had higher significance compared to amygdala volume features

Table 5: Experimental validation on Anxiety Disorders

Work	Disorder	Performance	Data	Participants	CV
[81]	PD & PDA	Training/Test Set: ACC=78.6%/81.3%, SEN=77.4%/75.0%, SPEC=79.7%/86.1%, AUC=0.85/0.84	Private	93 PDA and 120 HCs.	10-fold cross-validation
[79]	SAD	ACC=78.3%, Balanced ACC=77.7%, F1_SCORE=0.815	Private	58 LSA and 52 HSA	5-fold cross-validation
[74]	GAD	AD vs. HC/ GAD vs. HC: AUC=67%/69%	Healthy Brain Network (HBN)[1] [106]	200 AD (103 GAD) and 138 HCs.	10-fold cross-validation

The accuracies reported ranged from 67% to 81.3%, with an average of 76.7%. The best-performing model was presented by Bang et al. [81], achieving 81.3% accuracy and an AUC of 0.84 on the test set. The study used 29 radiomic features and implemented SHAP for model interpretability, identifying that the first-order energy features from the left and right long insula gyrus and central sulcus of the insula, were the most informative. Importantly, the authors addressed class imbalance using Bayesian optimization and showed no evidence of overfitting based on cross-validated results. Kim et al. [79] also reported strong performance on resting-state fMRI features, emphasizing the discriminative power of the orbitofrontal cortex. Also this study used the SHAP for model interpretability. Li et al. [74], using a public dataset, achieved lower AUC scores. Despite the larger sample size, performance was likely limited by using only localized amygdala radiomic features. All three studies used classical machine learning models and applied k-fold cross-validation to mitigate overfitting. Among the most consistently important brain regions across studies were the amygdala, left OFC, central sulcus of the insula, right ACC, and bilateral long insula gyrus. These areas are known to be involved in emotional regulation, sensory integration, cognitive control, and fear processing [81] supporting their role in anxiety pathology.

4.2. Bipolar and Related Disorders

Bipolar Disorder (BD) consists of the main causes related to disability and high mortality rates [107, 108]. Patients with bipolar disorder often experience long periods of depression, mania, or hypomania. In addition, sleep quality and duration, along with appetite and cognition, are also affected [109]. Unfortunately, the neurophysiology problems that cause this disorder are still unknown, and the diagnosis is based primarily on conversation and observation, which are not always accurate. However, neuroimaging has shown that there are anatomical differences between BD patients and healthy people brains. Those differences are related to volume reduction of the gray and white matter, the decrease in cortical thickness in the prefrontal region, and also in the amygdala and hippocampus. Furthermore, there are also connectivity abnormalities in the left orbitofrontal cortex and left ventrolateral prefrontal cortex, which were detected from functional MRI [110, 111, 7] and spontaneous local activity. In addition, widespread local functional abnormalities have been detected in the anterior cingulate cortex, thalamus, amygdala, hippocampus, and cerebellum [112, 113]. Other studies have also shown the existence of variations in the resting-state functional connectivity (RSFC) in the default mode network (DMN), the sensorimotor, frontoparietal, and also the salience network [114, 115, 116, 117, 118, 119, 109].

In the study of Wang et al. [109] rs-fMRI was used to detect radiomic features that are highly correlated with BD. Before the extraction process, image preprocessing methods were employed to increase the image quality of rs-fMRIs. The preprocessing procedure based on the MATLAB toolbox Data Processing Assistant for Resting-State fMRI (DPARSF) [120] and Statistical Parametric Mapping . Data preprocessing was implemented in several steps. Initially, the first 10 time points were removed. The

[1] https://fcon_1000.projects.nitrc.org/indi/cmi_health_brain_network/

middle slice was used as the reference frame for applying slice timing correction. With the regression of six motion signals, head motion correction was achieved. In addition, the T1-weighted data were logged to the functional images, on which motion correction was performed. It must be noted as this point, that the T1-weighted images are used only for preprocessing purposes and not for feature extraction or classification directly. These images are segmented into gray, white matter, and cerebrospinal fluid, utilizing the DARTEL algorithm. The functional data were mapped to the Montreal Neurological Institute (MNI) space with the normalization variables derived by segmentation, along with a resampling process to a defined size of voxel of $3\times3\times3$ mm^3. Nuisance covariates, comprising Friston 24 parameters of motion [121], cerebrospinal fluid and white matter signals, were mitigated. In addition, a band-pass filter (0.01–0.10 Hz) was employed in order to reduce high-frequency physiological noises, such as respiration, ensuring the quality of the images.

After the preprocessing, 7018 radiomic features were derived and can be categorized into four types: Voxel-Mirrored Homotopic Connectivity (VMHC), Mean Amplitude of Low-Frequency Fluctuation (mALFF), Mean Regional Homogeneity (mReHo), RSFC. The calculation of those radiomics is done as follows for each type of feature:

VMHC: The Voxel-Mirrored Homotopic Connectivity shows the functional connection between the two hemispheres of the brain for the mirrored voxels [122]. The maps were calculated with the Automated Anatomical Labeling (AAL) atlas for each ROI (116).

mALFF: The ALFF detects the strength of unconscious variations in the brain [123]. For each voxel, the ALFF map was computed, and the mALFF map for each ROI was created by normalizing these values to the whole brain mean. Also, for this type of feature for the identification of ROIs, the AAL was used as well.

mReHo: The Regional Homogeneity (ReHo), can reflect the neural activity's temporal homogeneity in neighboring voxels [124] and can be represented in the form of a map. The mean ReHo values were calculated by averaging the ReHo values for 116 ROIs that were detected according to the AAL atlas.

RSFC: In contrast with ReHo, the Resting-State Functional Connectivity reflects the temporal correlation of neural activity between different regions of the brain. Using the AAL atlas, the images were subtracted in 116 ROIs, and the average time series for each region was derived by calculating the average of the time signals of the entity of voxels in that area.

The total number of extracted features was 7018 divided as 116 for each of the mReHo, mALFF and VMHC categories and 6670 for the RSFC category.

However, the number of the extracted radiomics should be decreased in order to keep only the most important ones. For this reason, the authors used the Mann–Whitney U test which reduced the features to 1165. The features between patients with BD and the HC studies for statistical differences and those with p-value < 0.1 were kept for further analysis. Also, the features studied in terms of correlation. If the correlation coefficients of both features were bigger than 0.65, the one with the larger mean absolute correlation was removed. This technique reduced the number of radiomics to 248. Furthermore, LASSO regression was used in order for the most predictive features to be selected resulting in the reduction of the features to 65. The reduction that the authors achieved equals 99.07%. More specifically, the 65 features are divided into one mReHo, seven mALFF, three VMHC and 54 RSFC. The SVM model used for classifying these features achieved 87.3% and 0.919 and 80.5% and 0.838 accuracy and AUC on training and validation datasets, respectively. The findings of this paper show that the differences in the functional local activity can be used to identify patients with BD with high accuracy. In addition, the left superior temporal pole associated with the most connections (RSFC). The networks as well as the brain regions that the 65 radiomic features were extracted from are shown in Table 6. Additionally, details on key findings and evaluation performance metrics for BD are included in Tables 7 and 8, respectively.

Table 6: Networks and brain regions of the extracted radiomics by Wang et al. [109]

Network	Brain regions
DMN	Angular and Parahippocampal Gyrus, Precuneus, Medial Prefrontal and Anterior Cingulate Cortex
Affective Network	Amygdala, Temporal Poles, Pallidum, Insula
Visual Network	Occipital Regions (Superior, Middle, Inferior), Calcarine
Sensorimotor Network	Precentral Gyrus, Supplementary Motor Areas, Postcentral Gyrus
Cerebellar Network	Cerebellum Crus 1 & 2, Lobules 7b & 9, Vermis

Table 7: Analysis on Bipolar and Related Disorders

Work	Disorder	Selected features	Radiomics	Important Regions	Key Findings
[109]	BD	65	mReHo, mALFF, RSFC, VMHC	Precuneus, anterior cingulate cortex, parahippocampal gyrus, amygdala, insula, angular gyrus, occipital regions and medial prefrontal cortex	RSFC features from left superior temporal pole had an important role

Table 8: Experimental validation on Bipolar and Related Disorders

Work	Disorder	Performance	Data	Participants	CV
[109]	BD	Training/Validation: ACC=87.30%/80.5%, AUC=0.919/0.838	Private	90 BD II and 117 HCs.	10-fold cross-validation

The study addressing bipolar disorder by Wang et al. [109] used a private dataset, selecting 65 features derived from multiple radiomic measures, including mReHo, mALFF, RSFC, and VMHC. While the training performance was strong, a notable drop on the validation set suggests some degree of overfitting, despite the use of 10-fold cross-validation. Although the original dataset exhibited a class imbalance, the authors randomly split the subjects into two sets (primary and validation cohorts), ensuring balanced class proportions in each to reduce bias. The left superior temporal pole was identified as a key discriminative region. This structure plays a critical role in processing emotional tone, integrating sensory and emotional information, and supporting social cognition. Additional regions highlighted included the anterior cingulate cortex, amygdala, insula, medial prefrontal cortex, and parahippocampal gyrus, all of which contribute to affect regulation, salience detection, and autobiographical memory.

4.3. Depressive Disorders

4.3.1. Major Depressive Disorder (MDD) & Subthreshold Depression (StD)

Major Depressive Disorder (MDD) and Subthreshold Depression (StD) (or Subclinical / Subsyndromal Depression) are widespread and debilitating mental health disorders that significantly affect individuals. MDD is one of the primary contributors to disabilities globally, while StD often seen as a precursor to MDD, poses a significant risk of progression if left untreated [28]. MDD and StD diagnosis is a challenging process, as it is based on the self-report of symptoms, clinical interviews, and the experience of the psychiatrist. However, a diagnosis based exclusively on experience can lead to misdiagnosis and incorrect treatment. In addition, the neurological basis remains unknown and there is a lack of robust biomarkers [28, 125, 126]. MDD is defined mainly by an ongoing state of sadness combined with a reduced interest in activities, while patients with StD meet some of the symptoms of MDD but with less intensity. In the following paragraphs, papers will be presented aimed at identifying crucial radiomic features for differentiating patients with MDD, StD and HCs. Each of the related works followed a different approach that focused on structural or functional abnormalities of the brain, since MDD / STD are complex disorders which can have their basis in the different structures of specific regions of the brain or the malfunction of the regions, compared to HCs. The papers of this section aimed to diagnose MDD and StD. Key findings and evaluation performance metrics for Depressive disorders are included in Tables 11 and 12, respectively.

The work [126] by Sun et al. focused on creating an approach to differentiate MDD patients from HC people. In this approach, rs-fMRI and sMRI images were used. The MATLAB toolbox Data Processing Assistant for Resting-State fMRI DPARSF was used for standard data preprocessing [120]. This process included steps such as removing time points, slice-timing correction, segmentation, realignment, normalization, smoothing, and filtering. The extracted features were 7018. More specifically, from the rs-fMRI images three categories of features were identified: RSFC (6660), ALFF (116), and ReHo (116), and from the sMRI images, the evaluation of Gray Matter Volume (GMV) (116) was performed using Voxel-based Morphometry (VBM), a tool that can detect variations in the volume. In this work for ROI segmentation, the AAL used 116 regions as a result.

The selection process of the most important features consisted of multiple steps. The first step was the Two-Nested Leave-One-Out Cross-Validation (LOOCV) [127] algorithm to be performed for each of the feature categories. During the first loop (outer) of

the LOOCV each subject was included in the testing set, while the others were included in the training set. In addition, on the training set the second loop (inner) of the LOOCV was employed towards identifying the optimal parameters for the feature selection. Also, the statistical two-sided Student's t-test was used retaining the features which had p-values <0.1. In combination with the LOOCV also the LASSO logistic model was used. Furthermore, for the RSFC, since they had the highest dimensionality, in order for the total number to be reduced, additional steps were taken in order for the most relevant features to be identified by detecting the highest densely connected brain regions. In total, the number of features was reduced to 30 (RSFC: 9, ALFF: 8, ReHo: 5, and GMV: 8).

The SVM model was used to classify the selected features. The authors used different combinations of the feature categories. The optimal reported performance was an AUC of 0.916 and accuracy of 84.8% for the Validation Cohort (29 MDD vs. 52 HC) and AUC:0.919, accuracy: 87.1% on the primary cohort (140 MDD vs. 138 HC) was achieved using the GMV, RSFC and ALFF features, while the ReHo features show that although they provide some useful information, they are not so critical. Table 9 shows the selected radiomic features for each category as well as the identified region.

Table 9: Brain regions results in the work [126] by Sun et al.

Region	**Name**	**Radiomics Category**
Left Angular Gyrus (Default Mode Network)	Angular_L	ALFF
Left Precuneus (Default Mode Network)	Precuneus_L	ALFF
Right Precuneus (Default Mode Network)	Precuneus_R	ALFF
Right Pallidum (Affective Network)	Pallidum_R	ALFF
Right Temporal Pole (Superior Temporal Gyrus) (Affective Network)	Temporal_Pole_Sup_R	ALFF
Left Temporal Pole (Middle Temporal Gyrus) (Affective Network)	Temporal_Pole_Mid_L	ALFF
Left Cerebellum Crus 1 (Cerebellum)	Cerebellum_Crus1_L	ALFF
Left Inferior Frontal Gyrus (Orbital Part) (FCN)	Frontal_Inf_Orb_L	ALFF
Right Posterior Cingulate Gyrus (Default Mode Network)	Cingulum_Post_R	GMV
Left Cerebellum Crus 1 (Cerebellum)	Cerebellum_Crus1_L	GMV
Right Cerebellum 10 (Cerebellum)	Cerebellum_10_R	GMV
Vermis 9 (Cerebellum)	Vermis_9	GMV
Right Calcarine Cortex (Visual Network)	Calcarine_R	GMV
Left Inferior Occipital Gyrus (Visual Network)	Occipital_Inf_L	GMV
Left Olfactory Cortex (Sensorimotor Network)	Olfactory_L	GMV
Right Heschl's Gyrus (Sensorimotor Network)	Heschl_R	GMV
Left Angular Gyrus - Right Angular Gyrus (DMN - DMN)	Angular_L - Angular_R	RSFC
Left Thalamus - Right Temporal Pole (Middle Temporal Gyrus) (DMN - AN)	Thalamus_L - Temporal_Pole_Mid_R	RSFC
Right Angular Gyrus - Right Cerebellum Crus 3 (DMN - Cerebellum)	Angular_R - Cerebellum_3_R	RSFC
Right Thalamus - Right Cerebellum Crus 6 (DMN - Cerebellum)	Thalamus_R - Cerebellum_6_R	RSFC
Left Thalamus - Left Inferior Frontal Gyrus (Orbital Part) (DMN - FCN)	Thalamus_L - Frontal_Inf_Orb_L	RSFC

Continued on next page

Region	Name	Radiomics Category
Right Amygdala - Right Temporal Pole (Middle Temporal Gyrus) (AN - AN)	Amygdala_R - Temporal_Pole_Mid_R	RSFC
Right Cerebellum Crus 6 - Right Inferior Temporal Gyrus (Cerebellum - AN)	Cerebellum_6_R - Temporal_Inf_R	RSFC
Right Cerebellum Crus 6 - Right Cerebellum Crus 9 (Cerebellum - Cerebellum)	Cerebellum_6_R - Cerebellum_9_R	RSFC
Left Inferior Frontal Gyrus (Orbital Part) - Right Inferior Frontal Gyrus (Opercular Part) (FCN - FCN)	Frontal_Inf_Orb_L - Frontal_Inf_Oper_R	RSFC

Ma et al. [125] aimed to identify the characteristics that differentiate MDD and StD patients from HC using three-dimensional weighted T1 imaging (3D-T1WI) and diffusion tensor imaging (DTI) data. The ComBat technique used [128, 129] to harmonize radiomic features and to overall improve their quality and stability. For the preprocessing of the images, Surface-Based Morphometry (SBM) and VBM analyses of gray matter were performed, as well as diffusion property calculation for white matter. The extracted features are identified in three categories:

- **SBM radiomic features:** Features that indicate the shape or, in general, the surface-related variation of gray matter.
- **VBM radiomic features:** Features that indicate abnormalities in the volume or gray matter's density.
- **DTI radiomic features:** Quantified features related to the diffusion of white matter.

A total of 13,150 radiomic features were extracted. More specifically, 2338 SBM features, 10,044 VBM features, and 768 DTI features were detected. Furthermore, the next step was to select the most relevant features that were highly correlated with the disorder. For this reason, the extracted features were further harmonized using ComBat in order for the scanner variability to be minimized, and also Recursive Feature Elimination (RFE) and ANOVA were used for the reduction of the high-dimensionality and identification of the significant features. This process reduced the total number of radiomic features to 63. The selected features were used in an SVM model using a Radial Basis Function (RBF) kernel. The performance metrics for each classification were as follows:

- **MDD vs. HC:** AUC: 0.928, Sensitivity: 89.2%, Specificity: 93.2%, Accuracy: 90.5%, Precision: 93%, Recall: 92%
- **MDD vs. StD:** AUC: 0.821, Sensitivity: 73%, Specificity: 85%, Accuracy: 80.8%, Precision: 85%, Recall: 73%
- **StD vs. HC:** AUC: 0.836, Sensitivity: 82.4%, Specificity: 77.1%, Accuracy: 79.7%, Precision: 84%, Recall: 78%

The results showed that highly correlated features were extracted to differentiate between MDD, StD, and HC from the middle and superior temporal gyrus, bilateral medial orbitofrontal cortex and hippocampus, left posterior and right anterior cingulate, right cerebellar peduncle, left corpus callosum body, and anterior limb of the internal capsule. In addition, the research showed that the features of the cuneiform lobe and cerebellum had an important role.

In addition, Zhang et al. [130] sought radiomic features for the same separation between MDD, StD, and HC. At this point, it is worth noting that in the paper the subthreshold depression (StD) is called subclinical depression. In the case of this paper, rs-fMRI images were used to extract radiomic data, while sMRI data (high-resolution T1-weighted) were used as part of the preprocessing of the main data (rs-fMRI). For this process, DPARSF was used in the rs-fMRI data that discarded volumes to decrease the instability created during the acquisition of the MRI. In addition, slice timing correction and realignment were performed to remove artifacts (head movements, breathing, and heartbeats). The next step was the registration of the sMRI, which was acquired following the MPRAGE sequence, in the MNI space using the DARTEL algorithm [131] for segmentation and spatial normalization. The authors used the MNI space to standardize the brain images, enabling consistent alignment among the participants and performed ROI-based analysis. This is a common process that allows the integration of functional data with ROIs identified from the AAL atlas. Furthermore, preprocessing steps included nuisance covariate regression, functional image normalization, spatial smoothing, and temporal filtering to improve the quality of fMRI data. In addition, the Friston 24-parameter model [121] was used to regress out nuisance covariates, such as head motion effects. Data voxel size resamples to $3 \times 3 \times 3$ mm^3 and spatial smoothing used for noise reduction. Additional smoothing and filtering steps were performed before the calculation of specific radiomic features such as ReHo and ALFF.

After the preprocessing, three types of features were extracted: regional functional activity features (ALFF, fALFF, ReHo), RSFC features, and Global network topological features (node degree (Deg), betweenness centrality (BC) and nodal efficiency (Eff)). The total number of extracted radiomic features was 7366: 348 regional functional activity features, 6670 RSFC features, and 348 global network topological features. More specifically, the regional functional activity features capture spontaneous neural

activity within individual brain regions, the RSFC features reflect the temporal correlation between the activity of spatially distant brain regions, and the global network topological features describe the organization and efficiency of brain networks. Once again, ANOVA, RFE and LOOCV, SVM were used for the identification and classification of the most important features. Those features were one ALFF, two ReHo, one BCE, one Eff, two Deg, and 41 RSFC, 48 features in total. The performance of the classification was the following:

- **MDD vs. HC:** Sensitivity: 94.4%, Specificity: 93.94%, Accuracy: 94.2%
- **MDD vs. StD:** Sensitivity: 100%, Specificity: 92.31%, Accuracy: 96.77%
- **StD vs. HC:** Sensitivity: 61.54%, Specificity: 93.94%, Accuracy: 80%

The most crucial radiomic features detected in the networks of the Default Mode Network (DMN), Frontoparietal Network (FPN), discriminative regions, Affective Network (AN), Visual Network (VN) and Cerebellum. More specifically, the brain regions were Precuneus, medial frontal gyrus, hippocampus, and inferior frontal gyrus (IFG). In addition, the dorsolateral prefrontal cortex (DLPFC), superior frontal gyrus, superior parietal gyrus, Amygdala and caudate. Furthermore, important regions for radiomic features were the Lingual gyrus, occipital gyrus, and fusiform gyrus. The most significant features among all the classification tasks were the RSFC.

An additional work aimed to identify the crucial features between MDD and StD patients and HCs was the study of Ma et al. [28]. The authors of this work used 3D-T1WI and DTI data for the analysis of the gray matter morphometry and the white matter diffusion properties. For the preprocessing of the 3D-T1WI data, the software suite pipeline FreeSurfer was used. The steps included in this process were the conversion from DICOM to NIFTI format of the images, motion correction, intensity normalization, skull stripping ad smoothing, surface reconstruction, and labeling regions using the Desikan-Killiany-Tourville (DKT) atlas (124 labels) [132]. Regarding preprocessing of the DTI data, the software library FMRIB [133] was employed to correct head motion and eddy current, segmentation and tensor model fitting. In addition, in this study, the DTI data was used to develop a template tailored to the study through Diffusion Tensor Imaging Toolkit. This template was then registered with the Johns Hopkins University International Consortium of Brain Mapping (JHU-ICBM-DTI) atlas, allowing the identification and labeling of 48 regions of white matter [134]. Fractional anisotropy maps were generated to measure the directional coherence of water diffusion, and quality control was conducted by examining the direction encoding color and the fractional anisotropy.

The labeled brain regions were then processed using Mindboggle [135], an open source brain morphometry software. The feature extraction process was automated. The extracted features were the gray matter morphometry features of the T1WI and diffusion properties of the DTI data. In addition, statistical metrics from both types of images, such as mean, standard deviation, and kurtosis, were extracted. In total 3030 features were extracted, 2262 shape-related features, and 768 features from DTI. The next step in the approach of the paper was the feature selection. In total 25 features were selected as the most important: 10 features for differentiating MDD vs. HC, eight features for differentiating StD vs. HC. and seven features for differentiating MDD vs. StD. These features were cortical thickness (mean) in regions such as the medial orbitofrontal cortex, cuneus, anterior cingulate, and hippocampus, mean curvature (skew and kurtosis) in the superior frontal, superior temporal, medial orbitofrontal cortex, and amygdala, convexity (mean, skew, and kurtosis) in the superior temporal gyrus, cerebellar vermis and medial orbitofrontal cortex, geodesic depth (mean) in the hippocampus, and travel depth (skew) in the medial orbitofrontal cortex. Additionally, diffusion properties such as radial diffusivity, mean diffusivity, axial diffusivity, and fractional anisotropy along with their statistical metrics, were included for white matter regions. In the following Table 10 the mapping of the selected features is presented:

Table 10: Selected radiomic features by Ma et al. in the work [28]

Region	**Name**	**Radiomics Category**
Right Middle Temporal Gyrus	Convexity	Kurtosis
Right Superior Frontal Gyrus	Mean Curvature	Skew
Left Cuneus	Cortical Thickness	Mean
Left Hippocampus	Geodesic Depth	Mean
Left Medial Orbitofrontal Cortex	Cortical Thickness	Mean
Right Superior Temporal Gyrus	Mean Curvature	Kurtosis

Continued on next page

Region	Name	Radiomics Category
Right Anterior Cingulate Cortex	Mean Curvature	Kurtosis
Left Medial Orbitofrontal Cortex	Travel Depth	Skew
Right Anterior Cingulate Cortex	Cortical Thickness	Mean
Left Medial Orbitofrontal Cortex	Convexity	Skew
Right Superior Temporal Gyrus	Convexity	Kurtosis
Right Middle Temporal Gyrus	Cortical Thickness	Skew
Left Anterior Cingulate Cortex	Cortical Thickness	Kurtosis
Left Amygdala	Mean Curvature	Kurtosis
Left Cuneus	Cortical Thickness	Mean
Left Medial Orbitofrontal Cortex	Mean Curvature	Skew
Left Cerebellar Vermis	Convexity	Mean
Left Hippocampus	Mean Curvature	Skew
Left Medial Orbitofrontal Cortex	Cortical Thickness	Mean
Right Superior Frontal Gyrus	Mean Curvature	Kurtosis
Right Superior Temporal Gyrus	Mean Curvature	Kurtosis
Left Middle Temporal Gyrus	Cortical Thickness	Skew
Right Hippocampus	Mean Curvature	Skew
Right Anterior Cingulate Cortex	Cortical Thickness	Mean
Left Cuneus	Cortical Thickness	Mean

The features selected using the Boruta package [136] in the R software. Using Boruta were created shadow features (random copies of the original features), which were included in the dataset that the Random Forest classifier (RF) trained to identify the importance of the features. The criteria for the importance of each feature were how much each one contributes to improving the model's accuracy, and each feature should be more important than its shadow in order to be kept in the training dataset, this comparison was performed by the Boruta package. The most crucial features had significantly higher importance scores than the shadow features. The classification of the selected features for each category is performed by the RF with a 10-fold cross-validation. The scores for each of the cases were as follows:

- **MDD vs. HC:** AUC: 0.93, Sensitivity: 84.21%, Specificity: 88.89%, Accuracy: 86.75%
- **MDD vs. StD:** AUC: 0.66, Sensitivity: 54.55%, Specificity: 63.16%, Accuracy: 59.15%
- **StD vs. HC:** AUC: 0.69, Sensitivity: 57.58%, Specificity: 80%, Accuracy: 70.51%

Table 11: Analysis on Depressive Disorders

Work	Disorder	Selected features	Radiomics	Important Regions	Key Findings
[126]	MDD	30	ALFF, RSFC, GMV	Default mode network, prefrontal cortex, affective network	GMV, RSFC, and ALFF features were had high importance, while the ReHo features provided less useful information. The most important features detected in angular, precuneus, hippocampus, cingulum, prefrontal cortex, pallidum, temporal pole, amygdala, cerebellum
[125]	MDD & StD	63	SBM, VBM, DTI	GM, WM, hippocampus, anterior-posterior cingulate,	Features from the cuneiform lobe and cerebellum played a crucial role
[130]	MDD & StD	48	ALFF, fALFF, ReHo, RSFC, global network topology	Precuneus, medial frontal gyrus, hippocampus, inferior frontal gyrus, amygdala, DLPFC, superior parietal gyrus	Lingual gyrus, occipital gyrus, fusiform gyrus identified as important regions. The RSFC was the feature with the highest discriminative value for all the classifications
[28]	MDD & StD	25	Convexity kurtosis, cortical thickness skew, geodesic depth mean	Middle temporal gyrus, superior frontal gyrus, anterior cingulate, cerebellar vermis	Right superior, right anterior cingulate, left cuneus, middle temporal regions, cerebellar vermis, right superior frontal cortex, left medial orbitofrontal cortex

Table 12: Experimental validation on Depressive Disorders

Work	Disorder	Performance	Data	Participants	CV
[126]	MDD	Primary cohort/Validation set: ACC=87.1%/84.8%, AUC=0.919/0.916	Private	140 MDD and 138 HCs.	LOOCV
[125]	MDD & StD	MDD vs. HC: AUC=0.928, SEN=89.2%, SPE=93.2%, ACC=90.5%, PREC=93%, REC=92%; MDD vs. StD: AUC=0.821, SEN=73%, SPE=85%, ACC=80.8%, PREC=85%, REC=73%; StD vs. HC: AUC=0.836, SEN=82.4%, SPE=77.1%, ACC=79.7%, PREC=84%, REC=78%	Private	51 MDD, 50 StD and 46 HCs.	LOOCV
[130]	MDD & StD	MDD vs. StD: ACC=96.77%, SEN=100%, SPE=92.31%; MDD vs. HC: ACC=94.2%, SEN=94.44%, SPE=93.94%; StD vs. HC: ACC=80%, SEN=61.54%, SPE=93.94%	Private	36 MDD, 26 StD and 33 HCs.	LOOCV, 10-fold cross-validation

Continued on next page

Work	Disorder	Performance	Data	Participants	CV
[28]	MDD & StD	MDD vs. StD: ACC=59.15%, AUC=0.66; MDD vs. HC: ACC=86.75%, AUC=0.93; StD vs. HC: ACC=70.51%, AUC=0.69	Private	43 MDD, 49 Std and 50 HCs.	10-fold cross-validation

The analysis of the depressive disorders studies reveals important differences in performance and for MDD and related conditions. Sun et al. [126] reports solid and consistent performance across both their primary cohort and validation set, based on a large sample of 140 MDD and 138 HCs using 30 features. This consistency across datasets suggests good generalization ability without obvious overfitting. Ma et al. [125] achieved the best results for MDD vs. HC classification, while also addressing multiple classification tasks. Their use of LOOCV on a moderately sized but balanced sample (51 MDD, 50 StD, 46 HCs) supports the robustness of their findings. Furthermore, the authors implemented DeLong tests compared AUCs, and permutation tests assessed generalization. Zhang et al. [130] demonstrates extremely high performance in MDD vs. StD (ACC=96.77%, SEN=100%) and very high accuracy for MDD vs HC (94.2%), but the combination of LOOCV and 10-fold cross-validation on a relatively small dataset raises some concerns about potential overfitting and overly optimistic results, particularly given the perfect sensitivity reported. Ma et al. [28] shows a not so high overall performance, particularly in the MDD vs StD comparison, even though the MDD vs. HC classification was relatively better. Overall, Ma et al. [125] provides the most comprehensive and balanced performance, especially for distinguishing MDD from HC, while Sun et al. [126] shows commendable stability across independent cohorts. In contrast, despite high metrics, Zhang et al. [130] may be subject to overfitting risks due to small sample size and overly high sensitivity scores, and Ma et al. [28] struggles with generalization and lower discriminative power. Consistently important regions across studies include the amygdala, hippocampus, prefrontal cortex, ACC, and precuneus which are areas involved in emotion regulation, memory, and cognitive control.

4.4. Neurodevelopmental Disorders

4.4.1. Attention Deficit Hyperactivity Disorder (ADHD)

Attention Deficit Hyperactivity Disorder (ADHD) is an ordinary neurodevelopmental disorder defined by age-inappropriate inattention, hyperactivity, and impulsivity [137]. Globally, it influences an estimated 4% of adults and 5–10% of children, significantly affecting social, cognitive, educational, and emotional functioning [138, 139]. Related works in neuroimaging have revealed structural and functional defects in individuals with ADHD, including reduced brain volume, altered cortical morphometry, and disrupted white matter integrity. Key affected regions encompass the prefrontal cortex, which governs attention and decision-making, the basal ganglia, which regulate movement and behavior, and the cerebellum, which contributes to motor coordination and cognitive processes [139]. Despite these insights, ADHD diagnosis relies on behavioral assessments, which have a sensitivity of 70– 90% but often result in false-positive diagnoses due to symptom overlap with other psychiatric disorders [138, 137]. Beyond these methods, no biological or robust diagnostic test currently exists for the diagnosis of ADHD.

In the research of Shi et al. [138] T1-weighted sMRI images used from the ADHD-200 Consortium to identify robust biomarkers towards diagnosing of ADHD and also for its subtypes. The authors aimed to classify Typically Developing controls (TDCs) and children with ADHD, and also subjects with ADHD with different symptoms and severity reflecting in this way the clinical heterogeneity of the disorder. Initially, for the preprocessing of the images, the NIfTI data was reoriented and cropped using DCM2NII, and the quality of the image was assessed based on the absence of motion artifacts, the full coverage of brain tissue, and proper head orientation. Images that failed these quality criteria were excluded. Using the CAT12 toolbox, image reconstruction, correction, registration, and segmentation were performed. Key parameters included the Dartel spatial registration template, normalized voxel size, separate resampling for each hemisphere, and a smoothing filter size of full width at half maximum (FWHM) (FreeSurfer). The process produced standardized gray matter (GM), white matter (WM), and T1-weighted images with scalp stripping. Additional, smoothing and resampling applied to ensure the data conformed to a normal distribution. The extracted features which obtained can be divided into three types. Those types are the surface values, the volumetric measurements, and the radiomic features. Surface values (cortical thickness, gyrification, fractal dimension and sulcal depth) were derived from the Desikan–Killiany (DK) atlas after alignment to the MNI152 template using the CAT12 toolbox [140, 103] . Volumetric measurements of gray and white matter were obtained from 116 brain regions defined by the AAL atlas via DPABI software [141]. Furthermore, 209 radiomic features (first-order and texture features from GLCM, GLRLM, and NIDM) per AAL region (totaling 24244 radiomics) were extracted using IBEX software [142, 143] from the T1 images. The statistical analysis showed differences in brain features across all the participant groups. The Lilliefors and Bartlett tests confirmed normality and variance assumptions for certain features, which guided the use of ANOVA and Kruskal-Wallis tests for comparing group differences. Bonferroni correction was performed to control for multiple comparisons, with a corrected $P < .05$ considered significant. Spearman's rank correlation indicated varying connections among brain features and age in TDCs and ADHD patients, with a significant difference confirmed by a two-sample t-test ($P < 0.05$). Lasso algorithm was employed for feature selection to identify clinical factors, GM and WM volumes, surface values, and radiomic features as key variables. The latter features were subsequently utilized for training an SVM

classifier with an RBF kernel. The hybrid model, combining all three feature categories, achieved an accuracy score of 82.50% for ADHD vs. TDC. In comparison, the radiomic model alone achieved an accuracy score of 76.25% for ADHD vs. TDC and 84.3% for the classification of ADHD subtypes. After applying Bonferroni correction, 142 radiomic features (for the three groups) from 18 brain areas showed significant differences across the three participant groups. The most discriminative radiomic features were found in regions like left supramarginal, vermis, bilateral temporal lobe, insula, left olfactory lobe, right calcarine, right supplementary motor area, left occipital lobe, bilateral amygdala, right lingual lobe, left caudate, right frontal lobe, left paracentral lobule, gyrus, left hippocampus, and bilateral cerebellum. Specifically, the '30 percentile' and '0.25 quantile' of the right Heschl's gyrus, and the '10 percentile' of the left superior temporal gyrus displayed significant differences between all three groups. In addition to this, significant differences were observed between TDCs and ADHD patients, with ADHD patients exhibiting altered patterns of cortical thickness and radiomic features in areas like the 'linsula' (a surface value). Notably, 23 radiomic features were found to differentiate ADHD subtypes, with differences in brain areas such as the precentral gyrus, calcarine cortex, entorhinal cortex, posterior cingulate gyrus, and the angular gyrus, while nine radiomics showed important differences for the task ADHD vs. TDC. In terms of brain-age associations, an additional 30 radiomic features indicated notable differences among ADHD patients and TDCs, with ADHD patients exhibiting differences in both GM and WM volumes and cortical thickness Radiomic features outperformed traditional features in diagnosing ADHD and its subtypes. The hybrid model combining radiomics, surface values, GM volume, and clinical data improved overall accuracy but did not enhance subtype classification.

Furthermore, in the work of Liu et al. [137] resting-state functional magnetic resonance imaging (rs-fMRI) data was used to classify ADHD and HC children. The data obtained from the ADHD-200 consortium and the preprocessed data acquired from the R-fMRI Maps Project. The preprocessing performed with the Data Processing Assistant for Resting-State fMRI DPARSF, which relied on Statistical Parametric Mapping SPM. The process includes steps such as slice timing, correction of head motion, removal of white matter signal and cerebrospinal fluid, normalization to the standard MNI space, and resampling to $3\times3\times3$ mm^3. In addition, filtering to 0.01 - 0.1 Hz was applied. The metrics used in this study were ALFF, ReHo, VMHC, and Degree Centrality (DC). The ALFF measures the mean amplitude of the Fourier-transformed voxel time series within a specified range of frequency, while the ReHo assesses the similarity between the time series of a specified voxel and its closest neighbors. VMHC metric measures the Pearson correlation of Blood-Oxygen-Level-Dependent (BOLD) signal time series between a voxel and its mirrored and the DC reflects the functional connectivity intensity for each voxel and based on that the calculated functional connectivity (FC) calculated. Using the Pyradiomics [94] radiomics extracted from four metrics using the AAL atlas [144], resulting in 43152 features across 116 brain regions (93 features $\times$ 116 regions $\times$ 4 metrics). Specifically, extracted features were: five NGTDM, 14 GLDM, 16 GLRLM, 16 GLSZM, 24 GLCM, and 18 first-order features. Furthermore, the calculation of the p-value based on the two-sample two-sided t-test was performed, considering that features with p-values lower than 0.05 were more important for the separation of the ADHD subject and the HCs. Also, using the DPABI MATLAB-based toolbox, 116 mean signal (the average value of all voxel values within a specific brain area) features were extracted from each of the four metrics totaling 464 features across brain regions, totaling 43616 features. Unlike studies that focus on specific brain regions, the present study adopted a whole-brain approach, extracting features from all regions defined by the AAL atlas. This approach contributed to the high total summary of features. In order for the dimensionality of the radiomic features to be reduced, the most significant features were selected. Initially, the authors assessed whether each feature followed a normal distribution. For features that were normally distributed, a two-sample t-test was performed towards examining the difference between ADHD and HC groups. Moreover, the Mann–Whitney U test was applied to features that were not normally distributed. Features showing in-group variations were preserved ($p < 0.1$). Additionally, features with intense similarity (Spearman's rank coefficient > 0.8) were removed, retaining those with the lower p-values. To identify the most relevant features for classification, a sequential forward selection (SFS) method with 10-fold cross-validation was employed. The SFS algorithm first used all the features for training an SVM model with an RBF kernel, evaluating classification loss. Features were sequentially added, and if they improved classification performance, they were included in the final set of features. The significance of 19 features was determined using a linear kernel function. Both the radiomics and the mean signal features underwent the same process. The model reported an accuracy of 77.0% and an AUC of 0.797 in the test set. The most significant features were five ALFF, nine ReHo, three VMHC and two DC. As observed, all belong to the radiomics category and not the mean signal features category which their performance was 59.5% and 0.618 AUC. Finally, although the selected radiomics acquired from several brain areas such as the frontal, temporal and occipital cortex, and the limp system, but the majority and the most important of them identified in the cerebellum.

In addition, Sun et al. [139] focused on the fusion of T1-weighted images and diffusion-tensor images (DTI) aiming to classify HC and ADHD children, and also children with ADHD subtypes (inattentive and combined inattentive and hyperactive). The preprocessing of the T1-weighted images performed with the "recon-all" pipeline in FreeSurfer. The Desikan-Killiany-Tourville atlas was also used for the segmentation [132] and the Advanced Normalization Tools for the labeled brain generation [145] with the "antsCorticalThickness" pipeline. Regarding the preprocessing steps for the DTI data, eddy-current and head motion correction were performed, along with the removal of non-brain tissues and tensor model fitting. The latter process was implemented by using the FMRIB SoftwareLibrary. Using the Johns Hopkins University International Consortium of Brain Mapping Diffusion Tensor Imaging (JHU-ICBM-DTI-81) atlas, features from the white matter regions were identified. More specifically, 768 features including kurtosis, skew, standard deviation and mean identified. Those features were extracted after the calculation of several maps e.g., fractional anisotropy, mean, axial and radial diffusivity. Regarding the T1-weighted images, 2338 shape features from the gray

matter regions. For the feature extraction process the Mindboggle [135] used. The total extracted features from both types of data were 3106. For the reduction of the dimensionality of the extracted features, a random forest-based algorithm for features selection performed with R package, "Boruta" [136]. Each feature is categorized as relevant or irrelevant. The RF classifier incorporated a workflow that included an all-relevant feature selection procedure within a repeated k-fold (k = 10) cross-validation framework [146]. This workflow is applied using the package "caret" in R. In each iteration the features selected from various subsets, acquired with cross-validation. If a feature is selected in many iterations, then considered as a relevant selection. For validation purposes of the features' significance, 1000 random datasets were generated and the same process was repeated. The selection frequencies were analyzed with a binomial distribution model. Features that showed higher selection frequencies in the original dataset, as determined by Holm-Bonferroni corrected p-values (< 0.05), were classified as relevant and used for the classification [147]. The achieved classification accuracy for ADHD vs. HCs was 73.7%, while the accuracy score for discriminate the ADHD subtypes was 80.1%. The shape features (gray matter regions) that are shown as significant indicators in the first classification (ADHD vs. HC) were obtained from the left temporal lobe, bilateral cuneus, and regions around the left central sulcus. In addition,features from the default mode network and insular cortex could be considered as important indicators for the second classification task (ADHD subtypes). More specifically, the three most significant features discriminating ADHD and the HCs were the convexity skew, mean local thickness, kurtosis mean curvature, skew travel depth, skew mean curvature from the left superior temporal sulcus, right cuneus, left precentral, left superior temporal and left precentral, respectively. Regarding the discriminating between the subtypes, the features were mean, skew and kurtosis from the left circular sulcus, left posterior cingulate and left sylvian fissure.

4.4.2. Autism Spectrum Disorder (ASD)

ASD is a complex neurodevelopmental disorder with a wide spectrum of severity and manifestations. The disorder typically arises in early childhood, often before the age of three [148], and it involves difficulties in social interaction, communication, and engaging in repetitive behaviors. The reasons behind ASD are still not entirely comprehended but are considered to involve a combination of genetic, environmental, and developmental factors. Despite its high prevalence, the ASD treatment's development has been slow, largely due to the lack of objective, quantifiable diagnostic tools and a deep understanding of its underlying neurobiological mechanisms. Studies have identified several brain regions implicated in ASD, including the hippocampus, amygdala, cerebellum, and cerebral cortex, with abnormalities observed in their structure, volume, and connectivity. However, inconsistencies in findings across studies have hindered the identification of reliable biomarkers for the disorder [34].

Research [148] by Chaddad et al. investigates structural abnormalities between individuals with ASD and typically developing controls (DC). The authors used T1-weighted MRI data from the ABIDE database [149]. Studies have shown that there is a connection between ASD and hippocampus morphology since abnormalities in shape and neuronal size have been detected [150, 151]. In addition, amygdala connected to socio-emotional impairments in ASD [152, 153]. Both the hippocampus and the amygdala are correlated to memory formation. GLCM used to extract texture features from segmented regions. The GLCM is a statistical method that captures the spatial relationship between pairs of pixel intensities in an image, considering specific distances and directions between them. For each region, the GLCM matrices are computed in four different directions and at a distance of one pixel, resulting in four matrices. Twenty-two features, such as energy, entropy, contrast, and correlation, are then extracted from these matrices (eleven from the hippocampus, and eleven from the amygdala). These features quantify various aspects of the tissue structure, including uniformity, randomness, intensity contrast, and pixel intensity relationships. The features were: energy, entropy, correlation, contrast, homogeneity, variance, sum-mean, cluster shade, cluster tendency, max probability and inverse variance. After averaging the features across the slices and normalizing them (z-score), they form a comprehensive representation of tissue texture in the hippocampus and amygdala regions, which are appropriate for distinguishing between ASD and HCs. Statistical analysis was also performed with an ANOVA on the extracted features to identify significant differences between ASD and DC subjects. The p-values obtained from the ANOVA were corrected using the Holm–Bonferroni [154] method to account for multiple comparisons, and features with a p-value bigger than 0.05 were deemed important and those were the features were fed to the classifier. Those features were 11 from the hippocampus and four from the amygdala. At this point, worth mentioning that the dataset was separated into two groups: Group A comprised of subjects aged 4–15 years old, while Group B included subjects aged 10–24 years. This distinction allowed for comparison across both age categories. Of course, the separation between ASD subjects and DC applied to both of the groups. For the classification task, an SVM model was employed with an RBF kernel. The LOOCV was employed towards reducing biases, providing a robust performance. The model reported a performance with an accuracy score of 67.85% for Group A, and for Group B, the accuracy score was 75%. Those accuracy scores were the highest and achieved from the texture features extracted from the hippocampus. In addition, the feature importance process was further assessed using an RF classifier, which identified that the most distinctive features, were the hippocampal texture features and more specifically the correlation and the cluster tendency features.

Studies show that the hippocampus has a crucial value in the identification of ASD. Singh et al. [34] focused also on the hippocampus, among other regions such as the amygdala and corpus striatum, since all of them have been studied and are crucial regions for ASD [155]. The authors used multi-compartment diffusion-weighted imaging (MC-DWI) data acquired by rats. The target of the study were rats that all had genetic modifications, making them models of ASD. These genetic modifications are designed to replicate specific mutations or deletions associated with ASD in humans. The first preprocessing step regarding DWI data was the conversion of raw images to NIfTI (Neuroimaging Informatics Technology Initiative) using the DTI-TK software

package. Then, the diffusion tensor data were reconstructed, aligned, and normalized to a custom template specific to the study, followed by fitting them to the Neurite Orientation Dispersion and Density Imaging (NODDI) model (ODI, NDI, CSF) using the Microstructure Diffusion Toolbox (MDT) to compute quantitative indicators related to brain microstructure, which include ODI (Orientation Dispersion Index), NDI (Neurite Density Index), and CSF (Cerebrospinal Fluid). These indices help map and quantify microstructural features of the brain tissue. In addition, ROIs were identified and the DTI-based rat brain atlas was used to segment them. The segmentation process relied on a set of diffusion tensor reference labels, to precisely define anatomical regions [156, 157].

Using the Pyradiomics [94] package the texture features were extracted. All images were subjected to a grey-level discretization with a fixed bin-width of 0.1 [158, 159]. The analysis focused on extracting a range of radiomic features, which included 18 first-order statistics, 24 from the GLCM, 14 from the GLDM, 16 from the GLRLM, and 16 from the GLSZ. Using the ANOVA approach, seven features were identified as the most significant. These selected features were then used in an unsupervised hierarchical clustering model to reveal patterns in the microstructural differences between the ASD models. The model revealed different groupings among the ASD genetic models, highlighting the ability of the radiomic approach to identify key microstructural differences. The ODI-derived features, especially in the hippocampus, were crucial in this clustering, capturing unique variations and demonstrating the potential to reveal alterations in ASD.

In Tables 13 and 14, the key findings and evaluation performance metrics for both ADHD and ASD studies are summarized.

Table 13: Analysis on Neurodevelopmental Disorders

Work	**Disorder**	**Selected features**	**Radiomics**	**Important Regions**	**Key Findings**
[138]	ADHD	ADHD vs. TDC: 9-10 (depends on the model), ADHD-I vs. ADHD-C: 23, for all the groups: 142	First-order features and texture features	Bilateral temporal lobe, left olfactory lobe, insula, right supplementary motor area, left occipital lobe, right frontal lobe, left hippocampus, bilateral amygdala, right calcarine, right lingual lobe, left caudate, vermis, left paracentral lobule, left supramarginal gyrus, bilateral cerebellum, Precentral Gyrus, Calcarine Cortex, Entorhinal Cortex, Posterior Cingulate Gyrus, Angular Gyrus	'30 percentile' and '0.25 quantile' features of the right Heschl's gyrus, and the '10 percentile' feature of the left superior temporal gyrus were crucial
[137]	ADHD	19	ALFF, ReHo, VMHC, DC	Frontal cortex, temporal cortex, occipital cortex, cerebellum, limbic system	Radiomics features achieved better performance than mean signals. The majority of the significant features were from the cerebellum
[139]	ADHD	ADHD vs. HC: 8, ADHD-I vs. ADHD-C: 5	Mean local thickness, kurtosis mean curvature, skew travel depth, skew mean curvature	Left temporal lobe, bilateral cuneus, left central sulcus	The most significant statistics were the skew convexity, mean local thickness, and kurtosis mean curvature from left superior temporal sulcus, right cuneus and left precentral

Continued on next page

Work	Disorder	Selected features	Radiomics	Important Regions	Key Findings
[148]	ASD	15	Texture features	Hippocampus, amygdala	GLCM correlation features from hippocampus were important
[34]	ASD	7	First-order, GLCM, GLDM, GLSZM	Hippocampus, amygdala, corpus striatum	ODI-derived features, from hippocampus identified as significant

Table 14: Experimental validation on Neurodevelopmental Disorders

Work	Disorder	Performance	Data	Participants	CV
[138]	ADHD	ADHD vs. TDC (Training / Testing) (Hybrid model):ACC=82.50%, AUC=0.82/0.83, SEN=61.21%/68.57%, SPE=89.60%/93.33%; ADHD-I vs. ADHD-C (Radiomic model):ACC=89.9%/84.3%, AUC=0.94/0.85, SEN=95.65%/85.29%, SPE=84.21%/83.33%	ADHD-200 Consortium[2] [160]	65 ADHD-I, 86 ADHD-C and 170 TDCs.	10-fold cross-validation
[137]	ADHD	(Training/Testing): ACC=76.3%/77.0%, AUC=0.811/0.797	ADHD-200 Consortium	187 ADHD and 187 TDCs.	10-fold cross-validation
[139]	ADHD	ADHD vs. HC: ACC=73.7%, SPE=77%, SEN=70%; ADHD-I vs. ADHD-C: ACC=80.1%, SEN=71%	Private	40 ADHD-I, 43 ADHD-C and 87 TDCs.	10-fold cross-validation
[148]	ASD	GROUP A: ACC=67.85%, SEN=62.50%, SPE=71.42%, AUC=76.80%; GROUP B: ACC=75%, SEN=62%, SPE=85%, AUC=80.06%	ABIDE I[3] [149]	34 ASD and 30 TDCs.	LOOCV, 10-fold cross-validation
[34]	ASD	Clustering	Private	23 rats	-

Classification of ADHD and its subtypes has been addressed through various radiomic strategies with differing levels of performance. Shi et al. [138] achieved the strongest overall results for ADHD vs. TDC using a hybrid model combining radiomic features, surface values, and gray matter volume. In contrast, Liu et al. [137], using a larger but similarly structured ADHD-200 dataset, achieved slightly lower performance. However the DeLong test provided additional statistical support for their results. Sun et al. [139], working with a smaller private dataset, reported not so high metrics, likely due to limited sample size. Additionally, all the three studies used 10-fold cross-validation. Based on those studies, regions contributing most to classification included the Heschl's gyrus, left superior temporal gyrus, precentral gyrus, cerebellum, and cuneus—areas linked to sensory integration, motor control, language processing, and emotional regulation.

Two studies examined radiomics-based approaches for classification and subtyping in ASD. Chaddad et al. [148] employed texture analysis of the hippocampus and amygdala using GLCM-derived features from structural MRI, reporting moderate accuracy, but without external validation, raising concerns about overfitting. Singh et al. [34] implemented unsupervised hierarchical clustering on radiomic features extracted from NODDI diffusion MRI. Their study aimed at subtype discovery rather than diagnosis and evaluated clustering quality via permutation testing and ANOVA (FDR-corrected), without reporting traditional classification metrics. Alterations at hippocampus, which suggested by both studies, may thus contribute meaningfully to the cognitive and emotional symptoms observed in ASD. The hippocampus is known to be vital for memory processing, spatial navigation, and emotional regulation. It facilitates the retrieval of memories and plays a significant role in stress responses and learning. However,

[2] https://fcon_1000.projects.nitrc.org/indi/adhd200
[3] https://fcon_1000.projects.nitrc.org/indi/abide/abide_I.html

the generalizability of both studies is limited by small sample sizes and the absence of independent validation, highlighting the need for replication in larger and more diverse cohorts.

4.5. Schizophrenia Spectrum & Other Psychotic Disorders

This section mainly refers to schizophrenia (SZ), but schizoaffective disorder (SA) and psychotic episodes are also presented. SZ is an intense and debilitating mental disorder with unknown causes, involving mainly disrupted brain connectivity that affects thinking, perception, and emotions [161] and affects millions of people worldwide and arises from a mix of genetic, environmental, and social factors, leading to symptoms like hallucinations, delusions, emotional withdrawal, and cognitive impairments [162, 163]. The diagnosis still depends on clinical evaluations of symptoms rather than objective biological markers, which makes it essential to develop more accurate diagnostic methods [161]. Furthermore, research also shows that the cerebellum has a fundamental role in the SZ [164]. Diagnosis of schizophrenia remains difficult due to its reliance on behavioral assessments, emphasizing the importance of developing measurable biological indicators to enhance diagnostic precision [165]. Treatment is further complicated because nearly 30% of patients do not react favorably to antipsychotic medications. However, electroconvulsive therapy (ECT) and recurring transcranial magnetic stimulation (rTMS) are employed to treat patients, combined with antipsychotic medications. In the following papers, AI-based approaches for the diagnosis of SZ and for the prediction of the treatment response are presented. In addition, Tables 18 and 19 present a summary of the key findings and evaluation metrics.

The paper of Bang et al. [161] describes a multiparametric radiomic approach for the diagnosis of schizophrenia using DTI and T1- weighted images. The authors focused on the identification of radiomic features of the corpus callosum (CC), which is the largest structure of white matter and handles the transmission of information between the hemispheres [166]. CC has been chosen for the study since several abnormalities have been found in patients with schizophrenia in relation to the morphology and size of CC in its subregions [167, 168, 169, 170]. The T1-weighted images were used for the segmentation of the CC. This process was performed with FreeSurfer software, resulting in the segmentation of CC into five subregions: anterior, mid-anterior, central, mid-posterior and posterior. In terms of DTI images, the Diffusion Toolbox from the FMRIB software is used for preprocessing. For the DTI data, fractional anisotropy (FA) and apparent diffusion coefficient (ADC) maps were created, in which the T1 data were co-registered. In general, T1-weighted images were used to extract macrostructural alterations in CC, while DTI for microstructural characteristics. More specifically, using the Pyradiomics [94] library 1605 were extracted, 107 features for each of the 5 subregions of the 3 sequences of the CC (T1, FA, ADC). Those features were shape, first-order, and second-order statistical. For feature selection, the Scikit-Learn library was used and the extracted features normalized (min-max scaling), the Mutual Information technique [171] applied, and they analyzed for high correlations. The final outcome was the reduction of the features from 1605 to 30 (16 ADC, nine T1 and five FA). The next step was the classification. The authors used several classifiers, but the best performance was reported with the Bayesian optimized model which achieved an AUC score, precision, sensitivity, and specificity of 0.89, 80%, 83.3%, and 76.9%, respectively. One more important part of this study was the model interpretability using SHAP. This process showed that the second-order features of T1 and ADC of the posterior CC were the most crucial features.

Most of the works that have already been presented used fMRI or sMRI. In the work of Carrasco-Poves et al. [163], the authors used PET and T1-weighted MRI data. The two types of images, after they normalized the co-registered to the MNI space and VOI extracted from the frontal cortex, posterior cingulate cortex (PCC), temporal cortex, primary auditory cortex (PAC) and thalamus. Those regions were selected since the frontal cortex and cortical areas regions are usually associated to SZ. Research highlights that the crucial role of glutamatergic neurotransmission in the left temporal cortex region is highly correlated with SZ symptoms and impaired cognition linked to reduced temporal lobe volume. In addition, the PAC shows activation during auditory hallucinations. In addition, thalamic regions also play an important role, since metabotropic glutamate receptor 5 (mGluR5) is found in large amounts in patients with schizophrenia [172, 173, 174, 175, 176]. Except for the normalization step for the data, the gray levels were quantized in order to offer an improved signal-to-noise ratio, and also for PET images, there was an extra normalization step for brain volumes relative to the cerebellar gray matter to calculate Distribution Volume Ratio (DVR). which provides the availability of receptors in a region [177]. The radiomic features were extracted using the MATLAB Radiomics toolbox implemented in the work [178]. In total, 43 features were extracted, three from the first-order category or histogram, and 40 from the second-order category: 9 GLCM, 13 GLRLM, 13 GLSZM and 5 from NGTDM. For the selection of the most important features, the Relief algorithm was used [179], a filter-based method that assesses the significance of each feature, generating a ranking. The performance of the entire approach was evaluated separately for each of the five regions of the brain for the MRI and PET data. The best performance in PET images was achieved with the linear SVM for the features in the frontal cortex with AUC: 0.823; for the MRI data, the same classifier achieved AUC: 0.892 in the PCC. The five more used features for those cases in PET images were the GLCM, GLSZM, GLSZM, GLSZM, GLSZM, and for MR images were the GLRLM, GLRLM, Skewness, GLSZM, and the GLSZM. For PET and MRI performance, based on the AUC that has already been presented, the selected characteristics were 39 and 42 with 64 gray levels, respectively. At this point, it is worth noting that the options for the gray levels which were used were 16, 32, 64 and 128.

The work from Latha et al. [180], apart from SZ, deals with SA. SZ and SA are related disorders, but the difference is that SA is characterized by abnormal thoughts and deregulated emotions that cannot be regulated by the patient [181], while SZ has more complex symptoms. The authors of the paper aimed to identify and classify the most important radiomic features towards classifying SZ, SA, and HC. For these classifications, they used T1-weighted structural MRI data obtained from the National Alliance for Medical Image Computing (NA-MIC) and from the SchizConnect database the COBRE used. The preprocessing of

the images included removing the skull, dura, and arachnoid layers. The images were then segmented to define the ROIs, which in this case included the ventricle and cerebellum. Radiomics extracted from three regions: the ventricle, the cerebellum and also the whole brain to compare whether the radiomics of the cerebellum and the ventricle were more important and efficient than those obtained from the entire brain. In total, the features extracted for each region were: 30 features from the whole brain, 52 features from the ventricle, and 28 features from the Cerebellum, and can be categorized into four categories: Geometric, Hermite, Laws, and Structure tensors. It must be noted that the features that belong to the categories of Hermite, Laws, and Structure tensors are considered as texture features. The texture features deliver essential insights about the structure of the brain, while the geometric features assess the brain's shape variations. The feature selection process is performed using the Binary Particle Swarm Optimization (BPSO) [182], a metaheuristic algorithm designed to select the most important features. This was achieved by iteratively optimizing a subset of features to maximize classification performance.

The results of the use of the BPSO algorithm were the selection of the features shown in Table 15. The features were fed in a Fuzzy SVM (FSVM) model, reporting accuracies of up to 90.09%. This performance was achieved by using 28 combined features. The following step of the methodology was to identify which features were significantly varied across the SZ, SA, and Hc groups. Those features were the texture of the left cerebellum. This was achieved using ANOVA and more specifically the radiomic features of the Hermite, Law, and structure showed significant differences ($p < 0.0001$). In addition, Positive and Negative Syndrome Scale (PANSS) [183] correlation analysis was conducted towards identifying which features were related to the severity of clinical symptoms. With the PANSS tool, the symptoms' severity of SZ can be measured. There are three types of symptoms: positive (hallucinations, delusions), negative (lack of motivation), and general psychopathology (anxiety, mood disturbances). The total score reflects the overall severity of the symptoms. The results showed that the mean and E0 features and the R5L5 feature from the Hermite and Law category (texture features) from the cerebellum could be crucial features for the identification of the harshness of the disease.

Table 15: Extracted radiomics from the entire brain, cerebellum, and ventricle by Latha et al. in [180]

Category	**Radiomic Features**
Geometric	Area, extent, perimeter, convex area, solidity, eccentricity, major axis length, equivalent diameter, minor axis length (nine features)
Hermite	E3, E2, E1, E0, SD, mean, entropy, homogeneity up to order 4 (32 features)
Laws	Mean, SD, energy of E5L5, R5L5, S5E5, S5S5, R5R5, S5L5, E5E5, R5E5, R5S5 (27 features)
Structure tensors	Coherence, orientation, λ_1, λ_2, energy, anisotropy (six features)

An additional work focusing on the identification of important features that are capable of distinguishing SZ patients and HC people can be found in [184] where the authors specifically delve into subfields of the hippocampus. In this case, T1-weighted magnetic resonance imaging was also utilized. The preprocessing of the data began with the automated mask extraction of the hippocampus using the volBrain tool [185, 186]. First, adaptive filtering was employed for denoising [187], and then an affine registration was performed to align the image in the MNI space with the Advanced Normalization Tools [188], along with the normalization of the intensity of the images [189]. In addition, the nonuniformity of the low-frequency intensity was revised by using the N4ITK algorithm [190]. The next step was the segmentation of the hippocampus into three subfields (subicular complex, merged subfields of CA 1 to 3 and CA4-DG). In addition, a neurologist visually checked the results of the segmentation and the registration for possible errors. In addition, to improve the quality of preprocessing in stages such as segmentation or masking, the 3D Slicer software was used. Finally, no resampling was performed, as the images already had a resolution of 1 mm isovoxel. Using the Pyradiomics [94], we extracted 642 features for the six ROIs (three subfields for the right and left hippocampal subfields). More specifically, each ROI had 18 and 75 first and second-order features, respectively, as well as 14 shape features. With the usage of Mutual Information [171], the most important features were selected. With the MI the reduction of the redundancy was achieved while the most valuable features were selected. The result of this process was 30 features to be selected. These features were distributed across six ROIs: Right CA1- 3 (one feature), Right CA4-DG (nine features), Right Subiculum (nine features), Left CA1- 3 (four features), Left CA4-DG (four features) and Left Subiculum (three features). The selected features included one shape, eight first-order, and 21 second-order texture features. Those features were imported into a Logistic Regression model which achieved scores of 0.821 for AUC, 82.1% for accuracy, with a sensitivity of 76.9%, and 70% of specificity in the independent test set. As a conclusion for this study, the first-order features of the left CA 1-3 subfields are a strong biomarker that demonstrates a significant correlation with the gravity of positive symptoms scores evaluated with PANSS [183].

The authors of the previous study focused on the subfields of the hippocampal to identify schizophrenia. However, Bang et al. [164] focused exclusively on the cerebellum, since structural abnormalities have been found in schizophrenia. For this reason, high-resolution cerebellum T1- MRI data was used, which were preprocessed with the CERES service of volBrain, which is an automated pipeline for cerebellum segmentation. This pipeline has the highest quality scores, compared to other parcellation methods [191, 192]. The voxel size of the images was $1 \times 1 \times 1$ mm^3 while the non-uniformity was corrected with the use of the N4 algorithm. The outcome of the segmentation was to extract 12 subfields of the cerebellum based on the atlas presented in the study [193]. The subfields of the cerebellum were: lobule I-II, lobule III, lobule IV, lobule V, lobule VI, Crus I, Crus II, lobule VIIB, lobule VIIIA, lobule VIIIB, lobule IX, and lobule X. The features of the data, were exported by utilizing Pyradiomics [94] which conformed to the Image Biomarker Standardization Initiative (IBSI) [194]. The IBSI is an international effort to standardize the way radiomic features are extracted and analyzed from medical image data. In total, they extracted 2568 features, 107 for 12 subregions for the two hemispheres of the cerebellum. More specifically, the 107 radiomic features were 14 shape features, 18 first-order features, and 75 second-order features. The second-order features were 24 GLCM, 16 GLSZM, 14 GLDM, and 5 NGTDM. The extracted features are normalized using the Z-score method. Mutual Information (MI), is not the first time in this review that has been used. The authors of this paper used the MI for feature selection and concluded to 17 features that were subsequently fed into a Light Gradient Boosting Machine (LGBM) model, reporting AUC, accuracy, sensitivity, and specificity of 0.89, 78.8%, 88.5%, and 75.4%, respectively. The last and very important step in this approach was to evaluate the interpretability of the model. The SHAP method that the authors implemented, showed that the strongest biomarkers for diagnosing schizophrenia were the second-order GLSZM features of the right Lobule IX and the first-order energy of the right Lobules V and VI.

In contrast to the previous approach, the work presented in [165], is based on rs-fMRI, with T1-weighted sMRI used only for spatial normalization and anatomical registration during preprocessing. Both imaging modalities were acquired from Center for Biomedical Research Excellence (COBRE), in order to find neuroimaging biomarkers for the identification of schizophrenia. The authors used the images in order to calculate Degree Centrality (DC) and voxel-mirrored homotopic connectivity (VMHC) maps. The DC maps can measure, at the voxel level, how intense is the functional connectivity in the brain, while the VMHC maps, as already has been described, show the symmetry of functional connectivity between voxels which are placed in the two hemispheres. The authors based their preprocessing procedure and the methodology of the calculation of the maps in the study [195]. The preprocessing stage included the first 10 volumes removal, a common step in the preprocessing of rs-fMRI data, slice timing and realignment correction, segmentation, and spatial normalization using Diffeomorphic Anatomical Registration Through Exponentiated Lie Algebra (DARTEL), with a resampling resolution of $3\times3\times3$mm^3. Nuisance covariates such as white matter, cerebrospinal fluid signals, and head motion parameters were removed, and band-pass filtering (0.01–0.10Hz) was applied. The above steps were performed and the maps calculation was performed using the Data Processing & Assistant for Brain Imaging (DPABI) [141] and Statistical Parametric Mapping (SPM12). The segmentation of the brain was done with the Brainnetome atlas [196] and 246 regions were detected. The extraction of the 48 features was done with in-house scripts. Those features were 15 intensity-based histogram features and 33 texture features. In the feature selection process, the t-tests and the LASSO were used. A two-sample two-tailed t-test was used to filter the features that distinguish SZ patients from HC and then with the LASSO the most important features were identified. Those were 10 features, from each map, which were imported into an SVM model with a linear kernel for classification. Of course, the features were Z-score normalized. The achieved scores for the accuracy, AUC, sensitivity, and specificity of the model were 74.02%, 0.808, 69.11%, and 78.18%, respectively. After 200 cross-validation iterations and mean weight calculations for each feature, in order for the robustness and the generalizability to be ensured. The approach concluded with the identification of the most discriminative features, included in Table 16.

Table 16: The most discriminative features according to Shi et al. [165]

Lobes	**Radiomic Features**
Occipital Lobe	Median
Subcortical Nuclei	Cluster Shade, Correlation, LRLRE, skewness, Contrast, IDMN, Energy, Variance
Frontal Lobe	Sum Entropy, maximum
Insular Lobe	Cluster Prominence
Parietal Lobe	Sum Entropy

Continued on next page

Lobes	Radiomic Features
Temporal Lobe	Homogeneity1, Homogeneity2, Auto-correlation, Correlation, LRE, LRL-GLE, range

An additional case where two types of magnetic resonance imaging were used was presented in [162], where rs-fMRI and sMRI were combined. The software CONN was used for data preprocessing. The preprocessing stage included steps like discarding the first 10 images to ensure signal equilibrium, motion correction, co-registration of fMRI to T1 images, normalization of T1 images to MNI space, transformation of the fMRI to MNI, smoothing using Gaussian kernel, band-pass filtering to 0.01-0.1 Hz and resampling and regressing out nuisance signals. It can be noticed that the preprocessing stages, in most cases, have similar steps. In addition, brain segmentation was performed based on AAL and 90 non-cerebellar anatomical ROIs were detected. In addition, for each preprocessed pair of ROIs, Pearson's correlation coefficients were calculated to build a 90×90 correlation matrix. In total, they extracted 117 functional connectivity features from the cortical, subcortical, and limbic regions. For the selection of the most important features, we used LASSO regression. One more time, the LASSO is used for the feature selection process. The authors created two sets for the classification: the intra-data and the inter-data to evaluate the performance of the classification model (SVM). In the intra-data validation, the data were randomly divided for training and testing (80&- 20%), while in the inter-data they used two datasets for training and testing ensuring that no overlap between them will be shown. The LASSO regression led to the selection of 32 and 43 crucial features for the intra-data and inter-data, respectively. For the intra-data, the accuracy scores were 87.09% and 82.61% for the training and testing set, respectively, while for the inter-data the corresponding results were 83.15% and 80.07%, respectively. The reason why the authors had two approaches to evaluate the performance increases the robustness and generalizability of the approach.

So far, all the papers in this subsection refer to schizophrenia or schizoaffective disorder. One more thing that all the papers from this section have in common is that the classification model is a typical machine learning classifier and in many cases with several variations. In the study of Korda et al. [197] which will be described in the present paragraph, the approach and the disorder are different. The authors focused on first-episode psychosis (FEP) because it offers a critical window for early detection of structural abnormalities related to mental disorders. The sMRI data were obtained from the early detection study of the psychosis project (FePsy) conducted at the Department of Psychiatry, University of Basel, Switzerland [198]. The preprocessing pipeline on the paper included multiple stages. In order for the noise to be reduced Optimized Blockwise Nonlocal-Means filtering with Rician noise adaptation was used [199, 199]. Also, the segmentation process performed with the CAT12 toolbox, an extension of the SPM12 software package. The segmentation regions were the white matter (WM), gray matter (GM) and cerebrospinal fluid (CSF), which are areas capable of identifying schizophrenia or MDD [200]. Of course, before the segmentation inspection for significant artifacts and abnormalities was done by the authors and by neuroradiologist. Furthermore, with the CAT12 toolbox bias field correction addressed intensity inhomogeneities of the data. In addition, spatial normalization aligned all the images to MNI and histogram equalization was applied using Matlab's histeq function in order to adjust the contrast of the images. As the last step of this pipeline was the use of a 7×7×7 Gaussian kernel for voxel level smoothing. The features in this study were not extracted from the three above regions, but from the entire brain to detect microstructural changes. Segmentation of the brain into three regions, as described above, was performed only for preprocessing reasons to ensure data quality and consistency. It facilitated artifact removal, bias field correction, and accurate spatial normalization to MNI space. Furthermore, segmentation improved the precision of preprocessing steps, such as noise reduction and intensity correction, by focusing on specific tissue types. The feature extraction was performed using the GLCM algorithm for the non-segmented images. Six texture features were extracted from each voxel, including Entropy, Sum of Entropy, Difference of Entropy, Energy, Contrast, and Homogeneity. These features capture various aspects of texture, such as randomness, uniformity, and local intensity variations throughout the brain. In addition, the selection of the features was performed using a two-sample t-test to identify the most effectively distinguished between the target classes (FEP subjects vs. HC and FEP subjects vs. high-risk individuals who did not later progress to psychosis (CHR_NT)). The top 200 features were selected for each classification based on their significance. This process was incorporated into a 10×10 nested cross-validation, preventing over-fitting and ensuring the robustness of the selected features. Following feature selection, a deep learning classifier was employed using a five-hidden-layer neural network architecture, trained with the Levenberg-Marquardt algorithm [201]. The classifier achieved balanced accuracies of 75.24% for distinguishing FEP from HC and 73.21% for FEP vs. CHR_NT. To address the interpretability of the model, the authors used Layer-wise Relevance Propagation (LRP), a technique designed to provide insights into the decision-making process of neural networks by generating heatmaps [202]. These heatmaps visualized the brain areas that made the greatest contribution. The analysis revealed that the key areas, cerebellum, hippocampus, insula, thalamus, and amygdala, significantly contributed to distinguishing between FEP, CHR_NT, and HC groups. The most crucial features driving the classification decisions were the difference between entropy and contrast, which captured micro-structural abnormalities in brain tissue. This study significantly differs from others in the field, as it is the only one that employed Deep Learning while performing image segmentation exclusively for preprocessing purposes.

Although the previous papers described in the above paragraphs emphasized the detection and classification of schizophrenia, the following papers highlight how radiomics are used to predict treatment responses offering the potential for more effective and targeted interventions in the treatment of schizophrenia. One more study in which the authors employed a fusion of sMRI and fMRI, investigating the early prediction of treatment response in schizophrenia will be presented. Cui et al. [203] used two datasets. The first one included subjects with schizophrenia while the second one included subjects with SZ spectrum disorders (schizophrenia, psychotic disorder, schizophreniform disorder). The majority of patients received second-generation antipsychotics (risperidone, olanzapine, ziprasidone, quetiapine, paliperidone, aripiprazole, amisulpride and clozapine), while the remaining patients, which were the minority, received first-generation antipsychotics (haloperidol, chlorpromazine, perphenazine and sulpiride) for two to three weeks. Some patients also underwent electroconvulsive therapy (ECT) or repetitive transcranial magnetic stimulation (rTMS). For preprocessing of the fMRI data the CONN Functional Connectivity Toolbox toolbox is used. The first step was the exclusion of the 10 first volumes and the correction of head movements. In addition, co-registration to T1 images, normalization to MNI space, and smoothing were performed along with bandpass filtering on 0.01–0.1 Hz. For the preprocessing of the T1-weighted MRI data the FreeSurfer suite was used. Steps included skull stripping, bias-field correction, segmentation of the volumetric structures of subcortical white matter and gray matter, and registration to a spherical atlas and parcellation of the cerebral cortex into units based on the gyral and sulcal structures. The extracted features can be divided into the following two categories:

1. Functional Connectivity Features. The brain was segmented into 106 non-cerebellar ROIs using the FSL Harvard-Oxford Atlas. Those ROIs were 91 cortical and 15 subcortical regions. For every patient, the time series for each ROI was calculated by averaging them throughout all voxels of the region. Then, Pearson correlation coefficients were computed for every preprocessed ROI time series pair, resulting in a temporal correlation matrix of size 106×106 for each subject.
2. Cortical Features. The 408 cortical features extracted from the regions detected are based on the Desikan-Killiany Atlas. Those features were volumetric and geometric measures like cortical thickness, surface area, gray matter volume, curvature and sulcal depth. Those features were identified since they are related to cortical defects in patients with SZ.

The LASSO is a common technique for feature selection which has been presented several times in this review. This work also uses this technique in order to identify the most important features. With a 10-fold cross-validation-based LASSO algorithm selected nine functional connectivity features and three cortical features. The selected features show a reduction of 99.84% and 99.26% of the functional connectivity and cortical features, respectively. The selected features are shown in Table 17. The SVM classifier achieved the optimal performance by combining the two types of features predicting 92.04% of responders (patients with significant improvement) and 80.23% of non-responders (patients with insufficient response to their treatment), achieving an overall accuracy of 85.03% in early prediction antipsychotic treatment response offering a promising tool for personalized schizophrenia management.

Table 17: The 12 functional connectivity and cortical features according to Cui et al. in [203]

Type	Connectivity/Region	Feature
Functional Connectivity	Right Anterior Superior Temporal Gyrus - Left Anterior Superior Temporal Gyrus	-
Functional Connectivity	Left Temporal Pole - Right Inferior Lateral Occipital Cortex	-
Functional Connectivity	Left Caudate - Right Pallidum	-
Functional Connectivity	Left Inferior Lateral Occipital Cortex - Right Anterior Parahippocampal Gyrus	-
Functional Connectivity	Right Intracalcarine Cortex - Right Anterior Parahippocampal Gyrus	-
Functional Connectivity	Right Inferior Frontal Gyrus Pars Triangularis - Left Putamen	-
Functional Connectivity	Right Posterior Inferior Temporal Gyrus - Right Intracalcarine Cortex	-

Continued on next page

Type	Connectivity/Region	Feature
Functional Connectivity	Left Precentral Gyrus - Brain Stem	-
Functional Connectivity	Left Posterior Supramarginal Gyrus - Right Temporal Occipital Fusiform Cortex	-
Cortical Feature	Right Cuneus	Cortex Mean Curvature
Cortical Feature	Right Cingulate	Metric Distortion
Cortical Feature	Right Precuneus	Volume

Different types of treatments received by patients have been mentioned in the above works. However, Xi et al. [204] focus exclusively on ECT treatment. This treatment uses electrical currents which pass through the brain to induce a seizure, helping improve symptoms and has been proved that 66% of the patients who received this treatment have recovered [205]. The patients of this study had two to three sessions of ECT therapy per week over a period of three to four weeks. Each ECT session typically lasts between five and 10 minutes. T1-weighted sMRI was acquired before and after ECT to compare the structural changes in the brain. Data were analyzed using VBM analysis with the CAT12 toolbox in the SPM12 software, following its default settings. Image normalization and segmentation into gray matter (GM), white matter (WM), and cerebrospinal fluid (CSF) was performed. To adjust for individual brain sizes, the DARTEL algorithm [206] was applied for spatial normalization of the images. A two-sample t-test was conducted towards comparing GM volume differences between responders and non-responders to ECT, setting a threshold for significance of $P < 0.05$ uncorrected and a minimum size of cluster 100 voxels. The ROIs were defined using the AAL atlas [144], and areas showing significant changes were selected for feature extraction for machine learning purposes. The separation between responders and non-responders evaluated with PANSS [183]. If a patient showed a $\geq$ 70% decrease in the total PANSS score after the treatment when would be categorized as a responder. Those who showed a smaller reduction or no improvement were classified as non-responders. It is worth noting at this point that both categories had antipsychotic medications prior to ECT, with the responders receiving a higher dose compared to non-responders. For feature extraction, algorithms were implemented in MATLAB, resulting in 285 first-order statistical features per subject, derived from the histograms of GM volume values across ROIs. The features extracted from the GM since structural and functional changes in the GM are strongly related to the treatment response. Feature selection began with univariate two-sample t-tests to identify statistically significant differences between responders and non-responders. These were further refined using a regularized multivariate logistic regression model (LRM) with a LASSO penalty, which selected the most predictive features for classification. Based on the three selected GM features, a SVM classifier was also trained to validate the results. The LRM successfully distinguished between responders and non-responders, achieving an accuracy of 90.91% and 87.59% (training/validation). Additionally, SVM classifier achieved 90.91% and 91.78% accuracy in the training and validation set, respectively, showing that GM's first-order statistical features of hippocampus, inferior frontal gyrus, thalamus, cingulate cortex, insula, temporal and parietal lobes, are capable indicators for the prediction of ECT response in SZ patients who retrieving antipsychotics. To validate the performance a LOOCV framework was implemented. ECT combined with antipsychotic medications has been shown to produce enhanced therapeutic effects, making it a potentially secure and efficient option for patients with severe or treatment-resistant schizophrenia. Additionally, despite limited data, ECT has demonstrated rapid positive effects in reducing suicidal behavior in mood disorders. However, while about 66% of schizophrenia patients improve with ECT, a small group still shows minimal progress, even when ECT is used together with clozapine treatment [205, 207, 208, 209, 210].

The authors in [205] used T1-weighted sMRI and diffusion (dMRI) data from patients diagnosed with schizophrenia, including treatment-resistant cases, acute episodes, or suicide attempts, who received ECT combined with antipsychotic medications. The ECT process was 12 sessions, three times per week for four weeks. The sMRI and the dMRI data were acquired before the ECT. Also in this case the PANSS score [183] used to evaluate the symptoms of the subjects alongside mini-mental state examination (MMSE) for cognitive change measurements and Clinical Global Impression (CGI) were obtained before and after the ECT. Regarding the preprocessing of sMRI data, for the identification of the ROIs the AAL atlas was used resulting in 23 regions of gray matter. Also the CAT12 toolbox implemented in SPM12 (Statistical Parametric Mapping) was utilized to perform the VBM.

Regarding the preprocessing of the dMRI, multiple tools were used. The PANDA pipeline [211], which incorporates FMRIB Software Library [212], the Pipeline System for Octave and Matlab (PSOM) [213], the Diffusion Toolkit [214], and the MRIcron [215]. With this process, the binary maps of each white matter (WM) tract were built using data from healthy participants. For each schizophrenia patient, fractional anisotropy (FA) maps were overlaid onto these binary maps to generate FA-weighted WM tracts. In total, 37 FA-weighted white matter tracts were used for feature extraction. With this process, the authors were able to compare the microstructural changes in the WM between SZ patients and HC. Using MATLAB, the features for sMRI and dMRI were extracted. More specifically, 10 first-order statistical radiomic features were extracted for the 23 ROIs (230 GM radiomics) and 10 statistical features were extracted from each tract (370 WM radiomics). The total extracted features (600) were combined into

a 600-feature matrix for each patient. Furthermore, the researchers applied the LASSO technique to handle the high-dimensional data, in case of more features than patient samples. LASSO works by shrinking the coefficients of less important features to zero and keeping only the most significant predictors. To ensure that the feature selection was reliable and generalized across the dataset, LOOCV was also performed. In this approach, each subject's data was temporarily set aside as a test case, with the model being trained on the remaining samples. In addition, the regularization parameter λ was calculated using 10-fold cross-validation. The features were ranked according to their frequency of selection during the LOOCV process. In the following, the researchers evaluated model performance using various feature subsets within the LOOCV framework in the primary cohort. During this process, training samples were used to develop a Support Vector Regression (SVR) model, which was subsequently tested on the excluded sample. The model's accuracy was evaluated using Pearson's correlation coefficient (r) and Root Mean Square Error (RMSE). The SVR model demonstrated strong predictive performance for ECT response, achieving a Pearson's correlation of r=0.671 in the primary cohort and r=0.777 in the test cohort, with low RMSE values of 15.18 and 14.98, respectively. The results demonstrated that multi-parametric MRI features could predict treatment response to ECT. Crucial features from brain regions, including the left inferior frontal gyrus, right insula, left middle temporal gyrus, and right superior temporal gyrus, were important predictors, while the features from the dMRI data show that connecting the frontal and temporal regions, are connected to SZ.

The papers that have already been described focus only on one task, detection of SZ or prediction of treatment response, while the work presented in [216], consists of a holistic approach regarding both issues. The authors focused their study on the thalamus. Studies have shown that increased blood oxygenation levels in the thalamus to SZ patients [217]. Furthermore, abnormalities in connectivity have been reported between the thalamus and bilateral cerebellum, the anterior cingulate cortex, and multiple sensory-motor regions [218]. In addition, decreased sensitivity of the auditory cortex to its thalamic afferent has been shown, as well as partial disconnection of the thalamus and cerebellum in patients with schizophrenia [219, 220]. High dimensional sMRI data were used for the detection of SZ and for the prediction of the response of the treatment as well. The images were acquired before the treatment. The treatment was antipsychotic medication, with most patients receiving second-generation antipsychotics. Based on the PANSS, the patients with SZ are categorized as responders and non-responders. The images were preprocessed with the FreeSurfer. The stages were normalization standardized anatomical framework, skull stripping, correction for inhomogeneity, segmentation of subcortical WM and GM volumetric structures [221, 105], registration to a spherical atlas [222] and parcellation of the cerebral cortex [221]. The authors considered ROIs the bilateral thalami, based on previous studies [148, 184].

After the preprocessing of the images, using the AAL the thalamus of each subject was extracted. The feature extraction algorithms were implemented in MATLAB based on Image biomarker standardization initiative [158]. The extracted features can be categorized into four groups [142]: first and second order, wavelets, and texture features. The total number of features was 4019. The feature selection in this paper was conducted using a 10-fold CV, combined with LASSO. Through repeated CV, the 4019 radiomic features were iteratively reduced according to their importance, determined by the mean square error, as a cost function, and the MSE + 1SE criteria [223]. Features that appeared consistently across multiple iterations were selected as the most critical. With an RF classifier, 10-12 features discriminated SZ patients from the HCs with a mean accuracy score of 64.53% (inter-dataset) and four and five features forecasted the response of the treatment with a 66.78% (inter-dataset) mean accuracy. At this point, it should be noted that the 16 features were used towards identifying SZ and the prediction of the treatment response were wavelet-based radiomics features.

Table 18: Analysis on Schizophrenia Spectrum and Other Psychotic Disorders

Work	Disorder	Selected features	Radiomics	Important Regions	Key Findings
[163]	SZ	39, 42 (PET, MR Images)	First-order, GLCM, GLRLM, GLSZM, NGTDM	Frontal cortex, PCC	From the PET images the correlation , Large Zone High Gray-Level Emphasis, Large Zone Emphasis, Zone-Size Variance, and Zone Percentage was the most used and identified in the frontal cortex. For the MR images, those features were the Low Gray-Level Run Emphasis, Short Run Low Gray-Level Emphasis, Skewness, Zone Percentage, and the Low Gray-Level Zone Emphasis, detected in PCC
[180]	SZ & SA	28	Area, extent, perimeter, convex area, solidity, eccentricity, major axis length, equivalent diameter, minor axis length, Mean, SD, E0, E1, E2, E3, entropy, homogeneity, energy of E5L5, R5L5, S5E5, S5S5, R5R5, S5L5, E5E5, R5E5, R5S5, Coherence, orientation, λ_1, λ_2, energy, anisotropy	Cerebellum	High importance features were the mean and E0, and also the R5L5 from the Hermite and Law category and tensor features from the left cerebellum
[184]	SZ	30	Shape feature, first-order features, and second-order texture features	Right CA1- 3, right CA4-DG, right Subiculum, Left CA1- 3, left CA4-DG and left Subiculum.	The first-order features of the left CA 1-3 subfield were significant for the classification
[161]	SZ	30	FA, ADC, T1	Anterior, mid-anterior, central, mid-posterior and posterior CC	Significant second-order features of the posterior CC detected
[164]	SZ	17	Shape, first- order, second- order	Lobule I-II, lobule III, lobule IV, lobule V, lobule VI, Crus I, Crus II, lobule VIIB, lobule VIIIA, lobule VIIIB, lobule IX, and lobule X	Second-order GLSZM features of the right Lobule IX and the first-order and energy of the right Lobules V and VI were important

Continued on next page

Work	Disorder	Selected features	Radiomics	Important Regions	Key Findings
[165]	SZ	20	VMHC, DC	Default mode networks, bilateral dorsal ,front-parietal, somatomotor, limbic, caudate	Median, Subcortical Nuclei & Cluster Shade, Correlation, LRLRE, skewness, Contrast, IDMN, Energy, Variance, Sum Entropy, maximum, Cluster Prominence, Sum Entropy, Homogeneity1, Homogeneity2, Autocorrelation, Correlation, LRE, LRLGLE, range
[162]	SZ	32, 43 (intra, inter)	Functional connectivity features	Cortical, subcortical, and limbic regions	Results demonstrate an effective radiomics- based approach using functional connectivity to diagnose schizophrenia
[197]	Psychosis	6	Entropy, Sum of Entropy, Difference of Entropy, Energy, Contrast, Homogeneity	Anterior corona radiata left, Insular left, Lateral fronto-orbital gyrus left, Middle fronto-orbital gyrus left, Gyrus rectus left	Cerebellum, Thalamus, Amygdala, Hippocampus, Parahippocampus, and Insula, where significant regions along with the Difference of Entropy and contrast features
[203]	SZ-TR[4]	12	Cortex Mean Curvature, Metric Distortion, Volume, Functional connectivity	FC pairs: bilateral STG, TP-Occipital, Caudate–Pallidum, Parahippocampal-Occipital, Frontal-Putamen, Temporal-Intracalcarine, Precentral-Brainstem, Supramarginal-Fusiform; Cortical: Cuneus, Cingulate, Precuneus	Structural and functional radiomics predicted effectively the response to the treatment. An analytical table is provided in the paper
[204]	SZ- TR	3	Mean, Median, Standard, deviation, Root mean, square, Skewness, Kurtosis, Uniformity, Entropy	Thalamus, hippocampus, insula, cingulate cortex, temporal and parietal lobes, and inferior frontal gyrus	SGM's first-order statistical features of insula, inferior frontal gyrus, thalamus, Cingulate cortex, hippocampus Temporal and parietal lobes, had high importance value
[205]	SZ- TR	10	FA, VBM	Right insular cortex, right superior temporal gyrus, frontal and temporal gyri, left middle temporal pole, and left inferior frontal gyrus all contribute to various cognitive and neural processes	The right insula, right superior temporal gyrus, left middle temporal gyrus, and left inferior frontal gyrus were key regions, while dMRI-based features revealed a connection between the frontal and temporal regions in SZ

Continued on next page

[4]Treatment Response

Work	Disorder	Selected features	Radiomics	Important Regions	Key Findings
[216]	SZ- TR	4-17	W1.Mid, W1.Min, W1.Mid, W2.RMS, W2.Surface, W2.SVR, W2.Volume, W2.SRE_8, W2.Homo2_13, W3.Min, W4.Co_Corr_12, W4.Co_Var_13, W5.Co_Corr_11, W5.RLN_9, W6.Co_Corr_2, W6.Co_Corr_7, W7.IMC1_9 ,W1.SRLGLE_1, W1.Compactness1, W2.Energy, W2.MAD; W3.Min, W6.Cluster_Shade_mean, W8.Cluster_Shade_8	Thalamus	Wavelet-based radiomics features identified as high value

Table 19: Experimental validation on Schizophrenia Spectrum and Other Psychotic Disorders

Work	Disorder	Performance	Data	Participants	Evaluation	CV
[163]	SZ	MRI/PET:ACC=89%/82%, SEN=77.6%/71.8%, SPE=79.4%/71.8%, AUC=0.823/0.892	Private	17 SZ and 17 HCs.	-	5-fold cross-validation
[180]	SZ & SA	Cerebellum: ACC= 90.09%, SEN= 86.54% (Normal), 90.84% (SZ), SPE=93.53% (SZ), 95.48% (SA), AUC=0.917 (SZ), 0.956 (Normal), 0.945 (SA)	SchizConnect [5], COBRE[6], NA-MIC [7]	81 SZ, 31 SA and 84 HCs.	-	5-fold cross-validation
[184]	SZ	ACC=82.1%, SEN=76.9%, SPE=70%, AUC=0.821	Private	86 SZ and 66 HCs.	-	10-fold cross-validation
[161]	SZ	ACC=80%, SEN=83.3%, SPE=76.9%, AUC=0.89	Private	86 SZ and 79 HCs.	-	10-fold cross-validation
[164]	SZ	ACC=78.8%, SEN=78.8%, SPE=75.4%, AUC=0.89	Private	174 SZ and 162 HCs.	-	5-fold cross-validation

Continued on next page

[5] https://www.nitrc.org/projects/schizconnect/
[6] https://fcon_1000.projects.nitrc.org/indi/retro/cobre.html
[7] https://www.na-mic.org/

Work	Disorder	Performance	Data	Participants	Evaluation	CV
[165]	SZ	Brainetome atlas: ACC=74.02%, SEN=69.11%, SPE=78.18%, AUC=0.808, PRE=72.88%, F1_SCORE=70.94%	COBRE	72 SZ and 74 HCs.	-	Nested 10-fold cross-validation
[162]	SZ	Intra-data set: (Training/Testing) ACC=87.09%/82.61%, SEN=86.79%/88.00%, SPE=87.22%/76.19%; Inter-data set: (Training/Testing) ACC=83.15%/80.07%, SEN=80.79%/78.65%, SPE=83.63%/81.33%	Private	108 SZ and 121 HCs.	-	Intra- and Inter-dataset/ 10-fold cross-validation
[197]	Psychosis	FEP[8] vs. HC: ACC=75.24% (Contrast), SEN=76.48% (Contrast), SPE=88.02% (Difference of entropy); FEP vs. CHR_NT[9]: ACC=73.21% (Contrast), SEN=79.29% (Difference of entropy), SPE=73.20% (Sum of entropy)	Private	77 FEP, 58 CHR_NT, 15 CHR_T[10], and 44 HCs.	–	10 × 10 nested cross-validation
[203]	SZ- TR	ACC=85.03%, SEN=92.04%, SPE=80.23% (combined model)	Private [162, 224]	148 Schizophrenia Spectrum Disorder participants	After 17.4 - 20.3 days	10-fold cross-validation
[204]	SZ- TR	Training/Validation set ACC=90.91%/91.78%, AUC=0.9318/0.9034	Private	57 SZ (28 responders, 29 non- responders)	After 3.9 weeks	LOOCV
[205]	SZ- TR	r[11]=0.777, RMSE[12]=14.98	Private	57 SZ	After 4 weeks	LOOCV
[216]	SZ- TR	Diagnosis: (Intra/Inter set) ACC=68.37%/64.54%, SEN=71.15%/65.39%, SPE:70.62%/65.71%, AUC=0.64 TR (Intra/Inter set) ACC=71.01%/66.79%, SEN=72.53%/67.39, SPE=71.69%/67.04%, AUC=0.72	Private [162, 225, 226]	191 SZ and 199 HCs. (Diagnosis=390, TR=109)	After 15- 17 days	Intra- and Inter-dataset/ 10-fold cross-validation

Studies investigating schizophrenia spectrum disorders using radiomics have demonstrated a wide range of methodologies. Performance varied significantly across works, often influenced by dataset size, validation, and feature selection depth. For diagnosis, Carrasco et al. [163] reported high accuracy and AUCs using multi-modal radiomic features. However, the small sample size limits generalizability and raises overfitting concerns despite 5-fold cross-validation. In contrast, Cui et al. [162] employed both intra- and inter-dataset validation using a larger sample and functional connectivity features, achieving robust generalization. Shi et al. [165] used a large public dataset with nested 10-fold CV, achieving a balanced performance of ACC=74.02% and AUC=0.808. Bang et al. [161, 164] used texture and shape features from T1 and DTI modalities, identifying the corpus callosum and cerebellar lobules

[8] First-episode Psychosis Patients
[9] High-risk subjects with no later transition to psychosis
[10] Clinical high-risk subjects with later transition to psychosis
[11] Pearson's Correlation Coefficient
[12] Root Mean Square Error

as discriminative regions, achieving accuracy up to 80%. Latha et al. [180] presented strong multi-class classification across SZ, schizoaffective, and HC, with high AUCs and consistent feature importance. Korda et al. [197] extended the analysis to first-episode psychosis and high-risk groups, applying nested cross-validation with texture features, although imbalanced subgroups may bias classification performance. Across the reviewed diagnostic studies, a diverse range of radiomic features were used. The number of selected features varied substantially, from as few as six to over 40 in multi-modal approaches, reflecting differences in imaging modality, feature selection strategy, and model complexity. For TR, Cui et al. [203] integrated cortical morphometry and functional connectivity, achieving 85.03% accuracy, while Xi et al. [204] attained even higher performance ACC = 91.78% and AUC=0.9034 using first-order statistical features from subcortical gray matter. Cui et al. [216] conducted detailed intra- and inter-dataset TR classification using wavelet-based thalamic features, reporting ACC = 71.01%/66.79% and AUC = 0.72. Despite balanced cross-validation, performance dropped in the inter-dataset cohort, suggesting challenges in generalization. Gong et al. [205] approached treatment response prediction achieving a Pearson correlation of 0.777 and RMSE of 14.98, although classification performance was not reported. The brain regions identified across diagnostic and TR studies are primarily involved in emotional regulation, memory processing, sensory integration, and cognitive control. These areas also contribute to functions such as decision-making, social cognition, attention, motor coordination, and language processing. Those regions are the frontal cortex, PCC, thalamus, hippocampus, amygdala, insula, parahippocampus, inferior frontal gyrus, cingulate cortex, temporal and parietal lobes, cerebellum, corpus callosum (posterior segment), and hippocampal subfields. Functional regions such as the default mode network, dorsal fronto-parietal circuits, somatomotor, limbic networks, and caudate nuclei also emerged as relevant across multiple studies.

4.6. Trauma- and Stressor-Related Disorders

The Post-Traumatic Stress Disorder (PTSD) disorder occurs after a traumatic experience and its effects are physical, mental, and cognitive. The patient has negative thoughts and feelings, feelings of stress, increased alertness, and avoidance of situations similar to trauma. These kinds of traumatic events, such as natural disasters, military combat, traffic accidents, and COVID-19, had a crucial role in the increase in PTSD worldwide. Research has shown that neurometabolite alterations in the amygdala and hippocampus are associated with PTSD [227].

The study of Zheng et al. [228] focused on the classification of PTSD in rats, using radiomics. The rats have been chosen not because their brains are identical to the human's, but because they share common structural and functional similarities, especially in brain regions associated with stress and emotion control. In addition, as the current study shows, single-prolonged stress (SPS) rats have a high correlation with the clinical manifestations of PTSD in humans. In the Single Prolonged Stress (SPS) process [229], the rats were restrained for 2 hours, swam for 20 minutes and took a rest for 15 minutes. In the next step, they were exposed to anesthesia until they lost consciousness. When they regained consciousness, they moved into their homes and fed. This procedure was used to manifest PTSD symptoms in rats. In addition, the conducted tests during the experiments were the Morris Water Maze (MWM) and Elevated Plus Maze (EPM) tests.

The authors used T2-weighted images to study the brains of rats during the experiments. The images were preprocessed using anatomical references and stereotaxic coordinates to manually delineate the ROIs in the medial prefrontal cortex (mPFC), and the intensities were normalized as well. In addition, 262 textural radiomics were extracted from the 10 ROIs of the mPFC, using the MaZda v4.6 software. The mPFC has a very important role in regulating stress behaviors. The changes in the structure and functionality of the mPFC can affect the amygdala as a result of an overreaction to fear. In addition, the decrease in volume in mPFC shows a significant parameter for PTSD patients [230, 231, 232, 233, 234]. These extracted features are categorized into the categories of gray-level histogram, GLCM, gray absolute gradient matrices, GRLM and autoregressive model. In addition, for feature selection, Stepwise Discriminant Analysis (SDA) was employed towards identifying parameters of texture, and the LASSO regression was performed in order for the dimensionality to be reduced. The count of selected features ranges from 14-23, for the different periods after the SPS process. For the non-cross-validated SDA classification, the accuracies achieved ranged from 82% to 92% and the cross-validated accuracies ranged from 70% to 84%. The LASSO models achieved AUC values between 0.89 and 0.96. The outcomes of the study provide evidence that by using the radiomic approach, microstructural alterations and dysfunction within the mPFC are strongly associated with PTSD.

The authors also used the SDA and LASSO models to identify the importance of the features. SDA identified significant features by calculating canonical discriminant functions, where their coefficients showed how important they were. LASSO regression further refined feature selection by determining optimal lambda values, penalizing less important features, and reducing their coefficients to zero, retaining only the most important features with non-zero coefficients. The types of those features were: contrast, angscmom, invdfMom, entropy, difVarnc, sumaverg, correlation and difentrp. In conclusion, the textural radiomic features of the GLCM category of the mPFC could be a basis for the diagnosis of PTSD in humans.

The Tables 20 and 21 summarize the key findings and evaluation performance metrics for the PTSD study.

Table 20: Analysis on Trauma and Stressor Related Disorders

Work	Disorder	Selected features	Radiomics	Important Regions	Key Findings
[228]	PTSD	14- 23	Contrast, AngScMom, InvDfMom, Entropy, DifVarnc, SumAverg, Correlation, DifEntrp	mPFC	mPFC's textural radiomic features (GLCM category) were highly significant

Table 21: Experimental validation on Trauma and Stressor Related Disorders

Work	Disorder	Performance	Data	Participants	CV
[228]	PTSD	Non cross-validated/ cross-validated: ACC=86.5%/80.4%, AUC=Up to 0.967	Private	66 rats	10-fold cross-validation

The study by Zheng et al. [228] examined radiomics of PTSD extracted from the mPFC. The private dataset they used, was evaluated using internal cross-validation without an independent test set. The non-cross-validated and cross-validated classification accuracies were 86.5% and 80.4%, respectively, indicating potential overfitting. Also it is reported cross-validated AUCs of 0.944, 0.950, 0.959, and 0.936 for distinguishing control rats from SPS-exposed rats at 1, 4, 7, and 14 days post-stress, respectively, with AUCs ranging from 0.893 to 0.967 for classification between different SPS groups. While the reported AUCs are promising and cross-validation was implemented, the lack of an independent external validation set and the small dataset size may limit the generalizability of the results. Also, the dataset appears relatively balanced among groups (though small sample size overall). The mPFC emerged as a discriminative region, consistent with its known role in self-reflection, decision-making, emotional regulation, and social cognition, functions highly relevant to PTSD.

4.7. Conditions for Further Study

4.7.1. Internet Gaming Disorder

The evolution of Internet technology in recent years has made it an integral part of our daily routine. The Internet enables socializing, communication, knowledge sharing, and much more, including entertainment. Online gaming is a popular option for those who enjoy playing games with others on the Internet. The problem with online gaming is that it is highly addictive, if not used with moderation and self-control, and has become a global concern for mental health, particularly among young people, leading to various psychological negative effects [235, 236]. More specifically, research has shown that people with IGD have high levels of anxiety, depression, substance use disorder, and suicide-related behaviors [237, 238, 239]. In general, patients with Internet Gaming Disorder (IGD) show a high addiction to Internet games that causes a variety of behavioral changes that affect their psychological and cognitive abilities [240, 241]. Furthermore, the IGD was included as a new controversial disorder described in DSM-5 in 2013 [240]. In 2019, the WHO included this disorder in the ICD-11. This highlights the severity of this disorder, its impact on patients, and the seriousness with which psychologists and psychiatrists approach this problem. However, there is a discussion on this issue. According to DSM-5, this condition requires further study before it can be treated as a standalone mental disorder. In contrast, ICD-11 classifies IGD as a behavioral addiction, with multiple similarities and overlapping symptoms with other addictions, such as alcohol or drugs. Regardless of whether IGD is classified as a standalone mental disorder or a subcategory of behavioral disorders, it is a condition that requires a thorough study to develop effective solutions for affected patients. Many researchers have extensively investigated this issue. Based on neuroimaging, studies have found that patients with IGD exhibit larger volumes in certain areas like the striatum, thalamus, hippocampus, and amygdala [242, 243, 244, 240]. In what follows, an examination of radiomic biomarkers for the identification of IGD takes place, while the Tables 22 and 23 summarize the key findings and evaluation performance metrics.

The work presented in [241] shows a combination of T1-weighted and diffusion-tensor MRI images to discriminate IGD from HC patients. The authors focused on identifying the morphometric features of gray matter and the diffusion features of white matter. The T1-weighted MRI images were primarily analyzed using the FreeSurfer software with the "recon-all" processing pipeline, while diffusion-tensor MRI image data were processed by PANDA pipeline, which is based on FSL tools [211]. Features such as surface cortical thickness, geodesic depth, mean, volume, standard deviation, kurtosis, and skewness were extracted from gray matter,

totaling 1316 radiomic features. These features were calculated using Mindboggle after converting the images to surface meshes. Furthermore, 768 white matter-based radiomics were extracted by preprocessing the raw diffusion images into B0 images through affine transformation. The calculated parameters included fractional anisotropy (FA), mean diffusivity (MD), radial diffusivity (RD), and axial diffusivity (AD), with metrics such as mean, standard deviation, kurtosis, and skewness applied to each parameter. The extracted radiomics were 2084. In order for this number to be reduced, the authors used a one-way analysis of variance, and after applying coarse filters the total number was 179. The next step was to implement the Boruta algorithm in order to identify all the relevant features while eliminating noise and redundancy. With this step, the accuracy would be increased. The Random Forest classifier achieved an accuracy score of 73%. The most significant features in this study were the Local thickness, Mean diffusivity, Mean curvature, Mean diffusivity, and the Travel depth. This paper concludes that morphological abnormalities in the brain regions of the bilateral fusiform gyrus, left rostral middle frontal gyrus (rMFG), left cuneus, left parsopercularis, and areas surrounding the right uncinate fasciculus (UF) and left internal capsule (IC), are significant in distinguishing individuals with IGD from HCs. It should be noted that the areas of MFG, IFG, cuneus and fusiform regions are highly associated with reward processing, decision making, and cognitive control [245, 246, 247].

Another work focused on IGD can be found in [240]. The authors used High-resolution T1-weighted MRI for their study. The 3D Slicer software used for preprocessing as far as concern the ROIs selection. The ROIs were from the bilateral caudate nucleus (CAU), amygdala, thalamus, putamen, and hippocampus. Using Pyradiomics [94] for the 3D Slicer, 851 features were extracted for each ROI. Their total was around 8510 and included first-order radiomics, texture, wavelet, and shape features as well. Furthermore, SMOTE technology was used to handle imbalanced data, Z-score scaling for normalization, and Pearson's correlation coefficients to reduce feature redundancy. For feature selection, FeAture Explorer toolkit was used among four selection operators (analysis of variance (ANOVA), Kruskal–Wallis, recursive feature elimination, and relief). In addition, 10 classifiers were applied. The best performance was achieved with the ANOVA-LR method combined with the Logistic Regression (LR). The number of the selected features was 10 and the AUC metric was 0.96 and 0.89 in the training and testing set, respectively. The selected radiomic features were the followings: Complexity (NGTDM), Energy (First-Order), 10th Percentile (First-Order), Skewness (First-Order), Run Length Non-Uniformity (GLRLM), Zone Entropy (GLSZM), Gray-Level Non-Uniformity Normalized (GLSZM), Dependence Entropy (GLDM), Run Entropy (GLRLM), Coarseness (NGTDM), Sum Entropy (GLCM), Difference Entropy (GLCM), Gray-Level Non-Uniformity Normalized (GLRLM), Zone Entropy (GLSZM), Minimum (First-Order), Mean (First-Order), Gray-Level Non-Uniformity Normalized (GLSZM), Dependence Entropy (GLDM), Coarseness (NGTDM), and Zone Entropy (GLSZM). The results indicated that AMY and the right CAU are regions that could provide strong biomarkers for the detection of IGD.

Table 22: Analysis of Conditions for Further Study

Work	Disorder	Selected features	Radiomics	Important Regions	Key Findings
[241]	IGD	8	Local thickness, Mean diffusivity, Mean curvature, Mean diffusivity, Travel depth	Bilateral fusiform gyrus, left rostral, middle frontal gyrus, left cuneus, left parsopercularis, and areas surrounding the right uncinate fasciculus	Alterations in the morphology of the left rMFG, bilateral fusiform, left parsopercularis, left cuneus, right UF and left IC detected while the most significant radiomics were the local thickness and the mean diffusivity. An analytic table is provided in the paper
[240]	IGD	20	Complexity, Energy, Skewness, Zone Entropy	Bilateral caudate nucleus, amygdala, thalamus, putamen, hippocampus	As important features identified the texture and wavelet-based from the amygdala and the right CAU

Table 23: Experimental validation on Conditions for Further Study

Work	Disorder	Performance	Data	Participants	CV
[241]	IGD	ACC=73%, SEN=77%, SPE=68%	Private	59 IGD and 69 HCs.	5-fold cross-validation
[240]	IGD	Training/Test/Validation: AUC=0.961/0.895/0.916, ACC=73%	Private	133 IGD and 110 HCs.	10-fold cross-validation

Regarding the findings on IGD, two studies aimed to distinguish patients from healthy controls using private datasets and cross-validation techniques to reduce overfitting. However, the datasets in both studies had unequal numbers of IGD participants and healthy controls, which could affect model performance. To address this imbalance, Wang et al. [240] applied the SMOTE technique, achieving strong results with an AUC of 0.961 on the training set, 0.895 on the test set, and 0.916 on an independent validation set. The inclusion of a separate validation cohort is particularly important, suggesting their model generalizes well beyond the training data. Their relatively large sample size and use of 10-fold cross-validation further support the robustness of their findings. In contrast, Han et al. [241] did not employ resampling methods such as SMOTE to address dataset imbalance, achieving a mean classification accuracy of 73%, sensitivity of 77%, and specificity of 68% using 5-fold cross-validation. The lack of reported AUC and absence of independent validation in Han et al.'s study limits direct comparison and suggests a higher risk of overfitting or limited generalizability. Based on the findings from those two studies, morphological and texture-based radiomic features appear to exhibit strong discriminative power in identifying IGD. The most important brain regions associated with IGD, based on the above studies, include the bilateral fusiform gyrus, left rMFG, left cuneus, left pars opercularis, UF, left IC, amygdala, and right CAU. Morphological abnormalities in these regions are linked to impairments in language processing, visual attention, and emotional regulation. These areas are related to cognitive control, decision- making, memory, integration of emotional information and they are critical for cognitive tasks.

5. Discussion

5.1. Meta- Analysis of the Literature

The presented works used datasets designated for specific disorders. Most of the studies conducted their research using raw data manually obtained from MRI scanners and provided to them from hospitals, medical centers, or clinics. In addition, those datasets included a small number of data. However, in many cases, the studies mentioned that the data would be available upon request to the authors. Table 24 shows the databases / datasets found during the review. As it can be easily observed, the number of available datasets is quite limited and covers only a few mental disorders. This fact also limits researchers from investigating how radiomic technology combined with AI could potentially be used effectively for the diagnosis of several other disorders. The lack of public datasets covering a broad range of mental disorders poses a significant challenge for researchers. This limitation restricts the exploration of how radiomic technology, combined with AI, could enhance the diagnosis of various conditions.

Table 24: Public Databases/ Datasets used

Databases/ Datasets	Mental disorders	Image types	Participants	Access	Sources
ADHD-200 Consortium Database	ADHD	sMRI, rs-fMRI	776	Public, Requires registration	8 Datasets
ABIDE Database	ASD	sMRI, fMRI	1112 (I), 1114 (II)	Public, Requires registration	ABIDE I and ABIDE II

Continued on next page

Databases/ Datasets	Mental disorders	Image types	Parti- cipants	Access	Sources
SchizConnect Database	Schizophrenia Spectrum and Other Psychotic Disorders	sMRI, fMRI, DTI	490	Public, Requires registration/approval	COBRE, NMorphCH, MCIC
Healthy Brain Network (HBN) Dataset	ADHD, ASD, AD, Depression Disorders, Mood Disorders	sMRI, fMRI, dMRI, EEG	10,000 participants (age: 5–21)	Public, Requires registration/approval	-
NA-MIC Dataset	Schizophrenia Spectrum and Other Psychotic Disorders	sMRI, fMRI, dMRI	10 SZ subjects and 10 HCs	Public, Requires registration	-
COBRE Dataset	Schizophrenia Spectrum and Other Psychotic Disorders	sMRI, fMRI	72 SZ subjects and 75 HCs (age: 18–65)	Public, Requires registration/approval	-

In terms of preprocessing, the most commonly identified tools are summarized in Figure 5. FreeSurfer and CAT12 (SPM) are the most frequently used tools. FreeSurfer provides SBM analysis and high-quality measurements of surface area and cortical thickness, 3D surface reconstruction, as well as parcellation of subcortical regions, among other features. In contrast, the CAT12 toolbox focuses on VBM, making it ideal for whole brain analyses and for exploring gray and white matter changes. Furthermore, DPARSF appears to be the dominant tool for preprocessing rs-fMRI data. Furthermore, PANDA is widely used for the preprocessing of diffusion MRI data, while the CONN toolbox is primarily utilized for preprocessing and analyzing fMRI data, while the 3D Slicer is also used for segmentation.

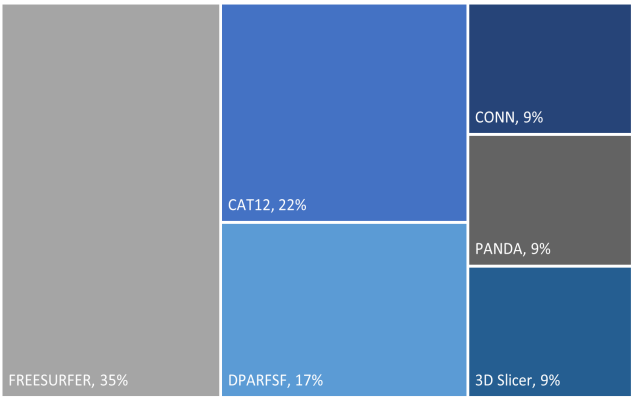

Figure 5: Most used preprocessing toolboxes

Additionally, the majority of the datasets were based on sMRI. As shown in Figure 6, 50% of the studies used sMRI, including T1-weighted, T2-weighted, and 3D-T1 images. Functional MRI and diffusion MRI (including DWI) were also used, with percentages of 18% and 4%, respectively. The pie chart of the figure illustrates the distribution of imaging modalities in studies that employed a single modality. Notably, also included a part for studies that used more than one neuroimaging modality (multimodal), which accounted for 29% [163, 161, 126, 28, 205, 165, 139, 130], making it the second most common approach after sMRI. The breakdown of the multimodal studies indicates that the most frequent combination was sMRI with dMRI (including DTI). This was followed

by the combination of sMRI and fMRI, while only one study was identified that used sMRI in combination with PET. In the reviewed multimodal approaches, sMRI was typically used during preprocessing (brain parcellation, segmentation, ROI etc.) and extraction of structural features, while diffusion and functional imaging contributed modality information such as white matter integrity or functional connectivity. Features from each modality were either combined into a single model or analyzed separately, with some studies applying feature selection independently. Notably, in the study involving PET, radiomic features from both PET and sMRI were extracted and evaluated independently to compare their diagnostic performance. Based on the above, the multimodal integrations aimed to improve classification accuracy by leveraging the complementary information provided by the different modalities. Furthermore, sMRI appears to be the most frequently used standalone modality and also serves as the core component in all multimodal approaches. Notably, every multimodal study included sMRI data, regardless of whether dMRI, fMRI, or PET was also incorporated.

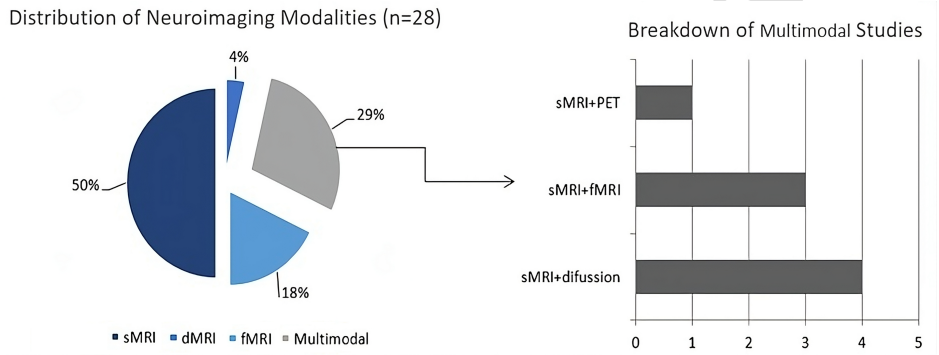

Figure 6: Distribution of neuroimaging modalities

With regard to the atlas most used in the studies, the AAL atlas was the most common. The AAL's ability to balance simplicity and computational efficiency makes it ideal for extracting radiomics from several brain regions. While other atlases, like the Brainnetome, provide more detailed segmentation (246 regions), the AAL (116 regions) significantly reduces computational demands, since the brain segmentation is less detailed compared to other atlases, without meaning that it is not a high-quality segmentation result. This efficiency reduces the total computational cost, making it more accessible for a wide range of studies. Furthermore, the AAL atlas has been widely adopted by neuroimaging preprocessing tools such as FreeSurfer and CAT12, ensuring its compatibility with various pipelines. In addition, the segmented regions provided by the AAL offer sufficient and detailed information about abnormalities in the structure or functionality of key brain regions associated with mental health. All these factors contribute to its frequent use, enhancing the reproducibility between studies, and making the AAL one of the most widely used atlases.

According to the conducted meta-analysis, Pyradiomics [94] is a widely adopted open-source tool for feature extraction from neuroimaging data. The tool supports the extraction of features from several neuroimaging modalities, sMRI, fMRI, and PET. It provides a wide range of radiomics, such as first-order statistics, second-order texture, shape, and higher-order features. Furthermore, its seamless integration into machine learning pipelines makes it an essential tool for radiomics-based research. Its adoption enables robust identification of imaging biomarkers, improving diagnostic precision, and improving understanding of mental disorders.

Furthermore, the analysis showed that LASSO has emerged as one of the most frequent methods for feature selection in radiomics research. Its ability to efficiently reduce high-dimensional datasets by penalizing less relevant features makes LASSO a widely used method for radiomics selection. Alongside LASSO, methods such as RFE and ANOVA played key roles in ensuring that only the most meaningful features were retained for further analysis. RFE is able to remove less significant features, helping to refine the dataset with only significant features, while the ANOVA provided a robust statistical framework for ranking features based on their ability to differentiate between specific classes, offering insights into the most impactful variables. Also, there is no doubt that SVM is the most commonly- used classifier. Other classifiers that achieved high accuracy were RF and XGBoost, while a DL model was reported in only one study [197].

5.2. Scientific Contributions

The conducted meta-analysis, beyond technical findings related to datasets, methods and algorithms, also yielded valuable results in terms of mental health, with a potential for practical investigation and application in mental disorders diagnosis and

treatment response. These critical findings include identified radiomics, and their association with certain brain regions and they have been presented separately for each mental disorder category.

The findings regarding the significance of specific brain regions, as well as the types of important extracted radiomic features, are summarized in the following:

1. Anxiety Disorders: The brain regions found as crucial, are related to emotional regulation, sensory integration, and decision-making. They process also internal body states, sensory and emotional information, and support cognitive control and error detection. These regions also play a role in regulating impulses, processing emotional responses, and contributing to reward-related decision-making. Collectively, they contribute to behaviors related to emotions, cognition, and stress management.
   Key brain regions: Amygdala, bilateral insula, central sulcus, right ACC, and left OFC.
2. Bipolar Disorder: The important regions related to this disorder are related to understanding emotional tone, integrating sensory and emotional information, and regulating social interactions.
   Key brain regions: Left superior temporal pole.
3. Depressive Disorders: The key findings brain regions are essential for visual processing, object and face recognition, scene interpretation, and memory. They have also been linked to emotional regulation, attention management, and potentially motor coordination.
   Key brain regions: Prefrontal cortex, cingulate cortex, amygdala, hippocampus, precuneus, temporal pole, cerebellum, fusiform and occipital gyrus, and pallidum.
4. PTSD: The mPFC is involved in self-reflection, decision-making, and emotional regulation. It plays a key role in social cognition, helping to process social interactions and understand others' emotions.
   Key brain regions: mPFC.
5. IGD: The morphological abnormalities were found in regions associated with visual attention, emotional regulation, and executive control, including areas also linked to speech production and cognitive inhibition. Those contribute also to cognitive control, decision-making, and memory, as well as the integration of emotional and sensory information. They are also important for executive functions and the coordination of motor and cognitive tasks.
   Key brain regions: Left rMFG, bilateral fusiform gyrus, left parsopercularis, left cuneus, right uncinate fasciculus, left internal capsule, amygdala, and right caudate nucleus.
6. ADHD: The regions are critical for ADHD and are associated with auditory processing, language comprehension, and visual perception. They support also motor control processes, spatial awareness, and emotional regulation while contributing to decision-making and sensory integration.
   Key brain regions: Cerebellum, left superior temporal sulcus, right Heschl's gyrus, right cuneus, left precentral gyrus.
7. Autism: The hippocampus is crucial for memory processing, spatial navigation, and emotional regulation. It helps retrieve memories, while also contributing to stress responses and learning.
   Key brain regions: Hippocampus.
8. Schizophrenia spectrum: The detected regions responsible for the diagnosis and also the prediction for the treatment response are associated with emotional regulation, memory processing, sensory integration, and cognitive control. They support also functions like decision-making, social cognition, and attention while contributing to motor coordination and language processing. Collectively, they form a network involved in integrating emotions, memory, and sensory information to guide behavior and thought processes.
   Key brain regions: For diagnosis- thalamus, insula, hippocampus, amygdala, OFC, IFG, cingulate cortex, PCC, temporal lobe, and cerebellum. For treatment response- thalamus, insula, hippocampus, cingulate cortex, temporal lobe, IFG, cerebellum, and striatum (caudate and putamen).

Furthermore, Figure 7 illustrates the distribution of significant features based on their categories. First-order features were the most frequently identified across approaches, followed closely by functional connectivity radiomics and second-order texture features and morphological features appeared less frequently, while higher-order and transform-based features were detected in only a few approaches. Some of the most frequent first-order radiomics according to the conducted review, are kurtosis, mean, entropy, skewness, median and energy. Regarding second-order features, the GLCM, GLRLM, GLSZM, and NGTDM, are identified. The morphological features include shape, volume and area, and the functional connectivity features of ReHo, fALFF, ALFF, RSFC and DC were also detected. Finally, for transform-based features, wavelets were identified, while for higher-order features (diffusion-delivered radiomics), FA and ODI were identified. In conclusion, the radiomic features of the first three categories are distributed slightly equally.

Regarding the papers focusing on treatment response for schizophrenia, it is important to emphasize the significance of the PANSS [183, 248], a scale which already discussed in previous sections. This scale is widely used to assess the severity of symptoms in patients with schizophrenia, with higher scores indicating greater symptom severity. Consequently, PANSS is a tool providing a clear indicator of treatment success. PANSS scores are calculated based on structured clinical questionnaires performed before the treatment (baseline) and again after its completion. In the paper of Cui et al. [203] as responders are defined the patients

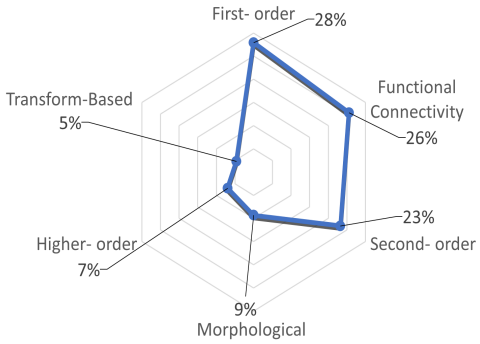

Figure 7: Distribution of radiomics based on their categories

who achieved at least a 30% reduction in PANSS total scores. In their study, responders achieved a 47-57% reduction, while non-responders showed only a 14-16% reduction after approximately 2–3 weeks. Similarly, Cui et al. [216] reported a 51% reduction in responders and a 16% reduction in non-responders after 17 and 16 days. In contrast, Xi et al. [204] used a stricter criterion, defining responders as those achieving more than a 70% reduction in PANSS scores. In this study, responders achieved a mean reduction of 84.7%, while non-responders still exhibited a substantial 51% reduction, with evaluations conducted after approximately 4 weeks of treatment. Furthermore, Gong et al. [205] reported a 67.5% reduction in PANSS scores after 4 weeks in a population of schizophrenia patients with treatment-resistant acute episodes or suicide attempts. These findings show a significant decrease in PANSS scores, which can be observed even in the short term following treatment with ECT combined with antipsychotics, with patients showing early improvements during the first few weeks of treatment. However, although the studies analyzed did not provide long-term data, existing literature supports the view that early symptom reduction is strongly associated with better long-term outcomes in schizophrenia [249]. Meta-analyses have demonstrated that patients who respond early to treatment are more likely to sustain clinical improvements over time. Thus, while the absence of long-term follow-up remains a limitation, the observed short-term improvements still provide meaningful prognostic information. Consequently, early PANSS reduction can be cautiously interpreted as a positive indicator of future clinical stability or even further improvement, although definitive conclusions would require extended long-term follow-up assessments in future studies.

Regarding the dataset- related challenges, the studies included in this review primarily relied on small sample sizes, with only one study [216] utilizing a dataset of 390 participants, which is considered a moderate size. There are several reasons for this limitation in mental health and neuroimaging research. First, recruiting large numbers of participants for studies involving mental health disorders can be challenging due to ethical, financial, and privacy constraints. Although, as highlighted in the introduction, millions of people suffer from mental health disorders, many individuals may be reluctant to participate in research due to the stigma surrounding mental illness or emotional reasons. Additionally, neuroimaging techniques, are costly and require access to specialized equipment and trained personnel, limiting the feasibility of large-scale studies, particularly in regions with fewer resources. This could be a reason for limited availability of large, publicly accessible neuroimaging datasets. As a result, the majority of the authors direct to collect their own small size of data from hospitals or clinics. Furthermore, data collected in clinical environments are typically restricted by privacy regulations and are often only available after a formal request. This is consistently reflected in the data availability statements of the reviewed studies. Furthermore, the limited size of datasets poses significant challenges for AI-based approaches. One of the primary concerns is the increased risk of overfitting, where models capture patterns specific to the training data rather than learning generalizable features. This often results in poor performance on unseen data. Overfitting is a common issue in studies using small sample sizes. Additionally, small datasets often fail to capture the full heterogeneity of mental health disorders, such as variations in symptom severity, reducing the generalizability and clinical relevance of the models. For the first limitation, techniques like the cross- validation or feature selection could me reduce the overfitting risk. Nevertheless, larger datasets are generally preferable, as they offer improved generalizability and robustness. Regarding the second limitation, except from larger, diverse datasets are crucial. Diversity of the data allow models to learn from a broader representation of the population. However, in the current review, the majority of the papers, approximately 79%, used their own data. It could be argued that some diversity in the patient population has been achieved, as not all participants shared the same age, gender, IQ, or severity of symptoms. While this diversity is certainly limited compared to larger datasets, it can still provide valuable insights for the results. Despite these limitations, studies have demonstrated strong methodological design can partly compensate for small sample sizes.

As shown in the tables of Section 4, many studies reported very high classification accuracies. For example, Xi et al. [204] achieved impressive accuracy in distinguishing ECT responders from non-responders, with training and validation accuracies of 90.91% and 91.78%, respectively. However, the dataset used in their study was small, comprising only 57 participants. Small sample sizes inherently increase the risk of overfitting, limiting the model's generalizability. Nevertheless, in the case of Xi et al., the use of LASSO for feature selection and LOOCV for model evaluation helped mitigate this risk. This is further supported by the reported AUC values which were 0.9318 for the training set and 0.9034 for the validation set, indicating a minimal drop in performance and suggesting good generalization. While larger datasets are undoubtedly preferable for developing more generalizable models, this and other studies demonstrate that, with appropriate feature selection and validation strategies, small-sample studies can still produce robust and meaningful results. Even though most of the studies reviewed used small datasets, they consistently employed methodological controls such as ANOVA, MI, 10-fold, and nested cross-validation to reduce overfitting and enhance model stability.

5.3. Limitations and Future Work

While radiomics has shown great promise in identifying neuroimaging biomarkers for mental disorders, this review highlights several critical limitations that must be considered when interpreting the current body of research. One of the most prominent challenges is the methodological heterogeneity across studies. The reviewed works employed varying pipelines for image preprocessing, radiomic feature extraction, feature selection, neuroimaging modalities, and machine learning approaches. Although tools such as PyRadiomics and commonly used atlases like AAL provide a degree of methodological consistency, notable variability remains across studies in terms of segmentation, preprocessing, and the categories of radiomic features extracted and the brain region for each disorder. While some recurring patterns in tools and methods were observed, as noted in the Conclusion, the overall lack of standardization continues to affect reproducibility and complicates the comparability of reported biomarkers and model performance. Furthermore, reproducibility is constrained by the limited availability of public datasets, the majority of studies relied on private datasets, making it difficult to validate or generalize findings across diverse populations. Beyond methodological variation, generalizability also poses a major concern. Many studies, except the fact that they are focused on the same disorders, use datasets with relatively small sizes that can not reflect the diversity of people. While demographic information such as gender, age, and IQ is often included, factors like ethnicity, socioeconomic status, or hereditary background are frequently missing. These factors could be valuable indicators to reflect the occurrence of mental disorders. For this reason, the findings of the studies may not be applicable to subjects with very different characteristics. To address this challenge, larger and more diverse datasets are needed. Moreover, fair machine learning techniques should be applied and validate the model's performance on a variety of different datasets. This approach would ensure consistent performance across all subjects, regardless of their differences.

Although only 28 studies ultimately met the inclusion criteria, this review remains comprehensive in scope, as it systematically examined all DSM-5 mental disorder categories in relation to radiomics and AI applications. The fact that a limited number of studies identified for certain categories (e.g. PTSD, BP, IGD) is not a limitation of the review itself, but reflects the current state of research in this field. This outcome shows the current imbalance in radiomics research across mental disorders and draws attention to categories with limited exploration. By maintaining the DSM-5 framework, the review not only synthesizes available evidence but also exposes critical gaps, providing a roadmap for future research in this emerging field.

Future research in the domain of radiomics and AI for mental disorders has a significant potential to build upon the current findings. As already has been mentioned, most of the studies are based on private datasets acquired from clinics or hospitals. A future study would expand the research to more types of mental disorders, as the studies which have already been reviewed are focusing on a limited number of disorders. As described in the first section, there are several mental disorders categorized in the DSM-5, offering a wide spectrum for research. Another promising research area is related to the investigation of alternative neuroimaging modalities, such as PET or SPECT, which were not identified in the current review, except in a few cases for PET. These types of data could provide useful insights into brain function and potentially reveal unique biomarkers. Although many studies used proprietary datasets, most of these could potentially become available after communicating with the corresponding authors. Another future research direction could explore more ML models which have not been presented, or even deploy DL models such as CNNs. While DL models have shown high performance in many domains, their application in radiomics for mental health introduces new challenges, particularly in the area of XAI.

5.4. Explainable Artificial Intelligence (XAI)

Explainable Artificial Intelligence (XAI) plays a crucial role in ensuring the transparency and interpretability of AI models, especially in sensitive medical fields where decision-making and fairness are essential. XAI refers to a set of techniques that help us understand how an AI model reaches its conclusions, rather than simply presenting a numeric prediction. These methods aim to answer a simple question: "Why did the model make this decision?" The terms transparency and interpretability are central to the concept of XAI. Transparency means being able to look inside the model and understand its structure and logic, instead of treating it as a "black box". Interpretability refers to how easily a human can make sense of the model's outputs. XAI algorithms make it easier for professionals from different scientific fields to understand how and why a model generates its results [250]. This clarity is especially important in mental health, where accurate diagnosis and treatment decisions can have a significant impact on patients' lives. By making the decision-making process visible, XAI increases the reliability of AI models and helps build trust in their use. In mental health applications, the need for interpretability is especially critical. Many mental health conditions are diagnosed based on

symptoms, behaviors, or clinical interviews rather than definitive biological markers. Specialists (e.g., psychiatrists, neurologists, and psychologists) must be able to relate model outputs to established diagnostic frameworks, such as DSM-5. XAI methods must therefore produce explanations that align with clinical reasoning, supporting more informed decisions. Through XAI, specialists can analyze, verify, or challenge AI predictions based on their expertise and knowledge. Ultimately, AI models in mental healthcare should serve as decision-support tools, not as replacements for clinical judgment. The role of XAI is to clearly show the logical and scientific reasoning behind a model's prediction, ensuring that the process is both transparent and trustworthy. In the current review, two types of XAI were identified: SHapley Additive exPlanations (SHAP) and Layer-wise Relevance Propagation (LRP). Specifically, four studies used the SHAP method [81, 79, 164, 161], while one focused on LRP [197]. SHAP, based on game theory, demonstrates how much each feature contributes to the final prediction [95]. LRP, on the other hand, generates relevance scores and heatmaps to visualize influential regions [202]. Both methods offer valuable insights into which features were important and why. Figure 8 illustrates the typical workflow of XAI in psychiatric applications. The process begins with input data such as MRI scans, which are analyzed by ML or DL models to produce diagnostic or predictive outputs. These outputs are then interpreted through explainability techniques like SHAP or LRP. The resulting explanations are clinically reviewed for validity, and the final decision remains with the human expert, who considers both the model's prediction and its justification. The five studies that applied an XAI method represented 17.86% of the reviewed literature. The LRP and SHAP methodologies were introduced in 2015 and 2017, respectively. Among these five studies, the first implementation of an XAI algorithm was published in 2021. Although XAI helps bridge the gap between AI-generated results and trustworthiness, the percentage could be considered low. One likely reason for the limited use of XAI is the combination of technical and practical challenges. Many researchers may not yet be familiar with these methods, as the field lacks standardized tools and evaluation protocols. In some cases, interpretability is viewed as secondary to predictive performance. Furthermore, implementing XAI in high-dimensional domains like brain imaging is particularly demanding. Deep learning models used in neuroimaging are complex, and extracting meaningful explanations from them requires significant computational resources and domain expertise. In addition, the broader field of radiomics in mental health is still emerging, and few studies prioritize explainability during early development. Nevertheless, in sensitive domains like psychiatry, reliability must be defined by more than accuracy alone. Ensuring that models are interpretable as well as accurate is critical to building clinical trust, supporting ethical deployment, and encouraging real-world adoption.

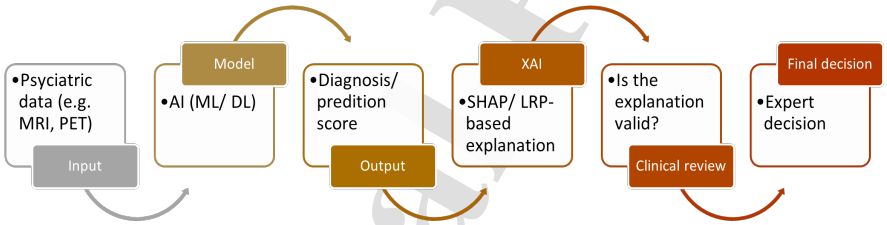

Figure 8: XAI in mental disorders

6. Conclusion

The present review explores the current status of radiomics combined with AI for diagnosing and predicting treatment responses for several mental disorders as classified in the DSM-5. The main constraint of this review lies in the absence of diversity among the investigated mental disorders. Most of the included studies focused on a limited number of disorders or their subtypes. The findings revealed that sMRI was the most commonly used neuroimaging modality. First-order radiomic features were the most frequently detected, while functional connectivity and second-order texture radiomic features showed slightly lower identification frequencies. SVM classifiers were the most commonly used across studies, with toolboxes like FreeSurfer and CAT12 for preprocessing, and Pyradiomics and LASSO for feature extraction and selection, frequently employed. Due to the limited availability of public datasets, most authors generated their own datasets in collaboration with clinics and hospitals. These datasets are often available upon request after communication with the corresponding authors. The use of XAI in mental disorder applications is crucial, as it bridges the gap between AI-generated results and healthcare professionals. Among XAI techniques, SHAP emerged as the most commonly utilized method. Finally, the results of this review suggest that integrating radiomics and AI into clinical practice has significant potential to transform mental health diagnostics and treatment. These technologies could facilitate the identification of early biomarkers for mental disorders, enabling earlier and more accurate diagnoses, as well as personalized treatment plans. However, despite encouraging trends in tool adoption, the lack of standardized pipelines across studies significantly limits the reproducibility findings. Addressing this issue is essential to building generalizable models and facilitating clinical translation.

Informed consent statement

Not applicable.

Declaration of competing interest

The authors declare that they have no known competing financial interests or personal relationships that could have appeared to influence the work reported in this paper.

Data availability

Not applicable.

References

[1] P. Hartmann, A. Ramseier, F. Gudat, M. J. Mihatsch, and W. Polasek. Normal weight of the brain in adults in relation to age, sex, body height and weight. *Der Pathologe*, 15(3):165–170, 1994.

[2] Anil Gulati. Understanding neurogenesis in the adult human brain, 2015. Issue: 6 Pages: 583–584 Publication Title: Indian journal of pharmacology Volume: 47.

[3] Institute for Health Metrics and Evaluation (IHME). Global Burden of Disease Study Results, 2024. = https://vizhub.healthdata.org/gbd-results/.

[4] John J. McGrath, Ali Al-Hamzawi, Jordi Alonso, Yasmin Altwaijri, Laura H. Andrade, Evelyn J. Bromet, Ronny Bruffaerts, José Miguel Caldas de Almeida, Stephanie Chardoul, and Wai Tat Chiu. Age of onset and cumulative risk of mental disorders: a cross-national analysis of population surveys from 29 countries. *The Lancet Psychiatry*, 10(9):668–681, 2023. Publisher: Elsevier.

[5] Daniel J Devoe, Aaron Peterson, and Jean Addington. Negative symptom interventions in youth at risk of psychosis: a systematic review and network meta-analysis. *Schizophrenia bulletin*, 44(4):807–823, 2018.

[6] Wesllei Felipe Heckler, Luan Paris Feijó, Juliano Varella de Carvalho, and Jorge Luis Victória Barbosa. Digital phenotyping for mental health based on data analytics: A systematic literature review. *Artificial intelligence in medicine*, page 103094, 2025.

[7] Mohammadreza Alizadeh, Manoj Tanwar, Amir H Sarrami, Ramin Shahidi, Aparna Singhal, and Houman Sotoudeh. Radiomics; a potential next "omics" in psychiatric disorders; an introduction. *Psychiatry Investigation*, 20(7):583, 2023.

[8] Long-Biao Cui, Xian Xu, and Feng Cao. Building the precision medicine for mental disorders via radiomics/machine learning and neuroimaging. *Frontiers in Neuroscience*, 15:685005, 2021.

[9] Xiao-Hui Wang, Angela Yu, Xia Zhu, Hong Yin, and Long-Biao Cui. Cardiopulmonary comorbidity, radiomics and machine learning, and therapeutic regimens for a cerebral fmri predictor study in psychotic disorders. *Neuroscience Bulletin*, 35:955–957, 2019.

[10] Orkun Aydin, Pinar Unal Aydin, and Ayla Arslan. Development of neuroimaging-based biomarkers in psychiatry. *Frontiers in Psychiatry: Artificial Intelligence, Precision Medicine, and Other Paradigm Shifts*, pages 159–195, 2019.

[11] Ahmed Naguy, Saxby Pridmore, Salem Alwetayan, Dalal Elsori, and Bibi Alamiri. Adhd-a clinician's bird's eye view of current status and new vistas! *Psychopharmacology Bulletin*, 53(1):46, 2023.

[12] Ahmad Chaddad, Jiali Li, Qizong Lu, Yujie Li, Idowu Paul Okuwobi, Camel Tanougast, Christian Desrosiers, and Tamim Niazi. Can autism be diagnosed with artificial intelligence? a narrative review. *Diagnostics*, 11(11):2032, 2021.

[13] Keita Watanabe, Jigar Jogia, and Reiji Yoshimura. Recent developments in neuroimaging in mood disorders. *Frontiers in Psychiatry*, 15:1371347, 2024.

[14] Lin Shi, Weidong Cai, and Feng Feng. Brain-image based computation for supporting clinical decision in neurological and psychiatric disorders, 2021.

[15] Zhi-An Huang, Zexuan Zhu, Chuen Heung Yau, and Kay Chen Tan. Identifying autism spectrum disorder from resting-state fmri using deep belief network. *IEEE Transactions on neural networks and learning systems*, 32(7):2847–2861, 2020.

[16] Rui Liu, Zhi-An Huang, Yao Hu, Zexuan Zhu, Ka-Chun Wong, and Kay Chen Tan. Spatial–temporal co-attention learning for diagnosis of mental disorders from resting-state fmri data. *IEEE transactions on neural networks and learning systems*, 2023.

[17] Benedetta Armocida, Lorenzo Monasta, Susan Sawyer, Flavia Bustreo, Giulia Segafredo, Giulio Castelpietra, Luca Ronfani, Maja Pasovic, Simon Hay, Susan M Sawyer, et al. Burden of non-communicable diseases among adolescents aged 10–24 years in the eu, 1990–2019: a systematic analysis of the global burden of diseases study 2019. *The Lancet Child & Adolescent Health*, 6(6):367–383, 2022.

[18] World Health Organization. Suicide, 2021. = https://www.who.int/news-room/fact-sheets/detail/suicide.

[19] American Foundation for Suicide Prevention (AFSP). Suicide statistics | AFSP, 2024. = https://afsp.org/suicide-statistics/.

[20] Rebecca C Rossom, Karen J Coleman, Brian K Ahmedani, Arne Beck, Eric Johnson, Malia Oliver, and Greg E Simon. Suicidal ideation reported on the phq9 and risk of suicidal behavior across age groups. *Journal of affective disorders*, 215:77–84, 2017.

[21] Elizabeth Reisinger Walker, Robin E. McGee, and Benjamin G. Druss. Mortality in mental disorders and global disease burden implications: a systematic review and meta-analysis. *JAMA psychiatry*, 72(4):334–341, 2015. Publisher: American Medical Association.

[22] Joe Kwun Nam Chan, Christoph U Correll, Corine Sau Man Wong, Ryan Sai Ting Chu, Vivian Shi Cheng Fung, Gabbie Hou Sem Wong, Janet Hiu Ching Lei, and Wing Chung Chang. Life expectancy and years of potential life lost in people with mental disorders: a systematic review and meta-analysis. *EClinicalMedicine*, 65, 2023.

[23] DSMTF American Psychiatric Association, DS American Psychiatric Association, et al. *Diagnostic and statistical manual of mental disorders: DSM-5*. American psychiatric association Washington, DC, 2013.

[24] Chi-Shin Wu, Chien-Hung Chen, Chu-Hsien Su, Yi-Ling Chien, Hong-Jie Dai, and Hsin-Hsi Chen. Augmenting dsm-5 diagnostic criteria with self-attention-based bilstm models for psychiatric diagnosis. *Artificial Intelligence in Medicine*, 136:102488, 2023.

[25] Carl C. Bell. DSM-IV: diagnostic and statistical manual of mental disorders. *Jama*, 272(10):828–829, 1994. Publisher: American Medical Association.

[26] Michael B. First M.D. *DSM-5-TR® Handbook of Differential Diagnosis*. American Psychiatric Pub, January 2024. Google-Books-ID: MTfxEAAAQBAJ.

[27] World Health Organization. Anxiety disorders fact sheet, 2024. url = https://www.who.int/news-room/fact-sheets/detail/anxiety-disorders.

[28] Huan Ma, Dafu Zhang, Dewei Sun, Hongbo Wang, and Jianzhong Yang. Gray and white matter structural examination for diagnosis of major depressive disorder and subthreshold depression in adolescents and young adults: a preliminary radiomics analysis. *BMC Medical Imaging*, 22(1):164, 2022.

[29] World Health Organization. Depression fact sheet, 2024. url = https://www.who.int/news-room/fact-sheets/detail/depression.

[30] World Health Organization. Bipolar disorder fact sheet, 2024. url = https://www.who.int/news-room/fact-sheets/detail/bipolar-disorder.

[31] World Health Organization. Schizophrenia fact sheet, 2024. url = https://www.who.int/news-room/fact-sheets/detail/schizophrenia.

[32] Fiona Charlson, Mark van Ommeren, Abraham Flaxman, Joseph Cornett, Harvey Whiteford, and Shekhar Saxena. New WHO prevalence estimates of mental disorders in conflict settings: a systematic review and meta-analysis. *The Lancet*, 394(10194):240–248, 2019. Publisher: Elsevier.

[33] World Health Organization. Autism spectrum disorders fact sheet, 2024. url = https://www.who.int/news-room/fact-sheets/detail/autism-spectrum-disorders.

[34] Ajay P Singh, Vansh S Jain, and J Yu John-Paul. Diffusion radiomics for subtyping and clustering in autism spectrum disorder: A preclinical study. *Magnetic resonance imaging*, 96:116–125, 2023.

[35] Ahmad Chaddad, Christian Desrosiers, and Matthew Toews. Multi-scale radiomic analysis of sub-cortical regions in mri related to autism, gender and age. *Scientific reports*, 7(1):45639, 2017.

[36] World Health Organization. Mental disorders - fact sheet, 2023. url = https://www.who.int/news-room/fact-sheets/detail/mental-disorders?

[37] Steven Walker. *Modern Mental Health: Critical Perspectives on Psychiatric Practice*. Taylor & Francis, 2025.

[38] J. Anthony Seibert. X-ray imaging physics for nuclear medicine technologists. Part 1: Basic principles of x-ray production. *Journal of nuclear medicine technology*, 32(3):139–147, 2004. Publisher: Soc Nuclear Med.

[39] Egwonor Loveth Irede, Omowunmi Rebecca Aworinde, Ogunnaike Korede Lekan, Osemudiamhen D Amienghemhen, Tochukwu Perpetua Okonkwo, Asishana Paul Onivefu, and Ikhazuagbe H Ifijen. Medical imaging: a critical review on x-ray imaging for the detection of infection. *Biomedical Materials & Devices*, pages 1–45, 2024.

[40] Md Shariful Alam, Dadong Wang, and Arcot Sowmya. Amfp-net: Adaptive multi-scale feature pyramid network for diagnosis of pneumoconiosis from chest x-ray images. *Artificial Intelligence in Medicine*, 154:102917, 2024.

[41] Caroline C Rodgers. Low-dose x-ray imaging may increase the risk of neurodegenerative diseases. *Medical hypotheses*, 142:109726, 2020.

[42] Wilhelm Conrad Röntgen. Discovery of X-rays. In *A Century of X-Rays and Radioactivity in Medicine*, pages 1–9. CRC Press, 2018.

[43] Toshihiro Sera. Computed Tomography. In Kohei Soga, Masakazu Umezawa, and Kyohei Okubo, editors, *Transparency in Biology: Making the Invisible Visible*, pages 167–187. Springer, Singapore, 2021.

[44] Aidan K Tirpack, Danyaal G Buttar, and Mandeep Kaur. Advancement in utilization of magnetic resonance imaging and biomarkers in the understanding of schizophrenia. *World Journal of Clinical Cases*, 13(1):96578, 2025.

[45] Beomsue Kim, Hongmin Kim, Songhui Kim, and Young-ran Hwang. A brief review of non-invasive brain imaging technologies and the near-infrared optical bioimaging. *Appl. Microsc.*, 51(1):9, December 2021.

[46] Denis Le Bihan, Jean-François Mangin, Cyril Poupon, Chris A. Clark, Sabina Pappata, Nicolas Molko, and Hughes Chabriat. Diffusion tensor imaging: Concepts and applications. *Magnetic Resonance Imaging*, 13(4):534–546, April 2001.

[47] Maija Pihlajamaki, Anne M. Jauhiainen, and Hilkka Soininen. Structural and functional MRI in mild cognitive impairment. *Current Alzheimer Research*, 6(2):179–185, 2009. Publisher: Bentham Science Publishers.

[48] M Chau, H Vu, T Debnath, and MG Rahman. A scoping review of automatic and semi-automatic mri segmentation in human brain imaging. *Radiography*, 31(2):102878, 2025.

[49] Michael P. Hartung, Thomas M. Grist, and Christopher J. François. Magnetic resonance angiography: current status and future directions. *Journal of Cardiovascular Magnetic Resonance*, 13(1):19, 2011. Publisher: Elsevier.

[50] Tommaso Ciceri, Letizia Squarcina, Alice Giubergia, Alessandra Bertoldo, Paolo Brambilla, and Denis Peruzzo. Review on deep learning fetal brain segmentation from magnetic resonance images. *Artificial intelligence in medicine*, 143:102608, 2023.

[51] Ranjeet Ranjan Jha, Arvind Muralie, Munish Daroch, Arnav Bhavsar, and Aditya Nigam. Enhancing autism spectrum disorder identification in multi-site mri imaging: A multi-head cross-attention and multi-context approach for addressing variability in un-harmonized data. *Artificial Intelligence in Medicine*, 157:102998, 2024.

[52] Y. F. Tai and P. Piccini. Applications of positron emission tomography (PET) in neurology. *Journal of Neurology, Neurosurgery & Psychiatry*, 75(5):669–676, 2004. Publisher: BMJ Publishing Group Ltd.

[53] Nicole R Zürcher, Jingyuan E Chen, and Hsiao-Ying Wey. Pet-mri applications and future prospects in psychiatry. *Journal of Magnetic Resonance Imaging*, 61(2):568–578, 2025.

[54] S. M. Landau, B. A. Thomas, L. Thurfjell, M. Schmidt, R. Margolin, M. Mintun, M. Pontecorvo, S. L. Baker, W. J. Jagust, and Alzheimer's Disease Neuroimaging Initiative. Amyloid PET imaging in Alzheimer's disease: a comparison of three radiotracers. *European journal of nuclear medicine and molecular imaging*, 41:1398–1407, 2014. Publisher: Springer.

[55] Yulin Wang, Wanchen Liao, Lei Wang, Jun Li, Dongqing Huang, Weibin Cheng, Junzhang Tian, and Ping Luan. Advance and prospect of positron emission tomography in alzheimer's disease research. *Molecular Psychiatry*, pages 1–11, 2025.

[56] Antoine Rogeau, Anne Jetske Boer, Eric Guedj, Arianna Sala, Iris E Sommer, Mattia Veronese, Monique van der Weijden-Germann, EANM Neuroimaging Committee Van Weehaeghe Donatienne Cecchin Diego Verger Antoine Albert Nathalie L. Brendel Matthias Yakushev Igor

Traub-Weidinger Tatjana Barthel Henryk Tolboom Nelleke, and Francesco Fraioli. Eanm perspective on clinical pet and spect imaging in schizophrenia-spectrum disorders: a systematic review of longitudinal studies. *European journal of nuclear medicine and molecular imaging*, 52(3):876–899, 2025.

[57] Tyler Wilson, Wesley Gohn, Francesc Massanes, Maximilian Reymann, and Hans Vija. SPECT simulation of a digital anthropomorphic brain phantom. In *Medical Imaging 2022: Physics of Medical Imaging*, volume 12031, pages 976–978. SPIE, 2022.

[58] Xiu Luo, Xiao Li, and Chang-Jing Zuo. SPECT Imaging with Tc-99m-labeled HYNIC-FAPI-04 to Extend the Differential Time Window in Evaluating Tumorous Fibrosis, 2023.

[59] Rui Wang, Debin Zhang, Yifan Hu, Zhenlei Lyu, and Tianyu Ma. High-sensitivity cardiac SPECT system design with collimator-less interspaced mosaic-patterned scintillators. *Frontiers in Medicine*, 10:1145351, 2023. Publisher: Frontiers.

[60] Takashi Ikeda, Kazuhiro Kitajima, Tatsuya Tsuchitani, Yoshiyuki Takahashi, Yasuhiko Hama, and Noriko Kotura. Effectiveness of quantitative bone SPECT/CT for bone metastasis diagnosis. *Hellenic Journal of Nuclear Medicine*, pages s002449912513–s002449912513, 2022.

[61] Philippe Lambin, Emmanuel Rios-Velazquez, Ralph Leijenaar, Sara Carvalho, Ruud GPM Van Stiphout, Patrick Granton, Catharina ML Zegers, Robert Gillies, Ronald Boellard, and André Dekker. Radiomics: extracting more information from medical images using advanced feature analysis. *European journal of cancer*, 48(4):441–446, 2012. Publisher: Elsevier.

[62] Robert J. Gillies, Paul E. Kinahan, and Hedvig Hricak. Radiomics: Images Are More than Pictures, They Are Data. *Radiology*, 278(2):563–577, February 2016.

[63] Mohammadreza Alizadeh, Manoj Tanwar, Amir H. Sarrami, Ramin Shahidi, Aparna Singhal, and Houman Sotoudeh. Radiomics; A Potential Next "Omics" in Psychiatric Disorders; An Introduction. *Psychiatry Investigation*, 20(7):583, 2023. Publisher: Korean Neuropsychiatric Association.

[64] Janita E Van Timmeren, Davide Cester, Stephanie Tanadini-Lang, Hatem Alkadhi, and Bettina Baessler. Radiomics in medical imaging—"how-to" guide and critical reflection. *Insights into imaging*, 11(1):91, 2020.

[65] Alican Kuran, Aytaç Üzel, Oğuz Baysal, Umut Seki, and Enver Alper Sinanoğlu. Repeatability of radiomics parameters in cone beam computed tomography volumes. *Chinese Journal of Academic Radiology*, pages 1–11, 2025.

[66] Xingping Zhang, Yanchun Zhang, Guijuan Zhang, Xingting Qiu, Wenjun Tan, Xiaoxia Yin, and Liefa Liao. Deep learning with radiomics for disease diagnosis and treatment: challenges and potential. *Frontiers in oncology*, 12:773840, 2022.

[67] Chunlei Liu, Nicole E Murphy, and Wei Li. Probing white-matter microstructure with higher-order diffusion tensors and susceptibility tensor mri. *Frontiers in integrative neuroscience*, 7:11, 2013.

[68] Mohammad Hasan Sarwer, Tui Rani Saha, Shake Ibna Abir, Shaharina Shoha, Md Miraj Hossain, Nigar Sultana, Shariar Islam Saimon, Intiser Islam, Mahmud Hasan, and Sarder Abdulla Al Shiam. Eeg functional connectivity and deep learning for automated diagnosis of alzheimer's disease and schizophrenia. *Journal of Computer Science and Technology Studies*, 7(1):82–99, 2025.

[69] Houman Sotoudeh, Amir Hossein Sarrami, Glenn H Roberson, Omid Shafaat, Zahra Sadaatpour, Ali Rezaei, Gagandeep Choudhary, Aparna Singhal, Ehsan Sotoudeh, and Manoj Tanwar. Emerging applications of radiomics in neurological disorders: a review. *Cureus*, 13(12), 2021.

[70] Baihua Zhang, Shouliang Qi, Xiaohuan Pan, Chen Li, Yudong Yao, Wei Qian, and Yubao Guan. Deep cnn model using ct radiomics feature mapping recognizes egfr gene mutation status of lung adenocarcinoma. *Frontiers in Oncology*, 10:598721, 2021.

[71] Cameron Severn, Krithika Suresh, Carsten Görg, Yoon Seong Choi, Rajan Jain, and Debashis Ghosh. A pipeline for the implementation and visualization of explainable machine learning for medical imaging using radiomics features. *Sensors*, 22(14):5205, 2022.

[72] Matthew J Page, Joanne E McKenzie, Patrick M Bossuyt, Isabelle Boutron, Tammy C Hoffmann, Cynthia D Mulrow, Larissa Shamseer, Jennifer M Tetzlaff, Elie A Akl, Sue E Brennan, et al. The prisma 2020 statement: an updated guideline for reporting systematic reviews. *bmj*, 372, 2021.

[73] Elizabeth R Duval, Arash Javanbakht, and Israel Liberzon. Neural circuits in anxiety and stress disorders: a focused review. *Therapeutics and clinical risk management*, pages 115–126, 2015.

[74] Qingfeng Li, Wenzheng Wang, and Zhishan Hu. Amygdala's t1-weighted image radiomics outperforms volume for differentiation of anxiety disorder and its subtype. *Frontiers in Psychiatry*, 14:1091730, 2023.

[75] Nataliya V Zharova, Artem S Osadchiy, Anastasia K Lobanova, Tatyana A Isakova, Nikolay A Zharov, Yury O Zharikov, André Pontes-Silva, and Tatiana S Zharikova. Functional anatomy of the structures of the limbic system involved in the development of neuropsychiatric disorders: A review. *Current Behavioral Neuroscience Reports*, 12(1):1–13, 2025.

[76] Leigh C Walker. A balancing act: The role of pro-and anti-stress peptides within the central amygdala in anxiety and alcohol use disorders. *Journal of neurochemistry*, 157(5):1615–1643, 2021.

[77] Jennifer YF Lau, David Goldman, Beata Buzas, Colin Hodgkinson, Ellen Leibenluft, Eric Nelson, Lindsey Sankin, Daniel S Pine, and Monique Ernst. Bdnf gene polymorphism (val66met) predicts amygdala and anterior hippocampus responses to emotional faces in anxious and depressed adolescents. *Neuroimage*, 53(3):952–961, 2010.

[78] Pankaj Sah. Fear, anxiety, and the amygdala. *Neuron*, 96(1):1–2, 2017.

[79] Byung-Hoon Kim, Min-Kyeong Kim, Hye-Jeong Jo, and Jae-Jin Kim. Predicting social anxiety in young adults with machine learning of resting-state brain functional radiomic features. *Scientific reports*, 12(1):13932, 2022.

[80] Lisa M Shin and Israel Liberzon. The neurocircuitry of fear, stress, and anxiety disorders. *Neuropsychopharmacology*, 35(1):169–191, 2010.

[81] Minji Bang, Yae Won Park, Jihwan Eom, Sung Soo Ahn, Jinna Kim, Seung-Koo Lee, and Sang-Hyuk Lee. An interpretable radiomics model for the diagnosis of panic disorder with or without agoraphobia using magnetic resonance imaging. *Journal of affective disorders*, 305:47–54, 2022.

[82] Amy B Locke, Nell Kirst, and Cameron G Shultz. Diagnosis and management of generalized anxiety disorder and panic disorder in adults. *American family physician*, 91(9):617–624, 2015.

[83] Thomas Dresler, Anne Guhn, Sara V Tupak, Ann-Christine Ehlis, Martin J Herrmann, Andreas J Fallgatter, Jürgen Deckert, and Katharina Domschke. Revise the revised? new dimensions of the neuroanatomical hypothesis of panic disorder. *Journal of neural transmission*,

120:3–29, 2013.

[84] Takeshi Asami, Ryota Nakamura, Masao Takaishi, Haruhisa Yoshida, Asuka Yoshimi, Thomas J Whitford, and Yoshio Hirayasu. Smaller volumes in the lateral and basal nuclei of the amygdala in patients with panic disorder. *PLoS One*, 13(11):e0207163, 2018.

[85] LR Demenescu, R Kortekaas, HR Cremers, RJ Renken, MJ Van Tol, NJA Van Der Wee, DJ Veltman, JA Den Boer, K Roelofs, and A Aleman. Amygdala activation and its functional connectivity during perception of emotional faces in social phobia and panic disorder. *Journal of psychiatric research*, 47(8):1024–1031, 2013.

[86] Fumi Hayano, Motoaki Nakamura, Takeshi Asami, Kumi Uehara, Takeshi Yoshida, Tomohide Roppongi, Tatsui Otsuka, Tomio Inoue, and Yoshio Hirayasu. Smaller amygdala is associated with anxiety in patients with panic disorder. *Psychiatry and clinical neurosciences*, 63(3):266–276, 2009.

[87] Judith Domínguez-Pérez, Wenceslao Peñate-Castro, and Francisco Luis Rivero-Pérez. Neural mechanisms of cognitive behavioral therapy efficacy in anxiety disorders: A scoping review of fmri-based studies that tested the dual model. *Life*, 15(3):493, 2025.

[88] Stefan Daniel Paul Dalton, Holly Cooper, Ben Jennings, and Survjit Cheeta. Neural correlates of implicit emotion regulation in mood and anxiety disorders: an fmri meta-analytic review. *Scientific Reports*, 15(1):1–17, 2025.

[89] Eun-Kyoung Kang, Kang Soo Lee, and Sang-Hyuk Lee. Reduced cortical thickness in the temporal pole, insula, and pars triangularis in patients with panic disorder. *Yonsei medical journal*, 58(5):1018, 2017.

[90] Chien-Han Lai and Yu-Te Wu. Fronto-temporo-insula gray matter alterations of first-episode, drug-naive and very late-onset panic disorder patients. *Journal of affective disorders*, 140(3):285–291, 2012.

[91] Ricardo R Uchida, Cristina M Del-Ben, Geraldo F Busatto, Fábio LS Duran, Francisco S Guimarães, José AS Crippa, David Araújo, Antonio C Santos, and Frederico G Graeff. Regional gray matter abnormalities in panic disorder: a voxel-based morphometry study. *Psychiatry Research: Neuroimaging*, 163(1):21–29, 2008.

[92] Takeshi Asami, Hidenori Yamasue, Fumi Hayano, Motoaki Nakamura, Kumi Uehara, Tatsui Otsuka, Tomohide Roppongi, Namiko Nihashi, Tomio Inoue, and Yoshio Hirayasu. Sexually dimorphic gray matter volume reduction in patients with panic disorder. *Psychiatry Research: Neuroimaging*, 173(2):128–134, 2009.

[93] Takeshi Asami, Fumi Hayano, Motoaki Nakamura, Hidenori Yamasue, Kumi Uehara, Tatsui Otsuka, Tomohide Roppongi, Namiko Nihashi, Tomio Inoue, and Yoshio Hirayasu. Anterior cingulate cortex volume reduction in patients with panic disorder. *Psychiatry and clinical neurosciences*, 62(3):322–330, 2008.

[94] Joost JM Van Griethuysen, Andriy Fedorov, Chintan Parmar, Ahmed Hosny, Nicole Aucoin, Vivek Narayan, Regina GH Beets-Tan, Jean-Christophe Fillion-Robin, Steve Pieper, and Hugo JWL Aerts. Computational radiomics system to decode the radiographic phenotype. *Cancer research*, 77(21):e104–e107, 2017.

[95] Scott Lundberg. A unified approach to interpreting model predictions. *arXiv preprint arXiv:1705.07874*, 2017.

[96] American Psychiatric Association et al. Diagnostic and statistical manual of mental disorders. *Text revision*, 2000.

[97] Antoine Bechara, Hanna Damasio, and Antonio R Damasio. Emotion, decision making and the orbitofrontal cortex. *Cerebral cortex*, 10(3):295–307, 2000.

[98] Vahid Nejati, Jamal Amani Rad, and Amir Hosein Hadian Rasanan. Neuromodulation of risk and reward processing during decision making in individuals with general anxiety disorder (gad). *Scientific Reports*, 15(1):371, 2025.

[99] Mohammed R Milad and Scott L Rauch. The role of the orbitofrontal cortex in anxiety disorders. *Annals of the new York Academy of Sciences*, 1121(1):546–561, 2007.

[100] Oscar Esteban, Christopher J Markiewicz, Ross W Blair, Craig A Moodie, A Ilkay Isik, Asier Erramuzpe, James D Kent, Mathias Goncalves, Elizabeth DuPre, Madeleine Snyder, et al. fmriprep: a robust preprocessing pipeline for functional mri. *Nature methods*, 16(1):111–116, 2019.

[101] Krzysztof Gorgolewski, Christopher D Burns, Cindee Madison, Dav Clark, Yaroslav O Halchenko, Michael L Waskom, and Satrajit S Ghosh. Nipype: a flexible, lightweight and extensible neuroimaging data processing framework in python. *Frontiers in neuroinformatics*, 5:12318, 2011.

[102] Robert W Cox. Afni: software for analysis and visualization of functional magnetic resonance neuroimages. *Computers and Biomedical research*, 29(3):162–173, 1996.

[103] Christian Gaser, Robert Dahnke, Paul M Thompson, Florian Kurth, Eileen Luders, Alzheimer's Disease Neuroimaging Initiative, et al. Cat: a computational anatomy toolbox for the analysis of structural mri data. *GigaScience*, 13:giae049, 2024.

[104] Bruce Fischl. Freesurfer. *Neuroimage*, 62(2):774–781, 2012.

[105] Bruce Fischl, David H Salat, Evelina Busa, Marilyn Albert, Megan Dieterich, Christian Haselgrove, Andre Van Der Kouwe, Ron Killiany, David Kennedy, Shuna Klaveness, et al. Whole brain segmentation: automated labeling of neuroanatomical structures in the human brain. *Neuron*, 33(3):341–355, 2002.

[106] Lindsay M Alexander, Jasmine Escalera, Lei Ai, Charissa Andreotti, Karina Febre, Alexander Mangone, Natan Vega-Potler, Nicolas Langer, Alexis Alexander, Meagan Kovacs, et al. An open resource for transdiagnostic research in pediatric mental health and learning disorders. *Scientific data*, 4(1):1–26, 2017.

[107] Colin D Mathers, Kim M Iburg, and Stephen Begg. Adjusting for dependent comorbidity in the calculation of healthy life expectancy. *Population Health Metrics*, 4:1–12, 2006.

[108] Kathleen R Merikangas, Robert Jin, Jian-Ping He, Ronald C Kessler, Sing Lee, Nancy A Sampson, Maria Carmen Viana, Laura Helena Andrade, Chiyi Hu, Elie G Karam, et al. Prevalence and correlates of bipolar spectrum disorder in the world mental health survey initiative. *Archives of general psychiatry*, 68(3):241–251, 2011.

[109] Ying Wang, Kai Sun, Zhenyu Liu, Guanmao Chen, Yanbin Jia, Shuming Zhong, Jiyang Pan, Li Huang, and Jie Tian. Classification of unmedicated bipolar disorder using whole-brain functional activity and connectivity: a radiomics analysis. *Cerebral Cortex*, 30(3):1117–1128, 2020.

[110] Mary L Phillips and Holly A Swartz. A critical appraisal of neuroimaging studies of bipolar disorder: toward a new conceptualization of underlying neural circuitry and a road map for future research. *American Journal of Psychiatry*, 171(8):829–843, 2014.
[111] Junyan Wang, Penghong Liu, Aixia Zhang, Chunxia Yang, Sha Liu, Jizhi Wang, Yong Xu, and Ning Sun. Specific gray matter volume changes of the brain in unipolar and bipolar depression. *Frontiers in Human Neuroscience*, 14:592419, 2021.
[112] Ying Wang, Shuming Zhong, Guanmao Chen, Tao Liu, Lianping Zhao, Yao Sun, Yanbin Jia, and Li Huang. Altered cerebellar functional connectivity in remitted bipolar disorder: a resting-state functional magnetic resonance imaging study. *Australian & New Zealand Journal of Psychiatry*, 52(10):962–971, 2018.
[113] Jianfeng Zhang, Paola Magioncalda, Zirui Huang, Zhonglin Tan, Xiwen Hu, Zhiguo Hu, Benedetta Conio, Mario Amore, Matilde Inglese, Matteo Martino, et al. Altered global signal topography and its different regional localization in motor cortex and hippocampus in mania and depression. *Schizophrenia bulletin*, 45(4):902–910, 2019.
[114] Paola Magioncalda, Matteo Martino, Benedetta Conio, Andrea Escelsior, Niccolò Piaggio, Andrea Presta, Valentina Marozzi, Giulio Rocchi, Loris Anastasio, Linda Vassallo, et al. Functional connectivity and neuronal variability of resting state activity in bipolar disorder—reduction and decoupling in anterior cortical midline structures. *Human brain mapping*, 36(2):666–682, 2015.
[115] Ying Wang, Shuming Zhong, Yanbin Jia, Yao Sun, Bing Wang, Tao Liu, Jiyang Pan, and Li Huang. Disrupted resting-state functional connectivity in nonmedicated bipolar disorder. *Radiology*, 280(2):529–536, 2016.
[116] Matteo Martino, Paola Magioncalda, Zirui Huang, Benedetta Conio, Niccolò Piaggio, Niall W Duncan, Giulio Rocchi, Andrea Escelsior, Valentina Marozzi, Annemarie Wolff, et al. Contrasting variability patterns in the default mode and sensorimotor networks balance in bipolar depression and mania. *Proceedings of the National Academy of Sciences*, 113(17):4824–4829, 2016.
[117] Cristian Vargas, Carlos López-Jaramillo, and Eduard Vieta. A systematic literature review of resting state network—functional mri in bipolar disorder. *Journal of affective disorders*, 150(3):727–735, 2013.
[118] Gaelle E Doucet, Danielle S Bassett, Nailin Yao, David C Glahn, and Sophia Frangou. The role of intrinsic brain functional connectivity in vulnerability and resilience to bipolar disorder. *American Journal of Psychiatry*, 174(12):1214–1222, 2017.
[119] Sabrina K Syan, Mara Smith, Benicio N Frey, Raheem Remtulla, Flavio Kapczinski, Geoffrey BC Hall, and Luciano Minuzzi. Resting-state functional connectivity in individuals with bipolar disorder during clinical remission: a systematic review. *Journal of Psychiatry and Neuroscience*, 43(5):298–316, 2018.
[120] Chaogan Yan and Yufeng Zang. Dparsf: a matlab toolbox for" pipeline" data analysis of resting-state fmri. *Frontiers in systems neuroscience*, 4:1377, 2010.
[121] Sihong Huang, Jungong Han, Hairong Zheng, Mengjun Li, Chuxin Huang, Xiaoyan Kui, and Jun Liu. Structural and functional connectivity of the whole brain and subnetworks in individuals with mild traumatic brain injury: predictors of patient prognosis. *Neural Regeneration Research*, 19(7):1553–1558, 2024.
[122] Xi-Nian Zuo, Clare Kelly, Adriana Di Martino, Maarten Mennes, Daniel S Margulies, Saroja Bangaru, Rebecca Grzadzinski, Alan C Evans, Yu-Feng Zang, F Xavier Castellanos, et al. Growing together and growing apart: regional and sex differences in the lifespan developmental trajectories of functional homotopy. *Journal of Neuroscience*, 30(45):15034–15043, 2010.
[123] Xuewei Qin, Xuanling Chen, Lan Yao, Fa Lu, Zhenhu Liang, Jianghong He, Xiangyang Guo, and Xiaoli Li. Differential brain activity in patients with disorders of consciousness: a 3-month rs-fmri study using amplitude of low-frequency fluctuation. *Frontiers in Neurology*, 15:1477596, 2024.
[124] Wensheng Chen, Guojun Xie, Caixia Xu, Jiaquan Liang, and Chunguo Zhang. The relationship between regional homogeneity in resting-state functional magnetic resonance imaging and cognitive function in depressive disorders with migraine. *Scientific Reports*, 15(1):11810, 2025.
[125] Huan Ma, Jing Yuan, Yao Wang, Dafu Zhang, Yingying Ding, Xiaoyong Zhang, Kun Li, and Jianzhong Yang. Combat harmonization of radiomics features to improve the diagnostic accuracy of major depressive disorder and subthreshold depression in adolescents with brain multiscale structural mri. *Asian journal of psychiatry*, 86:103681, 2023.
[126] Kai Sun, Zhenyu Liu, Guanmao Chen, Zhifeng Zhou, Shuming Zhong, Zhenchao Tang, Shuo Wang, Guifei Zhou, Xuezhi Zhou, Lizhi Shao, et al. A two-center radiomic analysis for differentiating major depressive disorder using multi-modality mri data under different parcellation methods. *Journal of affective disorders*, 300:1–9, 2022.
[127] Lixia Tian, Lin Ma, and Linlin Wang. Alterations of functional connectivities from early to middle adulthood: clues from multivariate pattern analysis of resting-state fmri data. *Neuroimage*, 129:389–400, 2016.
[128] Jean-Philippe Fortin, Nicholas Cullen, Yvette I Sheline, Warren D Taylor, Irem Aselcioglu, Philip A Cook, Phil Adams, Crystal Cooper, Maurizio Fava, Patrick J McGrath, et al. Harmonization of cortical thickness measurements across scanners and sites. *Neuroimage*, 167:104–120, 2018.
[129] W Evan Johnson, Cheng Li, and Ariel Rabinovic. Adjusting batch effects in microarray expression data using empirical bayes methods. *Biostatistics*, 8(1):118–127, 2007.
[130] Bo Zhang, Shuang Liu, Xiaoya Liu, Sitong Chen, Yufeng Ke, Shouliang Qi, Xinhua Wei, and Dong Ming. Discriminating subclinical depression from major depression using multi-scale brain functional features: a radiomics analysis. *Journal of Affective Disorders*, 297:542–552, 2022.
[131] Loretxu Bergouignan, Marie Chupin, Yvonne Czechowska, Serge Kinkingnéhun, Cédric Lemogne, Guillaume Le Bastard, Martin Lepage, Line Garnero, Olivier Colliot, and Philippe Fossati. Can voxel based morphometry, manual segmentation and automated segmentation equally detect hippocampal volume differences in acute depression? *Neuroimage*, 45(1):29–37, 2009.
[132] Arno Klein and Jason Tourville. 101 labeled brain images and a consistent human cortical labeling protocol. *Frontiers in neuroscience*, 6:171, 2012.
[133] Mark Jenkinson, Christian F Beckmann, Timothy EJ Behrens, Mark W Woolrich, and Stephen M Smith. Fsl. *Neuroimage*, 62(2):782–790, 2012.
[134] Susumu Mori, Kenichi Oishi, Hangyi Jiang, Li Jiang, Xin Li, Kazi Akhter, Kegang Hua, Andreia V Faria, Asif Mahmood, Roger Woods, et al. Stereotaxic white matter atlas based on diffusion tensor imaging in an icbm template. *Neuroimage*, 40(2):570–582, 2008.

[135] Arno Klein, Satrajit S Ghosh, Forrest S Bao, Joachim Giard, Yrjö Häme, Eliezer Stavsky, Noah Lee, Brian Rossa, Martin Reuter, Elias Chaibub Neto, et al. Mindboggling morphometry of human brains. *PLoS computational biology*, 13(2):e1005350, 2017.
[136] Miron B Kursa and Witold R Rudnicki. Feature selection with the boruta package. *Journal of statistical software*, 36:1–13, 2010.
[137] Guanlu Liu, Weizhao Lu, Jianfeng Qiu, and Liting Shi. Identifying individuals with attention-deficit/hyperactivity disorder based on multisite resting-state functional magnetic resonance imaging: a radiomics analysis. *Human Brain Mapping*, 44(8):3433–3445, 2023.
[138] Liting Shi, Xuechun Liu, Keqing Wu, Kui Sun, Chunsen Lin, Zhengmei Li, Shuying Zhao, and Xiuqin Fan. Surface values, volumetric measurements and radiomics of structural mri for the diagnosis and subtyping of attention-deficit/hyperactivity disorder. *European Journal of Neuroscience*, 54(10):7654–7667, 2021.
[139] Huaiqiang Sun, Ying Chen, Qiang Huang, Su Lui, Xiaoqi Huang, Yan Shi, Xin Xu, John A Sweeney, and Qiyong Gong. Psychoradiologic utility of mr imaging for diagnosis of attention deficit hyperactivity disorder: a radiomics analysis. *Radiology*, 287(2):620–630, 2018.
[140] Rachel A Yotter, Igor Nenadic, Gabriel Ziegler, Paul M Thompson, and Christian Gaser. Local cortical surface complexity maps from spherical harmonic reconstructions. *NeuroImage*, 56(3):961–973, 2011.
[141] Chao-Gan Yan, Xin-Di Wang, Xi-Nian Zuo, and Yu-Feng Zang. Dpabi: data processing & analysis for (resting-state) brain imaging. *Neuroinformatics*, 14:339–351, 2016.
[142] Hugo JWL Aerts, Emmanuel Rios Velazquez, Ralph TH Leijenaar, Chintan Parmar, Patrick Grossmann, Sara Carvalho, Johan Bussink, René Monshouwer, Benjamin Haibe-Kains, Derek Rietveld, et al. Decoding tumour phenotype by noninvasive imaging using a quantitative radiomics approach. *Nature communications*, 5(1):4006, 2014.
[143] Lifei Zhang, David V Fried, Xenia J Fave, Luke A Hunter, Jinzhong Yang, and Laurence E Court. Ibex: an open infrastructure software platform to facilitate collaborative work in radiomics. *Medical physics*, 42(3):1341–1353, 2015.
[144] Nathalie Tzourio-Mazoyer, Brigitte Landeau, Dimitri Papathanassiou, Fabrice Crivello, Octave Etard, Nicolas Delcroix, Bernard Mazoyer, and Marc Joliot. Automated anatomical labeling of activations in spm using a macroscopic anatomical parcellation of the mni mri single-subject brain. *Neuroimage*, 15(1):273–289, 2002.
[145] Nicholas J Tustison, Philip A Cook, Arno Klein, Gang Song, Sandhitsu R Das, Jeffrey T Duda, Benjamin M Kandel, Niels van Strien, James R Stone, James C Gee, et al. Large-scale evaluation of ants and freesurfer cortical thickness measurements. *Neuroimage*, 99:166–179, 2014.
[146] Ji-Hyun Kim. Estimating classification error rate: Repeated cross-validation, repeated hold-out and bootstrap. *Computational statistics & data analysis*, 53(11):3735–3745, 2009.
[147] S Paul Wright. Adjusted p-values for simultaneous inference. *Biometrics*, pages 1005–1013, 1992.
[148] Ahmad Chaddad, Christian Desrosiers, Lama Hassan, and Camel Tanougast. Hippocampus and amygdala radiomic biomarkers for the study of autism spectrum disorder. *BMC neuroscience*, 18:1–12, 2017.
[149] Adriana Di Martino, Chao-Gan Yan, Qingyang Li, Erin Denio, Francisco X Castellanos, Kaat Alaerts, Jeffrey S Anderson, Michal Assaf, Susan Y Bookheimer, Mirella Dapretto, et al. The autism brain imaging data exchange: towards a large-scale evaluation of the intrinsic brain architecture in autism. *Molecular psychiatry*, 19(6):659–667, 2014.
[150] Stephen R Dager, L Wang, SD Friedman, DW Shaw, JN Constantino, AA Artru, G Dawson, and JG Csernansky. Shape mapping of the hippocampus in young children with autism spectrum disorder. *American journal of neuroradiology*, 28(4):672–677, 2007.
[151] Lindsay E Rexrode, Joshua Hartley, Kurt C Showmaker, Lavanya Challagundla, Michael W Vandewege, Brigitte E Martin, Estelle Blair, Ratna Bollavarapu, Rhenius B Antonyraj, Keauna Hilton, et al. Molecular profiling of the hippocampus of children with autism spectrum disorder. *Molecular psychiatry*, 29(7):1968–1979, 2024.
[152] Elizabeth Kuenzel, Sarah Al-Saoud, Michelle Fang, and Emma G Duerden. Early childhood stress and amygdala structure in children and adolescents with neurodevelopmental disorders. *Brain Structure and Function*, 230(1):1–12, 2025.
[153] Tiziana Zalla and Marco Sperduti. The amygdala and the relevance detection theory of autism: an evolutionary perspective. *Frontiers in human neuroscience*, 7:894, 2013.
[154] Sture Holm. A simple sequentially rejective multiple test procedure. *Scandinavian journal of statistics*, pages 65–70, 1979.
[155] Marc V Fuccillo. Striatal circuits as a common node for autism pathophysiology. *Frontiers in neuroscience*, 10:27, 2016.
[156] Yi Jiang and G Allan Johnson. Microscopic diffusion tensor atlas of the mouse brain. *Neuroimage*, 56(3):1235–1243, 2011.
[157] Robbert L Harms, Francisco J Fritz, Alexandra Tobisch, Rainer Goebel, and Alard Roebroeck. Robust and fast nonlinear optimization of diffusion mri microstructure models. *Neuroimage*, 155:82–96, 2017.
[158] Alex Zwanenburg, Stefan Leger, Martin Vallières, and Steffen Löck. Image biomarker standardisation initiative. *arXiv preprint arXiv:1612.07003*, 2016.
[159] Loïc Duron, Daniel Balvay, Saskia Vande Perre, Afef Bouchouicha, Julien Savatovsky, Jean-Claude Sadik, Isabelle Thomassin-Naggara, Laure Fournier, and Augustin Lecler. Gray-level discretization impacts reproducible mri radiomics texture features. *PLoS One*, 14(3):e0213459, 2019.
[160] ADHD-200 consortium. The adhd-200 consortium: a model to advance the translational potential of neuroimaging in clinical neuroscience. *Frontiers in systems neuroscience*, 6:62, 2012.
[161] Minji Bang, Jihwan Eom, Chansik An, Sooyon Kim, Yae Won Park, Sung Soo Ahn, Jinna Kim, Seung-Koo Lee, and Sang-Hyuk Lee. An interpretable multiparametric radiomics model for the diagnosis of schizophrenia using magnetic resonance imaging of the corpus callosum. *Translational psychiatry*, 11(1):462, 2021.
[162] Long-Biao Cui, Lin Liu, Hua-Ning Wang, Liu-Xian Wang, Fan Guo, Yi-Bin Xi, Ting-Ting Liu, Chen Li, Ping Tian, Kang Liu, et al. Disease definition for schizophrenia by functional connectivity using radiomics strategy. *Schizophrenia bulletin*, 44(5):1053–1059, 2018.
[163] Alejandro Carrasco-Poves, Silvia Ruiz-Espana, Claudia Regio Brambilla, Irene Neuner, Ravichandran Rajkumar, Shukti Ramkiran, Christoph Lerche, and David Moratal. Analysis of new biomarkers for the study of schizophrenia following a radiomics approach on mr and pet imaging. In *2022 44th Annual International Conference of the IEEE Engineering in Medicine & Biology Society (EMBC)*, pages 234–237. IEEE, 2022.
[164] Minji Bang, Kisung Park, Seoung-Ho Choi, Sung Soo Ahn, Jinna Kim, Seung-Koo Lee, Yae Won Park, and Sang-Hyuk Lee. Identification of schizophrenia by applying interpretable radiomics modeling with structural magnetic resonance imaging of the cerebellum. *Psychiatry*

and Clinical Neurosciences, 78(9):527–535, 2024.
[165] Dafa Shi, Haoran Zhang, Guangsong Wang, Xiang Yao, Yanfei Li, Siyuan Wang, and Ke Ren. Neuroimaging biomarkers for detecting schizophrenia: a resting-state functional mri-based radiomics analysis. *Heliyon*, 8(12), 2022.
[166] Michael S Gazzaniga. Cerebral specialization and interhemispheric communication: does the corpus callosum enable the human condition? *Brain*, 123(7):1293–1326, 2000.
[167] Katherine L Narr, Paul M Thompson, Tonmoy Sharma, Jacob Moussai, Andrew F Cannestra, and Arthur W Toga. Mapping morphology of the corpus callosum in schizophrenia. *Cerebral Cortex*, 10(1):40–49, 2000.
[168] Mark Walterfang, Amanda G Wood, David C Reutens, Stephen J Wood, Jian Chen, Dennis Velakoulis, Patrick D McGorry, and Christos Pantelis. Corpus callosum size and shape in first-episode affective and schizophrenia-spectrum psychosis. *Psychiatry Research: Neuroimaging*, 173(1):77–82, 2009.
[169] Danilo Arnone, AM McIntosh, GMY Tan, and KP Ebmeier. Meta-analysis of magnetic resonance imaging studies of the corpus callosum in schizophrenia. *Schizophrenia research*, 101(1-3):124–132, 2008.
[170] Vina M Goghari, Donna J Lang, Sean W Flynn, Alex L MacKay, and William G Honer. Smaller corpus callosum subregions containing motor fibers in schizophrenia. *Schizophrenia research*, 73(1):59–68, 2005.
[171] Roberto Battiti. Using mutual information for selecting features in supervised neural net learning. *IEEE Transactions on neural networks*, 5(4):537–550, 1994.
[172] Corrado Corti, John Henry Xuereb, Luca Crepaldi, Mauro Corsi, Francesca Michielin, and Francesco Ferraguti. Altered levels of glutamatergic receptors and na+/k+ atpase-α1 in the prefrontal cortex of subjects with schizophrenia. *Schizophrenia research*, 128(1-3):7–14, 2011.
[173] Cláudia Régio Brambilla, Tanja Veselinović, Ravichandran Rajkumar, Jörg Mauler, Linda Orth, Andrej Ruch, Shukti Ramkiran, Karsten Heekeren, Wolfram Kawohl, Christine Wyss, et al. mglur5 receptor availability is associated with lower levels of negative symptoms and better cognition in male patients with chronic schizophrenia. *Human brain mapping*, 41(10):2762–2781, 2020.
[174] David R Roalf, Megan Quarmley, Monica E Calkins, Theodore D Satterthwaite, Kosha Ruparel, Mark A Elliott, Tyler M Moore, Ruben C Gur, Raquel E Gur, Paul J Moberg, et al. Temporal lobe volume decrements in psychosis spectrum youths. *Schizophrenia bulletin*, 43(3):601–610, 2017.
[175] Wei-Xing Shi. The auditory cortex in schizophrenia. *Biological psychiatry*, 61(7):829–830, 2007.
[176] Natalie Matosin, Francesca Fernandez-Enright, Jeremy S Lum, and Kelly A Newell. Shifting towards a model of mglur5 dysregulation in schizophrenia: consequences for future schizophrenia treatment. *Neuropharmacology*, 115:73–91, 2017.
[177] Robert B Innis, Vincent J Cunningham, Jacques Delforge, Masahiro Fujita, Albert Gjedde, Roger N Gunn, James Holden, Sylvain Houle, Sung-Cheng Huang, Masanori Ichise, et al. Consensus nomenclature for in vivo imaging of reversibly binding radioligands. *Journal of Cerebral Blood Flow & Metabolism*, 27(9):1533–1539, 2007.
[178] Martin Vallières, Carolyn R Freeman, Sonia R Skamene, and Issam El Naqa. A radiomics model from joint fdg-pet and mri texture features for the prediction of lung metastases in soft-tissue sarcomas of the extremities. *Physics in Medicine & Biology*, 60(14):5471, 2015.
[179] Ryan J Urbanowicz, Melissa Meeker, William La Cava, Randal S Olson, and Jason H Moore. Relief-based feature selection: Introduction and review. *Journal of biomedical informatics*, 85:189–203, 2018.
[180] M Latha and G Kavitha. Combined metaheuristic algorithm and radiomics strategy for the analysis of neuroanatomical structures in schizophrenia and schizoaffective disorders. *IRBM*, 42(5):353–368, 2021.
[181] Daniel J Abrams, Donald C Rojas, and David B Arciniegas. Is schizoaffective disorder a distinct categorical diagnosis? a critical review of the literature. *Neuropsychiatric Disease and Treatment*, 4(6):1089–1109, 2008.
[182] Manohar Latha and Ganesan Kavitha. Assessment of severity in neuropsychiatric disorders based on radiomic features with prior shape level set and metaheuristic algorithms. *International Journal of Imaging Systems and Technology*, 29(3):210–221, 2019.
[183] Stanley R Kay, Abraham Fiszbein, and Lewis A Opler. The positive and negative syndrome scale (panss) for schizophrenia. *Schizophrenia bulletin*, 13(2):261–276, 1987.
[184] Yae Won Park, Dongmin Choi, Joonho Lee, Sung Soo Ahn, Seung-Koo Lee, Sang-Hyuk Lee, and Minji Bang. Differentiating patients with schizophrenia from healthy controls by hippocampal subfields using radiomics. *Schizophrenia Research*, 223:337–344, 2020.
[185] José V Manjón and Pierrick Coupé. volbrain: an online mri brain volumetry system. *Frontiers in neuroinformatics*, 10:30, 2016.
[186] José E Romero, Pierrick Coupé, and José V Manjón. Corrigendum to" hips: A new hippocampus subfield segmentation method"[neuroimage 163 (2017) 286-295]. *NeuroImage*, 172:914, 2018.
[187] José V Manjón, Pierrick Coupé, Luis Martí-Bonmatí, D Louis Collins, and Montserrat Robles. Adaptive non-local means denoising of mr images with spatially varying noise levels. *Journal of Magnetic Resonance Imaging*, 31(1):192–203, 2010.
[188] Brian B Avants, Nick Tustison, Gang Song, et al. Advanced normalization tools (ants). *Insight j*, 2(365):1–35, 2009.
[189] László G Nyúl and Jayaram K Udupa. On standardizing the mr image intensity scale. *Magnetic Resonance in Medicine: An Official Journal of the International Society for Magnetic Resonance in Medicine*, 42(6):1072–1081, 1999.
[190] Nicholas J Tustison, Brian B Avants, Philip A Cook, Yuanjie Zheng, Alexander Egan, Paul A Yushkevich, and James C Gee. N4itk: improved n3 bias correction. *IEEE transactions on medical imaging*, 29(6):1310–1320, 2010.
[191] Aaron Carass, Jennifer L Cuzzocreo, Shuo Han, Carlos R Hernandez-Castillo, Paul E Rasser, Melanie Ganz, Vincent Beliveau, Jose Dolz, Ismail Ben Ayed, Christian Desrosiers, et al. Comparing fully automated state-of-the-art cerebellum parcellation from magnetic resonance images. *Neuroimage*, 183:150–172, 2018.
[192] Jose E Romero, Pierrick Coupé, Rémi Giraud, Vinh-Thong Ta, Vladimir Fonov, Min Tae M Park, M Mallar Chakravarty, Aristotle N Voineskos, and Jose V Manjón. Ceres: a new cerebellum lobule segmentation method. *Neuroimage*, 147:916–924, 2017.
[193] Min Tae M Park, Jon Pipitone, Lawrence H Baer, Julie L Winterburn, Yashvi Shah, Sofia Chavez, Mark M Schira, Nancy J Lobaugh, Jason P Lerch, Aristotle N Voineskos, et al. Derivation of high-resolution mri atlases of the human cerebellum at 3 t and segmentation using multiple automatically generated templates. *Neuroimage*, 95:217–231, 2014.

[194] Alex Zwanenburg, Martin Vallières, Mahmoud A Abdalah, Hugo JWL Aerts, Vincent Andrearczyk, Aditya Apte, Saeed Ashrafinia, Spyridon Bakas, Roelof J Beukinga, Ronald Boellaard, et al. The image biomarker standardization initiative: standardized quantitative radiomics for high-throughput image-based phenotyping. *Radiology*, 295(2):328–338, 2020.

[195] Dafa Shi, Yanfei Li, Haoran Zhang, Xiang Yao, Siyuan Wang, Guangsong Wang, and Ke Ren. Machine learning of schizophrenia detection with structural and functional neuroimaging. *Disease markers*, 2021(1):9963824, 2021.

[196] Lingzhong Fan, Hai Li, Junjie Zhuo, Yu Zhang, Jiaojian Wang, Liangfu Chen, Zhengyi Yang, Congying Chu, Sangma Xie, Angela R Laird, et al. The human brainnetome atlas: a new brain atlas based on connectional architecture. *Cerebral cortex*, 26(8):3508–3526, 2016.

[197] Alexandra I Korda, Christina Andreou, Helena Victoria Rogg, Mihai Avram, Anne Ruef, Christos Davatzikos, Nikolaos Koutsouleris, and Stefan Borgwardt. Identification of texture mri brain abnormalities on first-episode psychosis and clinical high-risk subjects using explainable artificial intelligence. *Translational Psychiatry*, 12(1):481, 2022.

[198] A Riecher-Rössler, U Gschwandtner, J Aston, S Borgwardt, M Drewe, P Fuhr, M Pflüger, W Radü, Ch Schindler, and R-D Stieglitz. The basel early-detection-of-psychosis (fepsy)-study–design and preliminary results. *Acta Psychiatrica Scandinavica*, 115(2):114–125, 2007.

[199] Pierrick Coupé, Pierre Yger, Sylvain Prima, Pierre Hellier, Charles Kervrann, and Christian Barillot. An optimized blockwise nonlocal means denoising filter for 3-d magnetic resonance images. *IEEE transactions on medical imaging*, 27(4):425–441, 2008.

[200] AI Korda, A Ruef, S Neufang, C Davatzikos, S Borgwardt, EM Meisenzahl, and N Koutsouleris. Identification of voxel-based texture abnormalities as new biomarkers for schizophrenia and major depressive patients using layer-wise relevance propagation on deep learning decisions. *Psychiatry Research: Neuroimaging*, 313:111303, 2021.

[201] Manolis IA Lourakis et al. A brief description of the levenberg-marquardt algorithm implemented by levmar. *Foundation of Research and Technology*, 4(1):1–6, 2005.

[202] Sebastian Bach, Alexander Binder, Grégoire Montavon, Frederick Klauschen, Klaus-Robert Müller, and Wojciech Samek. On pixel-wise explanations for non-linear classifier decisions by layer-wise relevance propagation. *PloS one*, 10(7):e0130140, 2015.

[203] Long-Biao Cui, Yu-Fei Fu, Lin Liu, Xu-Sha Wu, Yi-Bin Xi, Hua-Ning Wang, Wei Qin, and Hong Yin. Baseline structural and functional magnetic resonance imaging predicts early treatment response in schizophrenia with radiomics strategy. *European Journal of Neuroscience*, 53(6):1961–1975, 2021.

[204] Yi-Bin Xi, Long-Biao Cui, Jie Gong, Yu-Fei Fu, Xu-Sha Wu, Fan Guo, Xuejuan Yang, Chen Li, Xing-Rui Wang, Ping Li, et al. Neuroanatomical features that predict response to electroconvulsive therapy combined with antipsychotics in schizophrenia: a magnetic resonance imaging study using radiomics strategy. *Frontiers in psychiatry*, 11:456, 2020.

[205] Jie Gong, Long-Biao Cui, Yi-Bin Xi, Ying-Song Zhao, Xue-Juan Yang, Zi-liang Xu, Jin-Bo Sun, Peng Liu, Jie Jia, Ping Li, et al. Predicting response to electroconvulsive therapy combined with antipsychotics in schizophrenia using multi-parametric magnetic resonance imaging. *Schizophrenia research*, 216:262–271, 2020.

[206] John Ashburner. A fast diffeomorphic image registration algorithm. *Neuroimage*, 38(1):95–113, 2007.

[207] Saeed Ahmed, Ali Mahmood Khan, Hema Madhuri Mekala, Hema Venigalla, Rizwan Ahmed, Amira Etman, Michael Esang, and Mustafa Qureshi. Combined use of electroconvulsive therapy and antipsychotics (both clozapine and non-clozapine) in treatment resistant schizophrenia: a comparative meta-analysis. *Heliyon*, 3(11), 2017.

[208] Sohag N Sanghani, Georgios Petrides, and Charles H Kellner. Electroconvulsive therapy (ect) in schizophrenia: a review of recent literature. *Current opinion in psychiatry*, 31(3):213–222, 2018.

[209] Richard D Weiner and Irving M Reti. Key updates in the clinical application of electroconvulsive therapy. *International Review of Psychiatry*, 29(2):54–62, 2017.

[210] John Lally, John Tully, Dene Robertson, Brendon Stubbs, Fiona Gaughran, and James H MacCabe. Augmentation of clozapine with electroconvulsive therapy in treatment resistant schizophrenia: a systematic review and meta-analysis. *Schizophrenia research*, 171(1-3):215–224, 2016.

[211] Zaixu Cui, Suyu Zhong, Pengfei Xu, Yong He, and Gaolang Gong. Panda: a pipeline toolbox for analyzing brain diffusion images. *Frontiers in human neuroscience*, 7:42, 2013.

[212] Stephen M Smith, Mark Jenkinson, Mark W Woolrich, Christian F Beckmann, Timothy EJ Behrens, Heidi Johansen-Berg, Peter R Bannister, Marilena De Luca, Ivana Drobnjak, David E Flitney, et al. Advances in functional and structural mr image analysis and implementation as fsl. *Neuroimage*, 23:S208–S219, 2004.

[213] Pierre Bellec, Sébastien Lavoie-Courchesne, Phil Dickinson, Jason P Lerch, Alex P Zijdenbos, and Alan C Evans. The pipeline system for octave and matlab (psom): a lightweight scripting framework and execution engine for scientific workflows. *Frontiers in neuroinformatics*, 6:7, 2012.

[214] Ruopeng Wang, Thomas Benner, Alma Gregory Sorensen, and Van Jay Wedeen. Diffusion toolkit: a software package for diffusion imaging data processing and tractography. In *Proc Intl Soc Mag Reson Med*. Berlin, 2007.

[215] Chris Rorden, Hans-Otto Karnath, and Leonardo Bonilha. Improving lesion-symptom mapping. *Journal of cognitive neuroscience*, 19(7):1081–1088, 2007.

[216] Long-Biao Cui, Ya-Juan Zhang, Hong-Liang Lu, Lin Liu, Hai-Jun Zhang, Yu-Fei Fu, Xu-Sha Wu, Yong-Qiang Xu, Xiao-Sa Li, Yu-Ting Qiao, et al. Thalamus radiomics-based disease identification and prediction of early treatment response for schizophrenia. *Frontiers in neuroscience*, 15:682777, 2021.

[217] Erin Stolz, Krishna M Pancholi, Dhruman D Goradia, Sarah Paul, Matcheri S Keshavan, Vishwajit L Nimgaonkar, and Konasale M Prasad. Brain activation patterns during visual episodic memory processing among first-degree relatives of schizophrenia subjects. *Neuroimage*, 63(3):1154–1161, 2012.

[218] Jamie Ferri, JM Ford, BJ Roach, JA Turner, TG Van Erp, J Voyvodic, A Preda, A Belger, J Bustillo, D O'Leary, et al. Resting-state thalamic dysconnectivity in schizophrenia and relationships with symptoms. *Psychological medicine*, 48(15):2492–2499, 2018.

[219] Baojuan Li, Long-Biao Cui, Yi-Bin Xi, Karl J Friston, Fan Guo, Hua-Ning Wang, Lin-Chuan Zhang, Yuan-Han Bai, Qing-Rong Tan, Hong Yin, et al. Abnormal effective connectivity in the brain is involved in auditory verbal hallucinations in schizophrenia. *Neuroscience bulletin*,

33:281–291, 2017.
[220] Hu Liu, Guoguang Fan, Ke Xu, and Fei Wang. Changes in cerebellar functional connectivity and anatomical connectivity in schizophrenia: a combined resting-state functional mri and diffusion tensor imaging study. *Journal of magnetic resonance imaging*, 34(6):1430–1438, 2011.
[221] Bruce Fischl, André Van Der Kouwe, Christophe Destrieux, Eric Halgren, Florent Ségonne, David H Salat, Evelina Busa, Larry J Seidman, Jill Goldstein, David Kennedy, et al. Automatically parcellating the human cerebral cortex. *Cerebral cortex*, 14(1):11–22, 2004.
[222] BT Thomas Yeo, Mert R Sabuncu, Rahul Desikan, Bruce Fischl, and Polina Golland. Effects of registration regularization and atlas sharpness on segmentation accuracy. *Medical image analysis*, 12(5):603–615, 2008.
[223] Willi Sauerbrei, Patrick Royston, and Harald Binder. Selection of important variables and determination of functional form for continuous predictors in multivariable model building. *Statistics in medicine*, 26(30):5512–5528, 2007.
[224] Long-Biao Cui, Liu-Xian Wang, Ping Tian, Hua-Ning Wang, Min Cai, Fan Guo, Chen Li, Yu-Jing Wu, Peng-Gang Qiao, Zi-Liang Xu, et al. Aberrant perfusion and its connectivity within default mode network of first-episode drug-naïve schizophrenia patients and their unaffected first-degree relatives. *Scientific reports*, 7(1):16201, 2017.
[225] Long-Biao Cui, Min Cai, Xing-Rui Wang, Yuan-Qiang Zhu, Liu-Xian Wang, Yi-Bin Xi, Hua-Ning Wang, Xia Zhu, and Hong Yin. Prediction of early response to overall treatment for schizophrenia: a functional magnetic resonance imaging study. *Brain and Behavior*, 9(2):e01211, 2019.
[226] Long-Biao Cui, Yongbin Wei, Yi-Bin Xi, Alessandra Griffa, Siemon C De Lange, René S Kahn, Hong Yin, and Martijn P Van den Heuvel. Connectome-based patterns of first-episode medication-naïve patients with schizophrenia. *Schizophrenia bulletin*, 45(6):1291–1299, 2019.
[227] Fang Han, Bing Xiao, Lili Wen, and Yuxiu Shi. Effects of fluoxetine on the amygdala and the hippocampus after administration of a single prolonged stress to male wistar rates: In vivo proton magnetic resonance spectroscopy findings. *Psychiatry Research: Neuroimaging*, 232(2):154–161, 2015.
[228] Shilei Zheng, Han Wang, Fang Han, Jianyi Chu, Fan Zhang, Xianglin Zhang, Yuxiu Shi, and Lili Zhang. Detection of microstructural medial prefrontal cortex changes using magnetic resonance imaging texture analysis in a post-traumatic stress disorder rat model. *Frontiers in Psychiatry*, 13:805851, 2022.
[229] Rimenez R Souza, Lindsey J Noble, and Christa K McIntyre. Using the single prolonged stress model to examine the pathophysiology of ptsd. *Frontiers in pharmacology*, 8:615, 2017.
[230] Nathaniel G Harnett, Adam M Goodman, and David C Knight. Ptsd-related neuroimaging abnormalities in brain function, structure, and biochemistry. *Experimental neurology*, 330:113331, 2020.
[231] Thomas F Giustino and Stephen Maren. The role of the medial prefrontal cortex in the conditioning and extinction of fear. *Frontiers in behavioral neuroscience*, 9:298, 2015.
[232] Feng Chen, Jun Ke, Rongfeng Qi, Qiang Xu, Yuan Zhong, Tao Liu, Jianjun Li, Li Zhang, and Guangming Lu. Increased inhibition of the amygdala by the mpfc may reflect a resilience factor in post-traumatic stress disorder: a resting-state fmri granger causality analysis. *Frontiers in psychiatry*, 9:516, 2018.
[233] Neven Henigsberg, Petra Kalember, Zrnka Kovačić Petrović, and Ana Šečić. Neuroimaging research in posttraumatic stress disorder–focus on amygdala, hippocampus and prefrontal cortex. *Progress in Neuro-Psychopharmacology and Biological Psychiatry*, 90:37–42, 2019.
[234] Akira Kunimatsu, Koichiro Yasaka, Hiroyuki Akai, Natsuko Kunimatsu, and Osamu Abe. Mri findings in posttraumatic stress disorder. *Journal of Magnetic Resonance Imaging*, 52(2):380–396, 2020.
[235] Yuan-Xia Gao, Jiang-Yang Wang, and Guang-Heng Dong. The prevalence and possible risk factors of internet gaming disorder among adolescents and young adults: Systematic reviews and meta-analyses. *Journal of psychiatric research*, 154:35–43, 2022.
[236] Kun-Ru Song, Marc N Potenza, Xiao-Yi Fang, Gao-Lang Gong, Yuan-Wei Yao, Zi-Liang Wang, Lu Liu, Shan-Shan Ma, Cui-Cui Xia, Jing Lan, et al. Resting-state connectome-based support-vector-machine predictive modeling of internet gaming disorder. *Addiction Biology*, 26(4):e12969, 2021.
[237] Jin-Liang Wang, Jia-Rong Sheng, and Hai-Zhen Wang. The association between mobile game addiction and depression, social anxiety, and loneliness. *Frontiers in public health*, 7:247, 2019.
[238] Hee Ryung Wang, Hyun Cho, and Dai-Jin Kim. Prevalence and correlates of comorbid depression in a nonclinical online sample with dsm-5 internet gaming disorder. *Journal of affective disorders*, 226:1–5, 2018.
[239] Tyrone L Burleigh, Mark D Griffiths, Alexander Sumich, Grace Y Wang, Vasileios Stavropoulos, Lee Kannis-Dymand, and Daria J Kuss. Co-occurrence of gaming disorder and other potentially addictive behaviours between australia, new zealand, and the united kingdom. *International Journal of Environmental Research and Public Health*, 19(23):16078, 2022.
[240] Li Wang, Li Zhou, Shengdan Liu, Yurong Zheng, Qianhan Liu, Minglin Yu, Xiaofei Lu, Wei Lei, and Guangxiang Chen. Identification of patients with internet gaming disorder via a radiomics-based machine learning model of subcortical structures in high-resolution t1-weighted mri. *Progress in Neuro-Psychopharmacology and Biological Psychiatry*, 133:111026, 2024.
[241] Xu Han, Lei Wei, Yawen Sun, Ying Hu, Yao Wang, Weina Ding, Zhe Wang, Wenqing Jiang, He Wang, and Yan Zhou. Mri-based radiomic machine-learning model may accurately distinguish between subjects with internet gaming disorder and healthy controls. *Brain Sciences*, 12(1):44, 2021.
[242] Simone Kühn, A Romanowski, C Schilling, R Lorenz, C Mörsen, N Seiferth, T Banaschewski, A Barbot, GJ Barker, C Büchel, et al. The neural basis of video gaming. *Translational psychiatry*, 1(11):e53–e53, 2011.
[243] Doug Hyun Han, In Kyoon Lyoo, and Perry F Renshaw. Differential regional gray matter volumes in patients with on-line game addiction and professional gamers. *Journal of psychiatric research*, 46(4):507–515, 2012.
[244] Eun Jin Yoon, Jung-Seok Choi, Heejung Kim, Bo Kyung Sohn, Hee Yeon Jung, Jun-Young Lee, Dai-Jin Kim, Sun-Won Park, and Yu Kyeong Kim. Altered hippocampal volume and functional connectivity in males with internet gaming disorder comparing to those with alcohol use disorder. *Scientific reports*, 7(1):5744, 2017.
[245] Xin Du, Linlin Liu, Yongxin Yang, Xin Qi, Peihong Gao, Yang Zhang, Jiyu Zhu, Guijin Du, Shouping Dai, Xiaodong Li, et al. Diffusion tensor imaging of the structural integrity of white matter correlates with impulsivity in adolescents with internet gaming disorder. *Brain and*

behavior, 7(8):e00753, 2017.

[246] Bum Seok Jeong, Doug Hyun Han, Sun Mi Kim, Sang Won Lee, and Perry F Renshaw. White matter connectivity and internet gaming disorder. *Addiction biology*, 21(3):732–742, 2016.

[247] Kai Yuan, Ping Cheng, Tao Dong, Yanzhi Bi, Lihong Xing, Dahua Yu, Limei Zhao, Minghao Dong, Karen M von Deneen, Yijun Liu, et al. Cortical thickness abnormalities in late adolescence with online gaming addiction. *PloS one*, 8(1):e53055, 2013.

[248] Seungheon Yang and Jun Won Kim. Electrophysiological markers predicting antipsychotic treatment response in patients with schizophrenia: A retrospective study. *Neuropsychiatric Disease and Treatment*, pages 1387–1394, 2024.

[249] Myrto T Samara, Claudia Leucht, Mariska M Leeflang, Ion-George Anghelescu, Young-Chul Chung, Benedicto Crespo-Facorro, Helio Elkis, Kotaro Hatta, Ina Giegling, John M Kane, et al. Early improvement as a predictor of later response to antipsychotics in schizophrenia: a diagnostic test review. *American journal of psychiatry*, 172(7):617–629, 2015.

[250] Utku Kose, Nilgun Sengoz, Xi Chen, and Jose Antonio Marmolejo Saucedo. *Explainable Artificial Intelligence (XAI) in Healthcare*. CRC Press, 2024.

Acronyms

Acronyms	Meanings
AAL	Automated Anatomical Labeling
ACC	Anterior Cingulate Cortex
AD	Anxiety Disorder
ADC	Apparent Diffusion Coefficient
ADHD	Attention Deficit Hyperactivity Disorder
AFSP	American Foundation for Suicide Prevention
ALFF	Amplitude of Low-Frequency Fluctuation
AMY	Amygdala
ANOVA	Analysis of Variance
ANTS	Advanced Normalization Tools
ASD	Autism Spectrum Disorder
BOLD	Blood-Oxygen-Level-Dependent
BP	Bipolar Disorder
CAU	Caudate Nucleus
CSF	Cerebrospinal Fluid
CT	Computed Tomography
CV	Cross- validation
DC	Developing Controls
dMRI	Diffusion Magnetic Resonance Imaging
DC	Developmental Control
DSM	Diagnostic and Statistical Manual of Mental Disorders
DTI	Diffusion Tensor Imaging
DWI	Diffusion Weighted Imaging
FA	Fractional Anisotropy
FAE	FeAture Explorer
FDR	False Discovery Rate

Acronyms	Meanings
fMRI	Functional Magnetic Resonance Imaging
FSVM	Fuzzy Support Vector Machine
GAD	Generalized Anxiety Disorder
GI	Gyrification Index
GLCM	Grey Level Co-occurrence Matrix
GLDM	Grey Level Dependence Matrix
GLRLM	Grey Level Run Length Matrix
GLSZM	Grey Level Size Zone Matrix
GMW	Gray Matter Volume
HC	Healthy Control
HIP	Hippocampus
HSA	High Social Anxiety
IC	Internal Capsule
IFG	Inferior Frontal Gyrus
IGD	Internet Gaming Disorder
TIV	Intracranial Volume
LOOCV	Leave-One-Out Cross-Validation
LSA	Low Social Anxiety
LR	Logistic Regression
MDD	Major Depressive Disorder
MDT	Microstructure Diffusion Toolbox
MC-DWI	Multi-Compartment Diffusion Weighted Imaging
MNI	Montreal Neurological Institute
MRI	Magnetic Resonance Imaging
NDI	Neurite Density Index
NGTDM	Neighborhood Grey Tone Difference Matrix
NODDI	Neurite Orientation Dispersion and Density Imaging
ODI	Orientation Dispersion Index
PANDA	Pipeline Toolbox for Analyzing Brain Diffusion Images
PANSS	Positive and Negative Syndrome Scale
PET	Positron Emission Tomography
PD	Panic Disorder
PDA	Panic Disorder with Agoraphobia
PSOM	Pipeline System for Octave and Matlab
RBF	Radial Basis Function
rMFG	left Rostral Middle Frontal
ROIs	Region of Interest

Acronyms	Meanings
RSFC	Resting-State Functional Connectivity
rs-fMRI	Resting-State Functional Magnetic Resonance Imaging
SA	Schizoaffective Disorder
SAD	Social Anxiety Disorder
SBM	Surface-Based Morphology
SPECT	Single Photon Emission Computed Tomography
StD	Subthreshold Depression
sMRI	Structural Magnetic Resonance Imaging
SVM	Support Vector Machine
SZ	Schizophrenia
UF	Uncinate Fasciculus
VBM	Voxel-Based Morphology
VMHC	Voxel-Mirrored Homotopic Connectivity
VOI	Volume of Interest
WMV	White Matter Volume

Highlights

- Identification of key brain regions in mental disorders using radiomics approaches.
- Structural MRI (sMRI) is the most frequently used neuroimaging modality.
- FreeSurfer and CAT12 are widely used for neuroimaging preprocessing.
- Pyradiomics, LASSO, and SVM are the most commonly used tools for feature extraction, selection, and classification.
- First-order radiomic features are the most commonly extracted and selected.
- There is a limited availability of datasets for different mental disorders.
- Explainable AI (XAI) is rarely implemented in radiomics studies.

Declaration of interests

☒ The authors declare that they have no known competing financial interests or personal relationships that could have appeared to influence the work reported in this paper.

☐ The authors declare the following financial interests/personal relationships which may be considered as potential competing interests: